MINERALIZATION AND TECTONIC SETTING OF THE NORTON LAKE REGION, UCHI SUBPROVINCE

by

Justin R. Johnson

A thesis submitted in partial fulfillment of
the requirements for the degree of:

Master of Science in Geology

2005
Lakehead University
955 Oliver Road
Thunder Bay, ON
P7B 5E1

Abstract

The Norton Lake region is located approximately 50 km northeast of Fort Hope within the northernmost unnamed assemblage of the Miminiska-Fort Hope greenstone belt of the Uchi Subprovince, northwestern Ontario. An investigation of the region was initiated to attempt to correlate this region of the Superior Province with tectonic assemblages located to the southwest within other greenstone belts of the Uchi Subprovince, and to understand the mineralization of the Norton Lake Cu-Ni-Co-PGE deposit.

The geology of the area reveals a high degree of diversity within a relatively small area. The region is dominated by massive to pillowed mafic volcanic rocks with scattered pyroxenite and gabbro intrusions and sporadic sedimentary units. Trace element geochemistry has indicated that the volcanic rocks can be divided into three suites. Suite I consists of tholeiitic basalts to andesites characterized by weakly depleted to enriched LREE (La/Sm_{cn}= 0.8 – 1.2) and weakly fractionated HREE (Gd/Yb_{cn} = 1.0 – 1.4) in conjunction with slightly negative to slightly positive niobium anomalies. Suite II's tholeiitic basalts are characterized by LREE depleted basalts (La/Sm_{cn}= 0.5 - 0.7) with unfractionated HREE (Gd/Yb_{cn} = 0.9 - 1.0) and flat to negative niobium anomalies. Suite III is subdivided into two subsets: IIIa, calc-alkaline dacites, and IIIb, calc-alkaline basalts. All Suite III samples are strongly enriched in LREE (La/Sm_{cn}= 4.8 and 4.7 for IIIa, 1.1 – 3.1 for IIIb) with pronounce negative niobium anomalies. HREE vary from highly fractionated in Suite IIIa (Gd/Yb_{cn} = 2.3 and 1.8) to weakly fractionated and unfractionated in Suite IIIb (Gd/Yb_{cn} = 0.8 to 1.3).

The combination of trace element geochemistry and radiogenic isotope data indicates a complex tectonic environment. The sequence, from apparent oldest to youngest, of MORB (Suite II), subduction related volcanism (Suite III), ocean plateau (Suite I) and MORB (Suite II) is difficult to interpret. The obduction of an ocean plateau onto an immature island arc followed by the formation of a back-arc basin represents the most plausible explanation. The previous correlation of this region with the Northern Pickle assemblage of the Pickle Lake greenstone belt to the southwest, is supported by new trace element geochemistry and radiogenic isotope data.

The Norton Lake Cu-Ni-Co-PGE deposit (delineated in 1981 as 944,000 tonnes at 0.72% Ni and 0.56% Cu) is hosted within an ultramafic intrusion located along the contact between an upper mafic volcanic unit and a lower sheared amphibolite unit. Study of the mineralogy of the deposit has revealed two stages of mineralization. The first, due to sulphide saturation of the ultramafic intrusion through assimilation of an iron formation, accounts for formation of the primary sulphide phases. The second, a hydrothermal remobilization and enrichment of Cu and PGEs, resulted in the formation of crosscutting chalcopyrite veins and various Pd tellurides. The majority of Pt within the deposit has been found to be contained within the sulphide phases either as microinclusions, below the detection limit of a microprobe, or in solid solution with the sulphides. The Norton Lake deposit shows a similarity to the Thierry Mine, located within the Northern Pickle assemblage, in both mineralization history and geological setting.

Acknowledgements

I would like to thank Dr. P. Hollings for his suggestions, guidance, ability to take a joke and patience during my long journey. In addition Dr. S. Kissen insights into the economic aspects of this thesis were quite helpful. I would also like to thank R. Middleton (Bob) and East West Resource Corporation for unrestricted access to materials and information. In addition I wish to acknowledge the funding received through IRAP and East West Resource Corporation.

I also wish to thank most of the geology department who, in general, took the time to provided constructive criticism and new ideas to help strengthen this thesis. Ann Hammond and Alan MacKenzie provided valuable assistance with the preparation of material. I also wish to acknowledge the ability of the faculty to take the jokes played upon it.

Lastly, and most importantly, I wish to thank my family and friends without who I would have faltered and fallen long before now.

Table of contents

Title Page i
Abstract ii
Acknowledgements iii
Table of Contents iv
List of Figures vi
List of Tables viii
List of Appendices ix

1. Introduction and Methodology

1.1 Introduction 1
1.1 Scope of Study 1
1.2 Methods 2
1.2.1 Inductively Coupled Plasma-Mass Spectrometry and X-Ray Fluorescence Spetrometry 2
1.2.2 Thermal Ionization Mass Spectrometry 3
1.2.3 Scanning Electron Microscope-Energy Dispersion Spectrometry 4
1.2.4 Electron Microprobe 6
1.2.5 Bulk Element Analysis (ALS Chemex) 6

2. Regional Geology of the Uchi Subprovince

2.1. The Superior Province 7
2.2 Uchi Subprovince 7
2.2.1 Regional Geology 10
2.2.2 Overview of the Miminiska-Fort Hope Greenstone Belt 12
2.2.2.a General Geology of the Miminiska-Fort Hope Greenstone Belt 14
2.2.2.b Previous Work and Geology of the Norton Lake Study Area 17
2.2.3 Pickle Lake Greenstone Belt 19
2.2.4 Lake St. Joseph Greenstone Belt 24

3. Geological Mapping

3.1. Introduction 27
3.2.1 Summary of Field Mapping 29
3.2.2 Mafic Volcanic Rocks 31
3.2.3 Sedimentary Units 33
3.2.4 Iron Formation 34
3.2.5 Granite 34
3.2.6 Gabbroic/Pyroxenitic Units 34
3.2.8 Structure 35
3.3 Petrography 36
3.4 Summary 38

4. Whole Rock and Radiogenic Isotope Geochemistry

4.1 Introduction 40
4.2.1 Whole Rock and Rare Element Geochemistry of the Norton Lake Area 42
4.2.2 Results 45
4.2.3 Interpretation 53
4.3 Radiogenic Isotopes 58
4.4 Summary 61

5. Economic Mineralogy of the Norton Lake Deposit

5.1. Introduction 65
5.2. Norton Lake Ni-Cu-Co-PGE Deposit 66
5.2.1 Sulphides 68
5.2.2 Precious Metal Minerals 76
5.2.3 Oxides and Arsenides 81
5.3 Mineral Occurrences and Relationships 81
5.3.1 Constraints on Formation 87
5.4 Summary 91

6. Discussion and Conclusion 92

References 97

List of Figures

Figure 2.1	Generalized map of the Superior Province illustrating the various subprovinces.	8
Figure 2.2	Generalized geological map of the greenstone belts and intrusive rocks of the Uchi Subprovince.	9
Figure 2.3	Extent of previous studies (or mapping) undertaken in the Miminiska-Fort Hope greenstone belt.	11
Figure 2.4	Tectonic assemblages and plutonic suites of the Uchi Subprovince.	13
Figure 2.5	Simplified tectonic assemblages of the Miminiska-Fort Hope greenstone belt.	15
Figure 2.6	Geological map of the northeast portion of the Miminiska-Fort Hope greenstone belt. Outlined is the extent of the current study and Wasabi Resources Ltd.'s exploration.	18
Figure 2.7	Tectonic assemblages of the Pickle Lake belt.	20
Figure 2.8	Simplified geology of the Lake St. Joseph greenstone belt, U-Pb age determination sample locations.	26
Figure 3.1	Location of Locator Ltd. and Wasabi Resource Ltd. drill holes.	28
Figure 3.2	Geological compilation of the Norton Lake region based on surficial geology and diamond drill logs.	30
Figure 3.3	Photographs of outcrop exposure within the Norton Lake region.	32
Figure 3.4	Summary of structural features identified during mapping.	37
Figure 4.1	Location map of samples selected for whole rock geochemistry and radiogenic isotope analysis within the Norton Lake area.	41
Figure 4.2	Discrimination diagram for whole rock analysis with additional data from East West Resource Corporation.	43
Figure 4.3	MgO vs mobile and immobile elements.	44
Figure 4.4	Primitive mantle normalized diagrams for samples.	46-47
Figure 4.5	Variation plots for samples of Norton Lake area, East West Resource Corporation data is included.	54

Figure 4.6 Variation diagrams showing incompatible element abundances for samples from this study. 55

Figure 4.7 ϵ_{Nd} vs $^{147}Sm/^{144}Nd$ variation plot of isotope samples. 61

Figure 4.8 Interpreted trends of sample suites within Norton Lake region. 62

Figure 5.1 Longitudinal section of the mineralized zone. 67

Figure 5.2 A) Durchbewegung texture in drill core. B) Cartoon of drill core with select fragments highlighted. 68

Figure 5.3 Reflected light photomicrographs illustrating the various habits of pyrrhotite. 70

Figure 5.4 Fe-Ni-Co composition diagrams illustrating pyrrhotite and pentlandite compositions. Data from microprobe analyses and SEM analyses. 72

Figure 5.5 SEM backscattered images of sulphides 74

Figure 5.6 SEM backscattered images illustrating the occurrences of PMMs. 78

Figure 5.7 SEM backscattered images of composite PMM grains 78

Figure 5.8 Ternary diagram of SEM analyses illustrating the solid solution between michenerite and testibiopalladite. 79

Figure 5.9 Ternary diagram of SEM analysis of the melonite-merenskyite-moncheite solid solution. 80

Figure 5.10 SEM analyses of kotulskite plotted on the ternary Sb-Bi-Te diagram. 80

Figure 5.11 SEM backscattered images. 81

Figure 5.12 Element abundance diagrams, data from East West Resource Corporation drill core assays. 85

Figure 5.13 Superimposed predominance diagrams of the sulphides. 88

Figure 5.14 Superimposed predominance diagrams of tellurides and PGM. 89

List of Tables

Table 4.1	Summary of geochemical characteristics of samples	48
Table 4.2	Summary of isotope data	59
Table 5.1	Bulk assays by ALS Chemex of of ~1 m of drill core for samples studied by microprobe.	69
Table 5.2	Summary table of sulphide compositions as determined by microprobe.	71
Table 5.3	Summary of precious metal minerals identified.	77

List of Appendices

A. Sample Locations 106

B. Whole Rock and Radiogenic Isotope Geochemistry 113

C. SEM Analysis 123

D. Microprobe Analysis 144

Chapter 1

Introduction and Methodology

1. 1 Introduction

The geology of the northern greenstone belts of the Superior Province has received relatively little study, by both industry and academia, in comparison to the better known southern belts of the Abitibi and Wawa subprovinces. Sparse infrastructure combined with a short field season and limited outcrop make work in such areas difficult. Mapping has been concentrated around large bodies of water (which provide easier accessibility), communities (such as Fort Hope) and areas of economic interest (like the Norton Lake region).

Following initial provincial government regional mapping and airborne geophysical surveys within the Norton Lake region of the Uchi Subprovince, exploration companies have examined the area from the early 1970s to present. During the 1980s a Ni-Cu ore body, the Norton Lake deposit determined to be sub-economic at the time, was identified within the area between Norton Lake and Sturrock Lake hereafter referred to as the Norton Lake region.

1.1 Scope of Study

This study was undertaken to ascertain what mineral phases contained the economically important elements (platinum, palladium and cobalt) of the Norton Lake

mineralized zone, and to attempt a correlation between the geology and geochemistry of the Norton Lake region with the greenstone belts of the Uchi Subprovince located to the west-southwest. To achieve these goals the study was undertaken in two sections: a) geological mapping combined with high-precision geochemical analyses of key units; and, b) sulphide and precious metal mineral (PMM) mineralogy and interpretation of bulk-rock assays.

1.2 Methods

Whole rock geochemistry was carried out using Inductively Coupled Plasma – Mass Spectrometry (ICP-MS) and X-Ray Fluorescence Spectrometry (XRF). Radiogenic isotope analysis was carried out utilizing Thermal Ionization Mass Spectrometry (TIMS). Sulphide and PMM analyses were determined by Scanning Electron Microscope – Energy Dispersive Spectrometer (SEM-EDS) and electron microprobe. Additional whole rock geochemistry and bulk element analyses previously carried out by ALS Chemex was used to supplement the available data.

1.2.1 Inductively Coupled Plasma-Mass Spectrometry and X-Ray Fluorescence Spectrometry

Least altered whole rock samples (defined as samples with less than 5 vol% of alteration minerals and no observed carbonate minerals or serpentine) were selected based on petrographic microscope examination. Samples were first crushed using a tungsten carbide mallet and plate with the samples wrapped in paper to minimize contamination, reducing samples to approximately 3-4 mm in size. Secondary crushing in an agate rotary mill reduced samples to -200 mesh (~75μm). In order to minimize

contamination silica sand was run through the mill between each sample. Major elements were determined with XRF by fused disk for major oxides and pressed powder pellet for minor and trace elements at XRAL (X-Ray Assay Labs); relative standard deviations (RSD) are within 5%, loss on ignition (LOI) ranged from <0.01 wt% to 2.6 wt% and totals for all samples were 100% ± 1%.

Trace elements were analyzed by ICP-MS (Perkin Elmer Elan 5000) at the University of Saskatchewan using the protocol of Jenner et al. (1990), with standard additions, and pure elemental standards for external calibration. Wet chemistry operations were conducted under class-100 clean lab conditions. Analysis of acids, distilled deionised water and procedural blanks yielded levels of <1ppb for rare earth elements (REEs), niobium, zircon and hafnium, referenced to concentrations in rock. Detection limits are defined as 3σ of the procedural blank. Due to the possibility of refractory minerals being resistant to complete digestion during HF + HNO_3 dissolution, a comparison was made with results for HF+ HNO_3 dissolution and Na_2O_2 peroxide sinter (Jenner et al., 1990) with sinter values on average giving a higher abundance but within 10 to 15% of values determined by acid digestion. Detailed analytical methodology is provided in Fan and Kerrich (1997).

1.2.2 Thermal Ionization Mass Spectrometry

Analysis of isotopes was carried out by thermal ionization mass spectrometry (TIMS) on a Finnigan Mat 261 at Carleton University, Ontario. Neodymium isotopic analyses was performed on crushed powders where between 100 and 200 mg of the samples were spiked with a mixed ^{149}Sm-^{148}Nd solution and then dissolved by HF + HNO_3 in Savillex Teflon beakers. Neodymium and samarium were separated following

standard cation exchange techniques. Strontium was separated in a borosilicate glass column using AG50-X8 cation resin and 2.5 N HCl, followed by the rare earth elements using 6 N HCl. The REE-bearing solution was dried and the residue dissolved in 0.26 N HCl, then loaded into a column containing a 2 cm high bed of Teflon powder coated with HDEHP (2-ethylhexyl) orthophosphoric acid (Richard et al., 1976). Neodymium was eluted using 0.26 N HCl. Total procedural blanks for neodymium were <400 pg. The $^{147}Sm/^{144}Nd$ ratios are reproducible to 1%. Samples were loaded with 1 N HNO_3 on one side of a rhenium double filament and run in a Finnigan MAT261 thermal ionization mass spectrometer at temperatures of 1780° to 1820°C. Isotope ratios were normalized to $^{146}Nd/^{144}Nd = 0.72190$ (Cousens, 1996). Analyses of the La Jolla standard correspond closely to those obtained by other laboratories and averaged $^{143}Nd/^{144}Nd = 0.511877 \pm 18$ during the period of analysis. An age of 2900 Ma, the assumed age for the Norton Lake area based on current interpretations, was used for the calculation of initial ε_{Nd} values. Epsilon values at time T were calculated using the following formula:

$$\varepsilon^{T}_{Nd} = [(^{143}Nd/^{144}Nd^{T}_{sample}/^{143}Nd/^{144}Nd^{T}_{CHUR}) - 1] \times 10000$$

where CHUR is the Chondrite Uniform Reservoir and T is the time the rock was formed.

1.2.3 Scanning Electron Microscope-Energy Dispersion Spectrometry

Samples were analysed at the Lakehead University Instrumentation Laboratory, using a JEOL 5900 scanning electron microscope equipped with an Oxford energy dispersion spectrometer (EDS) with a resolution of 139eV. All mineral compositions were determined using the LINK ISIS analytical system incorporating a Super ATW Light Element Detector. Raw EDS spectra were acquired for 60 – 300 seconds (live

time) with an accelerating voltage of 20 kV and a beam current of 0.475 nA. The spectra were processed with the LINK ISIS SEMQUANT software, with full ZAF algorithm matrix corrections applied. Sulphides were analysed for sulphur, copper, iron, nickel, cobalt, lead, and molybdenum. The precious metal minerals (PMMs) were analysed for platinum, palladium, silver, gold, tellurium, antimony and bismuth, with silicon, aluminium, magnesium, sulphur, copper, iron, nickel and cobalt analysed to determine the potential degree of contamination (see below). Standardization at the start of each session was carried out using both geological and pure metal standards. The instrument's calibration was checked each hour using a pure nickel metal standard. Accuracy is 0.2 to 1.0 wt% and precision of 0.5 to 1.0 wt% depending on the atomic weight of the element on major elements at 60s (live time). Precision in the composition of mineral analyses was calculated based on sigma % output from the SEM-EDS.

Due to the small size of many of the PMM grains analysed, activation of the surrounding minerals was probable. Iron, nickel and to a lesser extent sulphur, cobalt and silicon have been report within PMM at low levels (Cabri, 2002). In order to evaluate if there was contamination from the surrounding matrix or if the elements were in solid solution within the PMM was evaluated on a case by case basis dependant on the elements detected and the degree to which they occurred. In circumstances where there was determined to be greater than 5 wt% combined contamination from the surrounding matrix, only semi-quantitative data was collected.

1.2.4 Electron Microprobe

Additional mineral chemistry work was carried out at the University of Saskatchewan using a JEOL 8600 microprobe equipped with an energy dispersive spectrometer and three wavelength dispersive spectrometers, one with a lead stearate crystal and a layered dispersion element crystal for light element analysis. Analyses were carried out using an accelerating voltage of 1500 kV, 35 nA beam current and a 5 μm electron beam width. Standardization was carried out utilizing both natural and synthetic materials for the elements iron, cobalt, nickel, copper, zinc, ruthenium, rhodium, palladium, silver, cadmium, rhenium, osmium, iridium, platinum, gold, lead and sulphur with ZAF corrections applied to all microprobe analysis.

1.2.5 Bulk Element Analyses (ALS Chemex)

Bulk assays on the mineralized zone were obtained from the Ministry of Northern Development and Mines assessment files and unpublished data from East West Resource Corporation. Assays were conducted on 0.5 m – 1.5 m BQ-thinwall diamond drill core, sawn in half, where care was taken to include similar styles of mineralization within one assay interval (internal memo, East West Resource Corporation). Whole rock analyses was preformed on 3 – 10 cm lengths of uncut core. All samples were sent to ALS Chemex with sample preparation conducted in Thunder Bay, Ontario and analysis completed in Vancouver, British Columbia. The following internal order codes were used; CU-AA46, NI-AA46, ME-ICP41, ME-XRF06, PGM-ICP23 and PGM-MS26 resulting in variety of techniques being used (refer to www.alschemex.com for details).

CHAPTER 2

Regional Geology of the Uchi Subprovince

2.1 The Superior Province

The Superior Province spans an area of 1,572,000 km^2, making it the world's largest Archean craton. It consists of a series of subprovinces composed of plutonic, volcanic, gneissic and metasedimentary assemblages ranging in age from 3.1 to 2.7 Ga (Figure 2.1; Card and Ciesielski, 1986). Geochronological studies have shown a broad southward younging of ages within the Province (Thurston, 2002), reflecting north to south accretion in both the southern part of the Province (Card and Ciesielski, 1986) and in the northern part of the province (Stott, 1997).

2.2 Uchi Subprovince

The Uchi Subprovince is a linear east-west trending structure composed of a series of metavolcanic, metasedimentary and plutonic sequences (greenstone belts) spanning an east-west distance of approximately 600 km. Given that the majority of the volcanic and sedimentary rocks within the Uchi Subprovince have been metamorphosed to at least greenschist grade, the term "meta" will be taken as implicit throughout this thesis. The Uchi Subprovince is separated from the English River Subprovince, to the south, by the Sydney Lake-Lake St. Joseph Fault and is in gradational contact with the Berens River Subprovince to the north (Figure 2.2). The Uchi Subprovince is

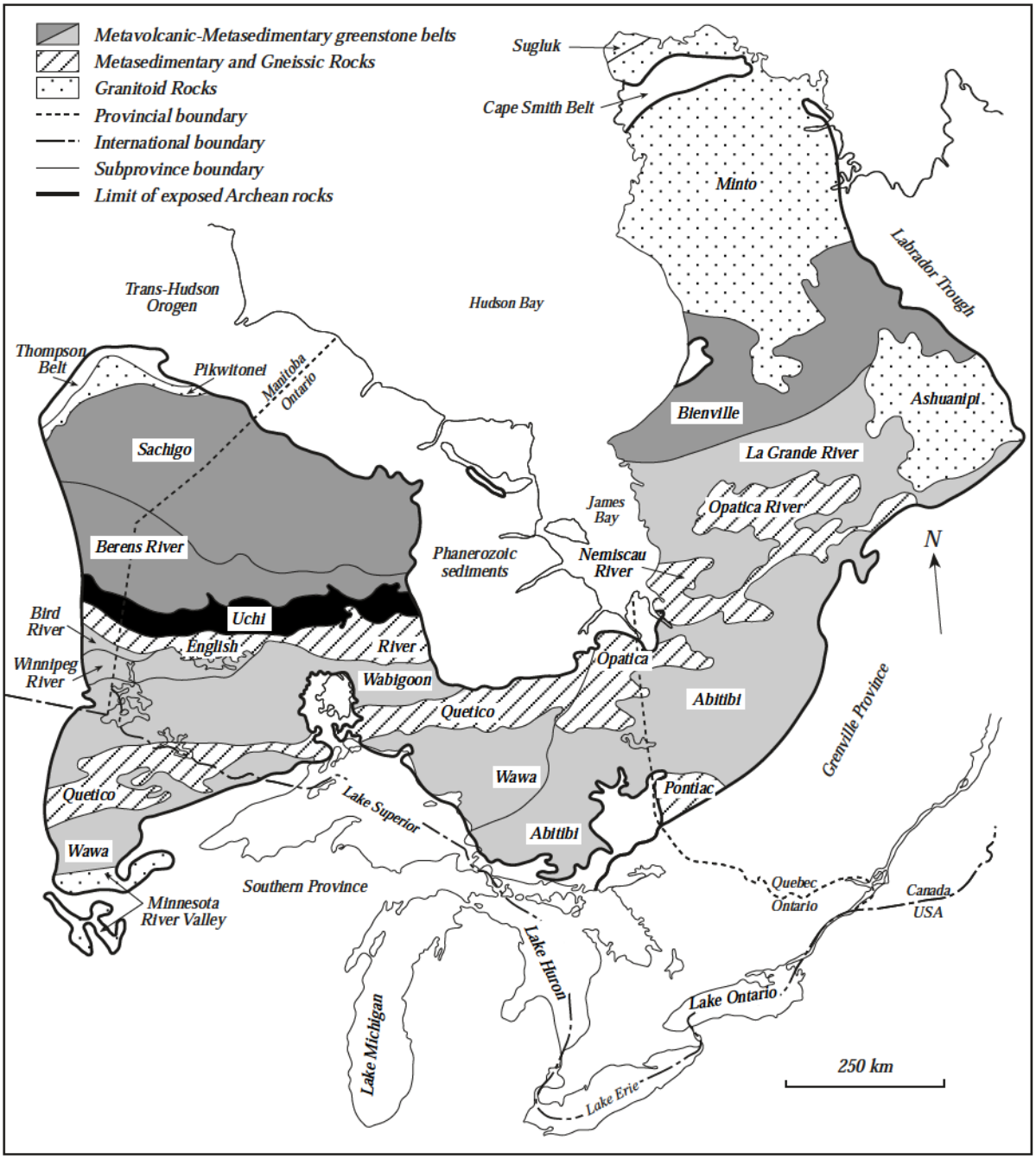

Figure 2.1: Generalized map of the Superior Province illustrating the various subprovinces. Uchi Subprovince highlighted in black (modified after Card and Ciesielski, 1986; Stottt, 1991).

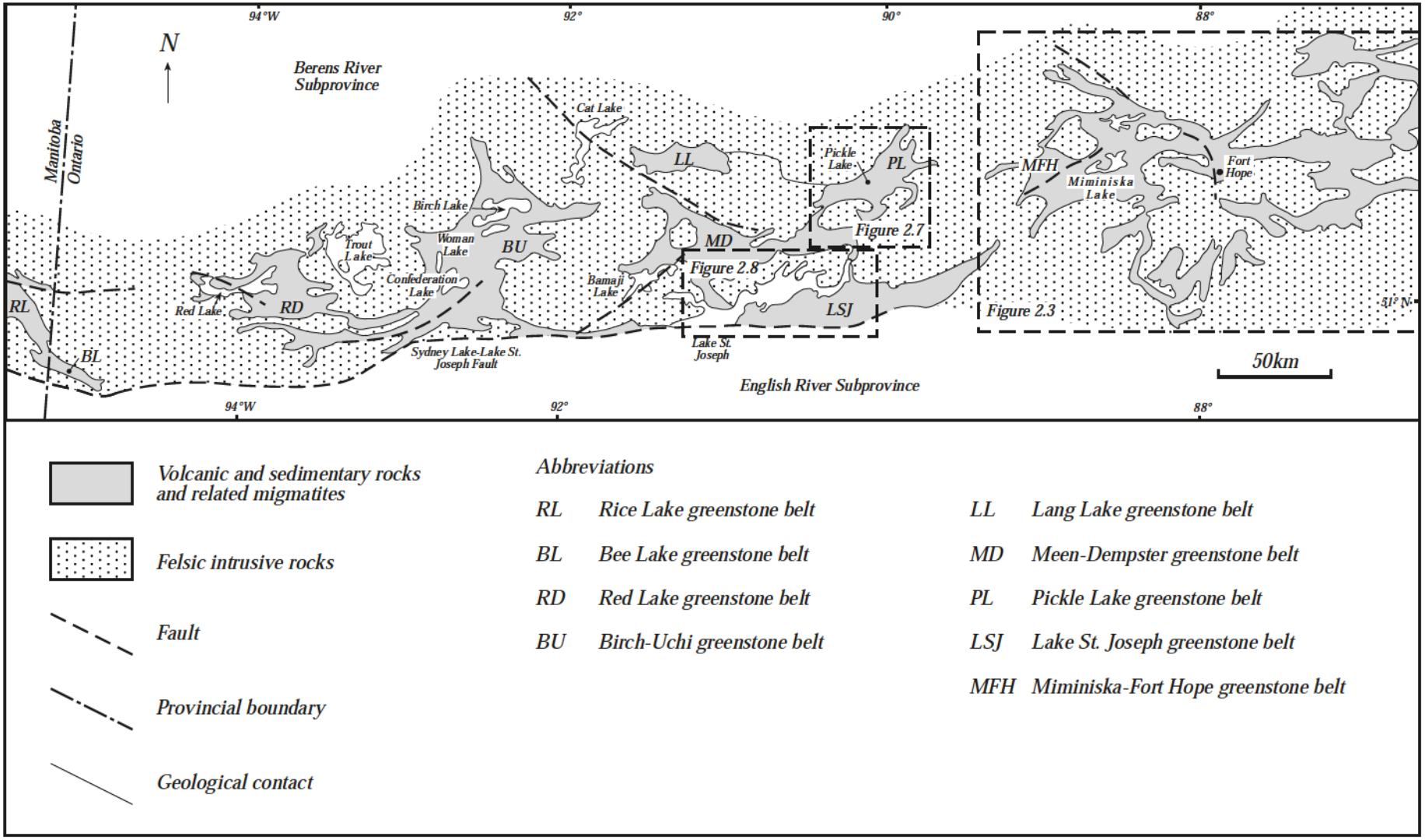

Figure 2.2: Generalized geological map of the greenstone belts and intrusive rocks of the Uchi Subprovince, modified after Stott and Corfu (1991).

distinguished from the Berens River Subprovince on the basis of lithology, with the Uchi Subprovince being dominated by greenstone belts and felsic plutons whereas the Berens River Subprovince is dominated by felsic plutons (Stott and Corfu, 1991). Thurston et al. (1991) have proposed that the ~2.9 – 3 Ga volcanic and plutonic sequences of the Uchi Subprovince should be grouped together with rocks of similar age in the Sachigo and Berens River Subprovinces to form the North Caribou Terrane.

Within the Uchi Subprovince several greenstone belts have been identified. From west to east these are the Rice Lake, Red Lake, Birch-Uchi, Meen-Dempster, Pickle Lake, Lake St. Joseph and the Miminiska-Fort Hope greenstone belts (Stott and Corfu, 1991; Figure 2.2). The greenstone belts are composed of distinct assemblages that are defined from a combination of field mapping, lithological and geochronological relationships. Thurston (p.77, 1991) defined an assemblage as "stratified volcanic and/or sedimentary rock units built during a discrete interval of time in a common depositional or volcanic setting". Within the subprovince there is a decrease in bedrock exposure towards the east due to a variable thick blanket of glacial till and the low relief of the eastern area (Stott and Corfu, 1991).

2.2.1 Regional Geology

Geochemical and geochronological data for the Miminiska-Fort Hope greenstone belt (MFGB) is quite limited. Thurston and Carter's (1970) Operation Fort Hope reconnaissance mapping along with Wallace's of more detailed work concentrated around the Miminiska Lake, Attwood Lake and Opikeigen Lake regions (Figure 2.3) represent the only published geochemical work done within the region while

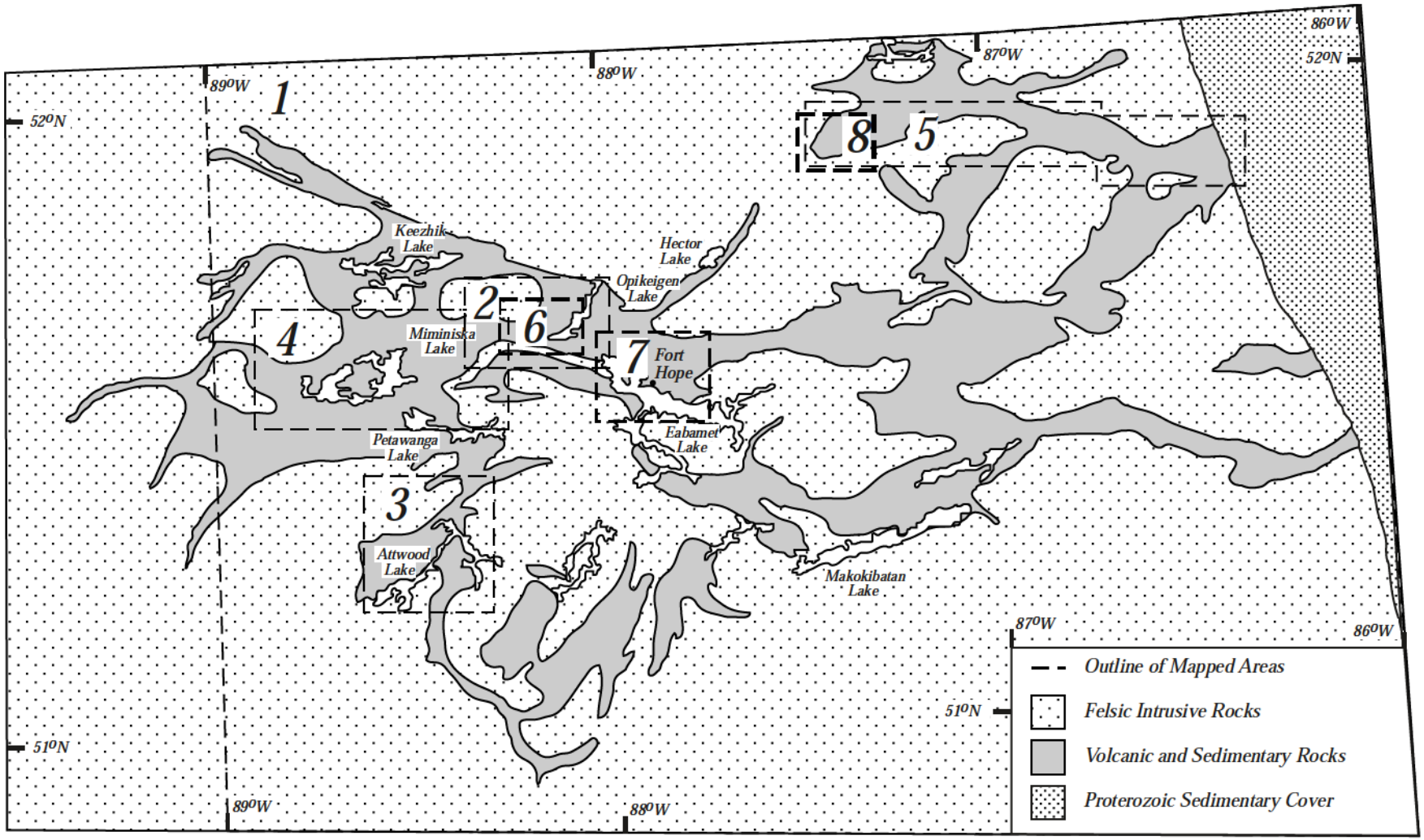

Figure 2.3: Extent of previous studies (or mapping) undertaken in the Miminiska-Fort Hope greenstone belt. 1. Thurston and Carter (1970) undertook regional scale mapping at a 1 inch to 2 miles encompassing 50º30' to 52º30' north and 86º to 89º west; 2. Wallace (1978) at 1:31,680; 3. Wallace (1981a) at 1:31,680; 4. Wallace (1981b) at 1:31,680; 5. Wasabi Resources Ltd. and Locator Exploration Ltd.; 6. Hall (2004); 7. Prest (1944); 8. Current Study.

geochronological work is restricted to Corfu and Stott's (1993a; 1993b) work. As a result of this limited data past correlations to other assemblages within the Uchi subprovince have been based primarily on the interpretation of aeromagnetic trends and general similarities in rock types and units. Stott and Corfu (1991) correlated the northern assemblages in the Miminiska-Fort Hope greenstone belt (MFGB) with those of the North Caribou terrain, the Pickle Lake greenstone belt and the St. Joseph greenstone belt (Figure 2.4). Recent work within the Uchi Subprovince (e.g. Hollings et al., 1999; Rogers, 2002; Young, 2003) has resulted in the redefinition of previous assemblages and new assemblages being defined. In order to evaluate these changes and how they affect the MFGB, the geology of these areas will be briefly summarized.

2.2.2 Overview of the Miminiska-Fort Hope Greenstone Belt (MFGB)

The MFGB has undergone limited mapping by the government with most of the work concentrated within the southern portion of the belt, with additional work around the Fort Hope Reserve, Miminiska Lake and Keezhik Lake (Figure 2.3: Prest, 1944; Thurston and Carter, 1970; Wallace, 1978, 1981a, 1981b). In addition, various exploration companies have carried out reconnaissance studies and small scale, detailed geological mapping since the 1970's. The subdivision of the MFGB has been difficult due to the limited geological mapping, the lack of outcrop exposure and the absence of age determinations for the dominantly mafic rocks of the area.

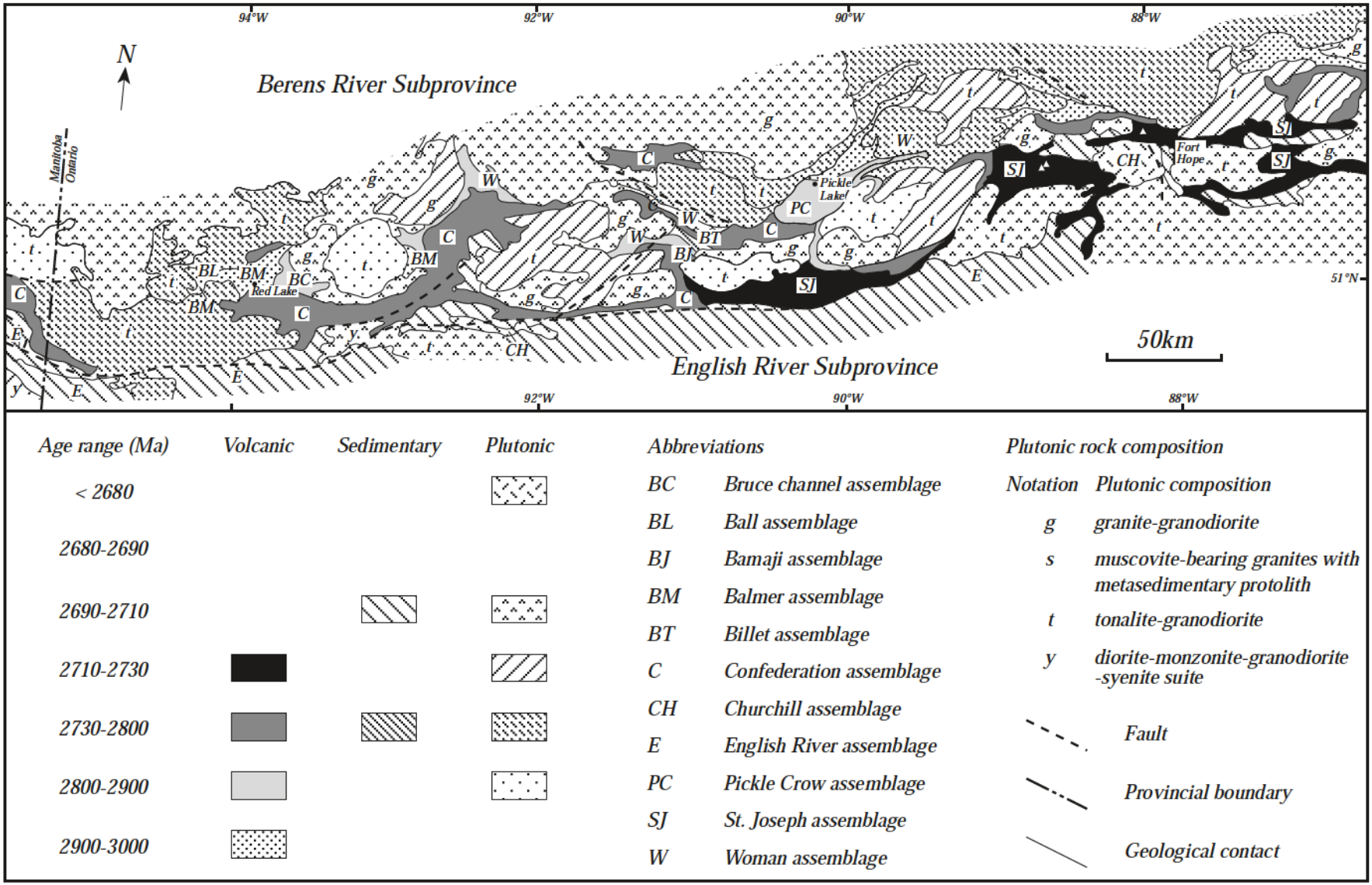

Figure 2.4: Tectonic assemblages and plutonic suites of the Uchi Subprovince. Modified after Stott and Corfu, 1991.

2.2.2.a General Geology of the Miminiska-Fort Hope Greenstone Belt

The MFGB was provisionally divided into five tectonic assemblages by Stott and Corfu (1991). It consists of three unnamed volcanic assemblages in the northern part of the belt, the St. Joseph assemblage and the sedimentary rocks of the Miminiska Lake area (Figure 2.5). Information on the northern three unnamed assemblages has come from the work undertaken in the Keezhik Lake area and has been extended to the east based on limited mapping and interpretation of geophysical airborne surveys. Only the Lake St. Joseph assemblage, the southernmost assemblage, has been dated with U – Pb zircon ages of 2723±1 Ma (MILv a lapilli tuff), 2716±1 Ma (MIMv a crystal tuff – breccia) and 2723±2 Ma (RLv a lapilli tuff, refer to Figure 2.5 for locations; Corfu and Stott, 1993a). The remaining assemblages' ages are based on interpreted correlations with assemblages from other belts (Stott and Corfu, 1991).

The northernmost assemblage (1 on Figure 2.5) is composed of basaltic flows with an east-northeast striking, three- to ten-metre wide banded magnetite iron formation located north of the east arm of Keezhik Lake and trending east-northeast (Thurston and Carter, 1969; Thurston and Carter, 1970; Stott and Corfu, 1991). The assemblage has been suggested as correlative with the McGruer assemblage of the North Caribou greenstone belt based on the similarity of rock types and a discontinuous aeromagnetic anomaly, interpreted to be a continuation of the iron formation marker unit at Keezhik Lake, implying an age of 2900-3000 Ma (Stott and Corfu, 1991).

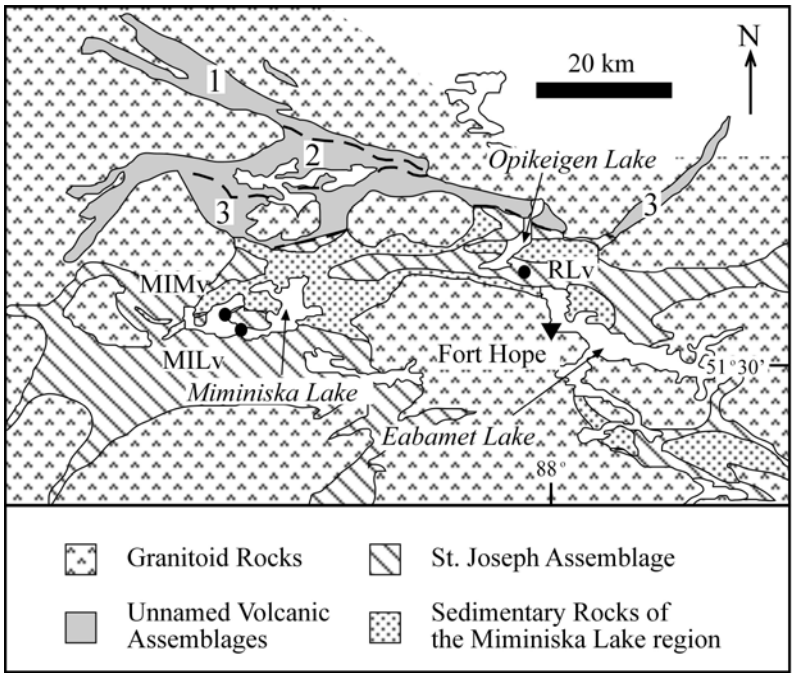

Figure 2.5: Simplified tectonic assemblage map of the northwest portion of the Miminiska-Fort Hope greenstone belt. 1, 2, and 3 denote the unnamed volcanic assemblages. Sample locations indicated for all U-Pb age determinations of Corfu and Stott (1993b) (modified after Corfu and Stott, 1993b).

The second assemblage (2 on Figure 2.5) is divided into a northern and southern portion. The northern portion consists of south-facing massive to pillowed basalt flows with a banded magnetite iron formation located north of Keezhik Lake (Thurston and Carter, 1969; Thurston and Carter, 1970; Stott and Corfu, 1991). Stott and Corfu (1991) have suggested that this iron formation is equivalent to one located in the First Loon Lake area within the Pickle Crow assemblage of the Pickle Lake greenstone belt. Basalts with a quartz porphyry intrusion accompanied by a unit of dacitic pyroclastic rocks (speculated to be an extension of the Woman assemblage, as defined by Stott and Corfu (1991), of the Pickle Lake greenstone belt) occur further to the south. The northern portion has an interpreted age of 2800 – 2900 Ma based on a U-Pb zircon age of 2836±3

Ma from a quartz-phyric tuff in the Woman assemblage of the Pickle Lake greenstone belt with which it has been correlated (see below; Stott and Corfu, 1991).

The third assemblage (3 on Figure 2.5), interpreted to be 2730 – 2800 Ma in age, is composed of southward facing, basaltic flows with minor felsic volcanic units (Stott and Corfu, 1991). The assemblage unconformably overlies a thin sedimentary unit west of Keezhik Lake (Stott and Corfu, 1991). It's contact with the St. Joseph assemblage, located to the south, is poorly established (Stott and Corfu, 1991). The contact is conditionally located where a change in the regional stratigraphic younging direction occurs, from south-facing in the third assemblage to north-facing within the St. Joseph assemblage located to the south. The change in younging is observed within the area surrounding Miminiska Lake.

The St. Joseph assemblage is interpreted to be the continuation of the Lake St. Joseph assemblage of the Lake St. Joseph greenstone belt and dominates the south half of the MFGB (Stott and Corfu, 1991). It is a sequence of north-facing tholeiitic and calc-alkalic basalt flows and calc-alkalic pyroclastic rocks that range in composition from andesitic to rhyolitic (Stott and Corfu, 1991). The assemblage becomes intercalated with clastic sedimentary sequences on a regional scale towards the east (Stott and Corfu, 1991). Its contact with the older assemblages is interpreted to continue to the east based solely on aeromagnetic interpretations (Stott and Corfu, 1991).

Stott and Corfu (1991) tentatively identified a fifth assemblage consisting of sedimentary rocks located around Miminiska Lake. Due to the uncertainty of the source and the original depositional setting for these rocks (they may have formed in their present location or they may have been transported as a tectonic wedge from the English

River assemblage located to the south) they are treated as an unnamed assemblage (Stott and Corfu, 1991). The assemblage contains evidence of folding and displays an overall north younging (Stott and Corfu, 1991). It is composed of medial to distal turbidite wacke sediments with interbeds of banded magnetite iron formation (Stott and Corfu, 1991). The assemblage displays characteristics similar to those identified in fore-arc accretionary prisms (i.e., interlayering with volcanic assemblages to the east; Stott and Corfu, 1991).

2.2.2.b Previous Work and Geology of the Norton Lake Study Area

The northeast area of the MFGB extending from Sturrock Lake to the eastern extent of the MFGB (see Figure 2.6) has been the subject of additional geological mapping that is summarized in Hill's (1981a) *Interim Report on the Norton Lake Area for Wasabi Resources Ltd.* with additional information from Ellington's (1988) Locator Exploration Ltd. (Duration Minerals Ltd.) *Norton Lake Property OMEP OM87-4-L-112 Geological Report*.

The northernmost portion of the MFGB is approximately 77 km in length and varies in width from 10-16 km (Figure 2.6). It is bordered on the north, south and west by granititic batholiths and on the east by the Paleozoic sediments of the Hudson Bay Lowlands. The main structural feature is a north-dipping, overturned syncline whose axis trends nearly east-west. The central part of this area has a north-south anticlinal cross fold that has resulted in the closing of the syncline. The banded iron formations, as interpreted from geophysics, highlight the folds (Figure 2.6; Hill, 1981a). The banded iron formations close in the centre, due to the cross fold, and are open to the west and east

resulting in two subsidiary anticlinal folds. The first folded iron formation is located in the area of the Norton Lake Deposit while the second occurs within the sediments and volcanics located further to the east in the Hale Lake area (Figure 2.6; Hill, 1981a).

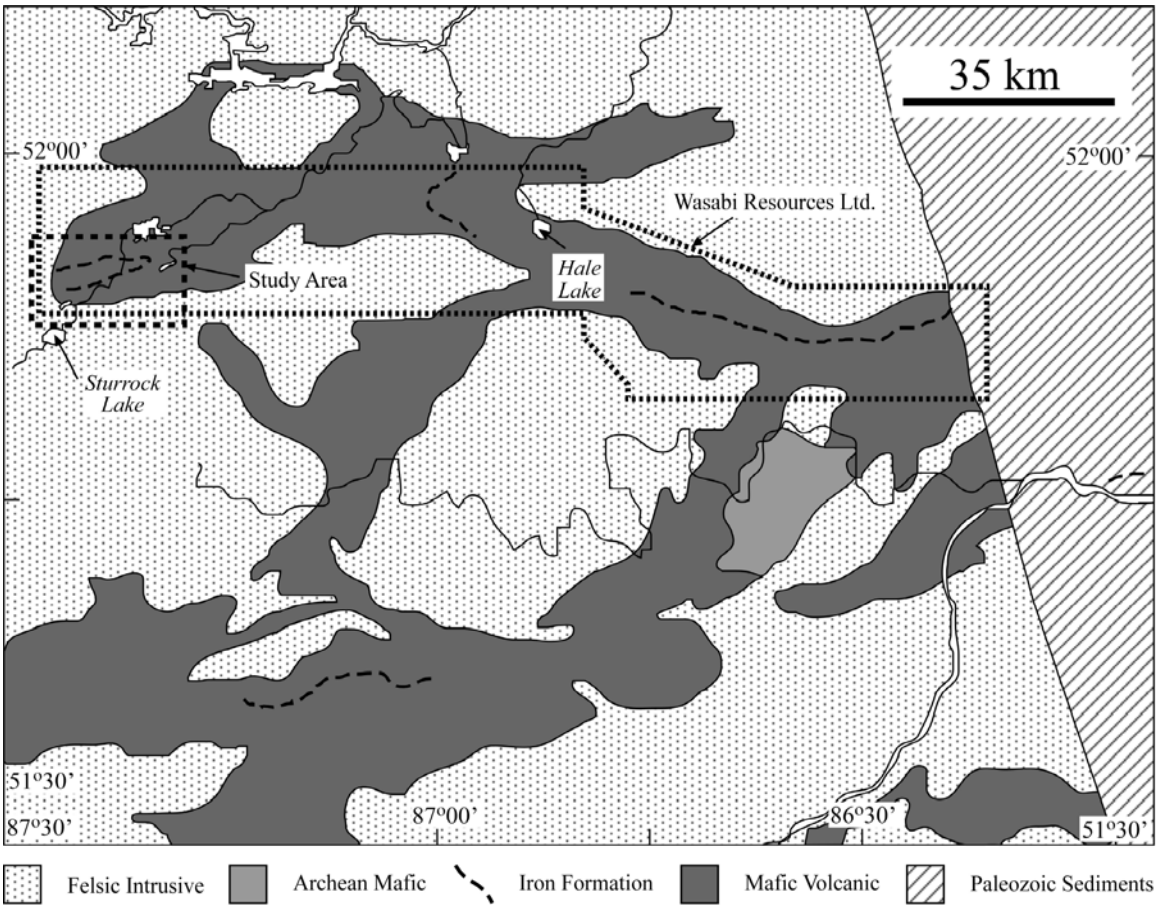

Figure 2.6: Geological map of the northeast portion of the Miminiska-Fort Hope greenstone belt. Outlined is the extent of the current study and Wasabi Resources Ltd.'s exploration (modified after Thurston and Carter, 1969; units as defined by Thurston and Carter, 1969).

Wasabi Resources Ltd. and Locator Exploration Ltd. identified four volcanic units within the region, three recognised in outcrop and one interpreted from geophysical data. These volcanic units consisted of: A) thin layers of massive to pillowed mafic flows, mafic tuffs, mafic to ultramafic sills or flows and interflow iron formations and

sedimentary beds; and B) mafic to felsic volcanic rocks consisting of amphibolitic mafic pillowed lavas, massive felsic rocks and foliated lapilli tuffs. Interpretation of whether these units are laterally continuous, grading from one to another, or if they are distinct units was not determined by Hill (1981a, b) or Ellington (1988) due to the scarcity of outcrop and the scale of the mapping.

2.2.3 Pickle Lake Greenstone Belt

Located within the centre of the Uchi Subprovince, the Pickle Lake greenstone belt was proposed by Stott and Corfu (1991) to consist of four volcanic assemblages. Young and Helmstaedt (2001) and Young (2003) have since redefined these assemblages (Figure 2.7).

The northernmost assemblage, identified by Stott and Corfu (1991) and described in detail by Stott (1996), is the Northern Pickle assemblage. It is a sequence of tabular volcanic and minor sedimentary strata that consists of massive and pillowed basalt flows with minor magnetite banded iron formation interbeds, mafic to ultramafic intrusive sheets and very limited tuff beds that are interpreted to run nearly the full length of the northern half of the Pickle Lake belt, based on aeromagnetic anomalies and marker beds (Stott, 1996). The assemblage was interpreted to resemble an Archean oceanic mafic plain sequence (Stott, 1996). The Northern Pickle assemblage was believed to be comparable to the McGruer assemblage of the North Caribou greenstone belt, located within the Sachigo Subprovince to the north, and consequently interpreted to have an age of 2990 Ma (Stott and Corfu, 1991; Stott, 1996).

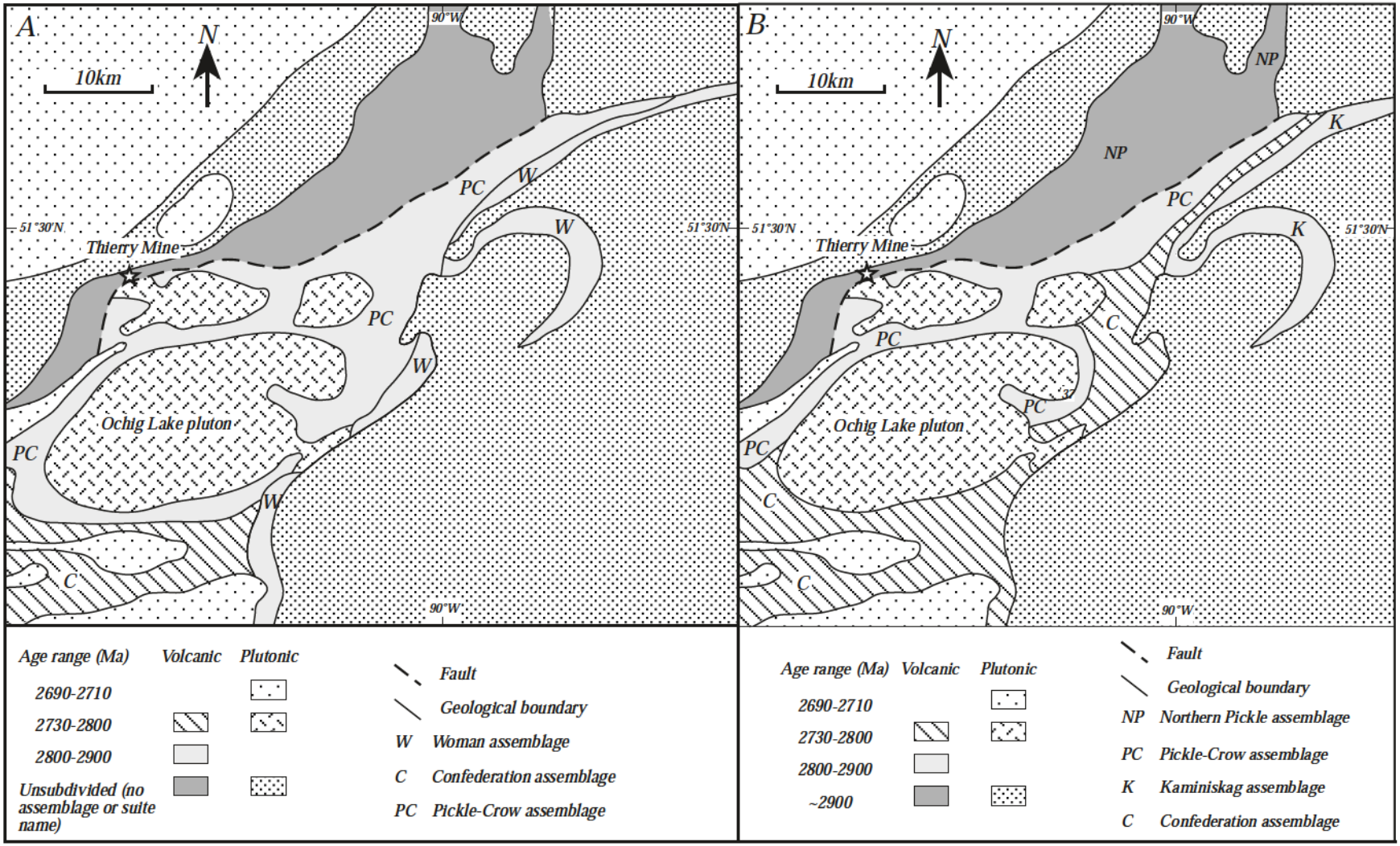

Figure 2.7: Tectonic assemblages of the Pickle Lake belt. A. Modified after Stott and Corfu (1991). B. Modified after Young (2003).

The Pickle Crow assemblage, as defined by Stott and Corfu (1991), is composed of a folded sequence of dominantly massive to pillowed basaltic flows, dacitic to rhyolitic pyroclastic flows, quartz porphyry intrusions and magnetite-banded iron formation with interbeds of thin graphitic schist. An age of 2860±2 Ma (Corfu and Stott, 1993b) has been determined for a quartz porphyry sill that intrudes the basalts at the base of the assemblage. Samples of the same sill contain inherited zircons that have an age of 2892+5/-2 Ma (Stott, 1996).

Young (2003) suggested that the Northern Pickle assemblage formed the base of the Pickle Crow assemblage to the southeast. Young's interpretations are based on recent work showing that there is a northwest younging of the strata rather than southeast younging (Young and Helmstaedt, 2001, Young, 2003) as would be indicated by a correlation with the North Caribou terrene (Stott, 1996). In addition there is a continuation of an aeromagnetic anomaly (Young and Helmstaedt, 2001; Young, 2003) through the proposed boundary between the Pickle Crow and Northern Pickle assemblages. Hollings (2002) determined that samples taken from the Northern Pickle have REE patterns broadly comparable to modern OIB but due to distinct thorium-niobium-lanthanum systematics should be termed niobium enriched basalts. Additional REE and samarium-neodymium isotope work of Young (2003) produced similar results.

The Woman assemblage, as defined by Stott and Corfu (1991), was interpreted to be present in three quarters of the Uchi Subprovince covering the Birch-Uchi, Meen-Dempster, Pickle Lake and Miminiska-Fort Hope greenstone belts. Recent mapping has restricted the Woman assemblage to occurring only in the Birch-Uchi greenstone belt (Hollings et al., 2000; Rogers et al., 2000; Young, 2003). The circa 2836 Ma rocks of the

former Woman assemblage have been reassigned to the Kaminiskag assemblage due to similarities in age, geochemistry and stratigraphy (Hollings et al., 2000; Young, 2003).

The Kaminiskag assemblage in the Pickle Lake belt is composed of an upper pyroclastic sequence followed by massive to pillowed tholeiitic basalts with minor gabbroic sills, beds of banded quartz-magnetite iron formation and dacitic to rhyolitic ash flows (Stott and Corfu, 1991; Young, 2003). The southern part of the assemblage is composed of a quartz-phyric tuff with an U-Pb zircon age of 2836±3 Ma (Corfu and Stott, 1993a). A stratigraphic correlation may occur with "a coarser, thicker suite of dacitic pyroclastic rocks and a quartz porphyry intrusion believed to lie close to a vent in an unnamed assemblage in the northern part of the Miminiska-Fort Hope greenstone belt" (p. 171, Stott and Corfu, 1991).

Stratigraphically above the Kaminiskag assemblage lies the Confederation assemblage. The boundaries of the Confederation assemblage have been expanded by Young (2003) further to the northwest on the basis of new U-Pb age determinations, similarities in rock types and aeromagnetic trends. The Confederation assemblage now includes parts of the former Pickle Crow assemblage and sections of the former Woman assemblage (see Figure 2.7). The newly expanded extent of the Confederation assemblage is composed of intercalated mafic to intermediate volcanic rocks (Young, 2003). The bulk of the assemblage occurs in the southwest area of the belt and is considered an extension of similar rocks in the Meen-Dempster belt to the west (Stott and Corfu, 1991).

The Pickle Lake greenstone belt has undergone considerable exploration in the past resulting in several past-producing mines. The majority of exploration in the belt

was undertaken for gold with a lesser amount being conducted for base metals, magmatic Cu-Ni and rare element pegmatites. Of the most interest to this study is the Thierry Cu-Ni mine operated from 1976 to 1982.

The Thierry mine is located to the west of the town of Pickle Lake within the Pickle Crow assemblage (see Figure 2.7). The mine has been interpreted to be a magmatic sulphide deposit that was remobilized and metamorphosed (Patterson and Watkinson, 1984a; 1984b). During its operation the Thierry mine processed approximately 4.9 million tons at a grade of 1.13 % copper and 0.14 % nickel with minor amounts of precious metals grading 0.0046 oz/ton gold, 0.004 oz/ton platinum and 0.020 oz/ton palladium. The mineral reserves are calculated at 2.7 million tonnes at a diluted grade of 1.65 % copper to the 1600 foot level and an additional measured mineral resource of 3.6 million tonnes at an undiluted grade of 1.78 % copper to the 1800 foot level. In addition there is an approximate 0.25 % nickel grade with an undetermined PGE grade. The mineralization within the Thierry mine is hosted within sheared mafic to ultramafic rocks of greenschist to amphibolite facies metamorphism (Patterson and Watkinson, 1984a; 1984b; Curtis, 2001).

The sulphides at the Thierry mine occur in four associations: disseminated sulphides (less than 1%), breccia ore (40 %), mylonite ore (58 %) and bornite ore (less than 1 %; Patterson and Watkinson, 1984a, b). Patterson and Watkinson (1984a, b) concluded that deformation and metamorphism at the Thierry Mine modified the uneconomical, primary magmatic sulphides to a copper rich, ore grade assemblage.

The PGEs within the Thierry mine are enriched in bismuth tellurides with palladium values elevated relative to platinum (Patterson, 1980; Patterson and

Watkinson, 1984b; Curtis, 2001). The PGE grades were found to be structurally controlled with a positive correlation to higher nickel, copper and cobalt values and a strong correlation between palladium and nickel (WGM, 1991 reference in Curtis, 2001). Within the mine sequence there is a chert-magnetite iron formation (Curtis, 2001 and references within). This sedimentary horizon may have acted as a zone of weakness allowing the intrusion of the mafic to ultramafic body and the subsequent shearing and remobilization of the mineralization within the Thierry mine (Patterson, 1980; Curtis, 2001).

2.2.4 Lake St. Joseph Greenstone Belt

The Lake St. Joseph greenstone belt is composed of three assemblages, the Confederation assemblage, the St. Joseph assemblage and the Eagle Island assemblage. (Figure 2.8). The Confederation assemblage is a continuation of the Confederation assemblage of the Birch-Uchi greenstone belt (Stott, 1996). Within the Lake St. Joseph greenstone belt the Confederation assemblage consists of two volcanic cycles (Cycle I and Cycle III) that are separated by a volcanic cycle of the St. Joseph (Cycle II) assemblage (Stott, 1996). The similarities in geochemistry of the mafic and felsic units in Cycle I and III imply that they have been tectonically shuffled out of sequence. Cycle III has been tectonically separated and thrust-stacked on to the top of Cycle II (Stott, 1996). The Confederation assemblage volcanic cycles are composed of basaltic flows with overlying dacitic to rhyolitic pyroclastic rocks with comparable geochemical signatures and ages (2733 +3/-2 Ma and 2730±1 Ma, Corfu and Stott, 1993b; Stott, 1996).

The Eagle Island assemblage is a volumetrically minor assemblage located in the western part of Lake St. Joseph belt, near Eagle Island. The assemblage is composed of clastic and chemical sedimentary rocks that unconformable overly the Confederation and St. Joseph assemblages. The assemblage is interpreted as a submarine fan and contains numerous well preserved sedimentary structures.

The St. Joseph assemblage (Cycle II and IV) is the youngest assemblage in the Uchi subprovince (2730±1 Ma, 2737+5/-4 Ma and 2733+3/-2 Ma; Corfu and Stott, 1993b). It is composed of tholeiitic basalt and calc-alkalic andesite, dacite and rhyolite most prominently exposed in the vicinity of Lake St. Joseph and the southern half of the Miminiska-Fort Hope greenstone belt (Figure 2.5; Stott and Corfu, 1991). The base of the assemblage is composed of basaltic flows, which is overlain by a thick layer of rhyolitic to dacitic pyroclastic deposits (Stott, 1996).

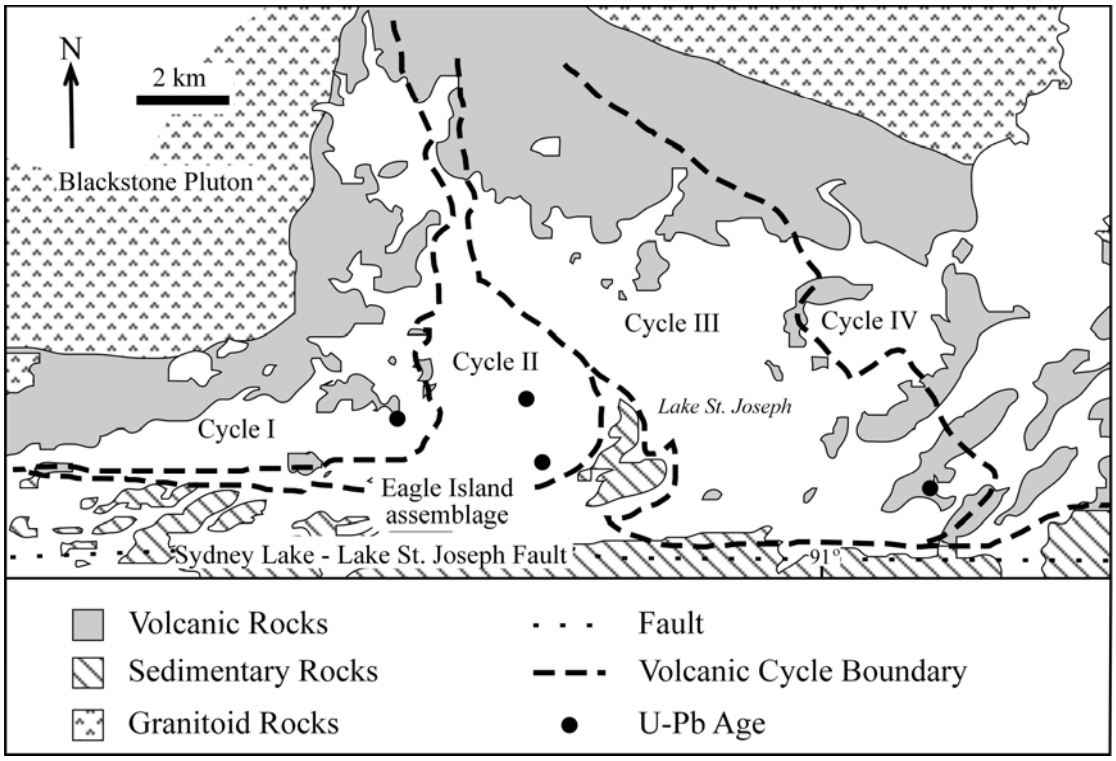

Figure 2.8: Simplified geology of the Lake St. Joseph greenstone belt, U-Pb age determination sample locations (modified after Corfu and Stott, 1993b).

CHAPTER 3

Geological Mapping

3.1 Introduction

A reconnaissance mapping project, covering approximately 30 km^2, was carried out in 2003 and 2004. Access in the area is poor despite the presence of numerous rivers. Low water levels, low topographic relief, beaver activity and numerous areas of muskeg restricted movement through the map area. Access to the area is restricted to float planes on the deeper and large bodies of water, or by helicopter. Outcrop exposure within the study area was generally poor and concentrated in east-west trending ridges. In order to further understand the geology of the region, drill core abandoned by previous exploration programs because of the prohibitive costs of flying it out, was re-examined (Figure 3.1). Drill hole locations were obtained from the assessment files of the Ministry of Northern Development and Mines.

Since the 1970's numerous companies have undertaken fieldwork in the Norton Lake region; the following is a summary of their findings and results. In 1970 Questor Surveys flew an INPUT Mark V airborne survey for Union Mineral Exploration (UMEX) and Imperial Oil (joint venture) that was followed up by a limited ground exploration program consisting of three 'winky' (a man portable diamond drill) drill holes (Hill, 1981a). Work in the area was continued by UMEX & Imperial Oil (1970 - 1972), but no

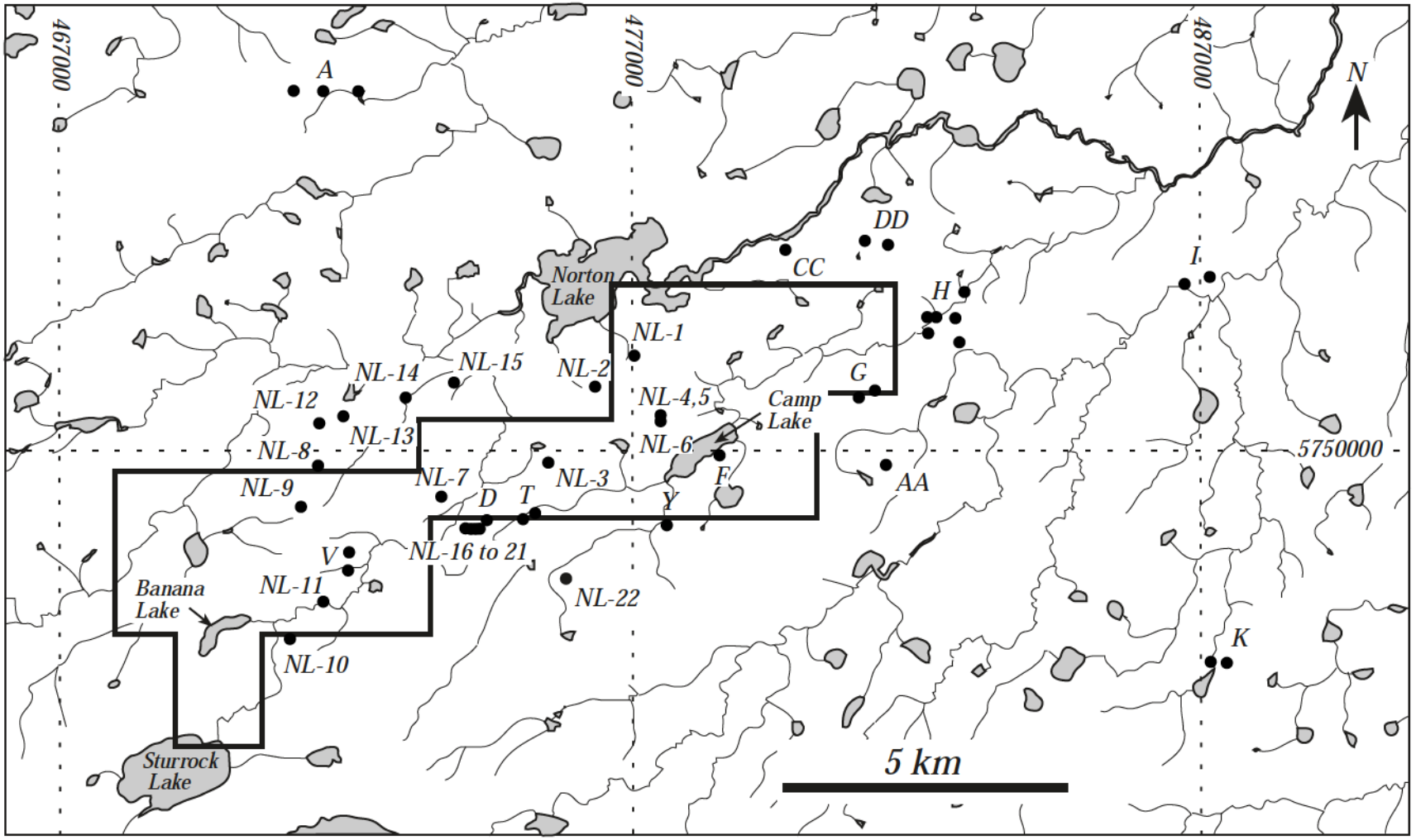

Figure 3.1: Location of Locator Ltd. (NL-##) and Wasabi Resources Ltd. (single letter) diamond drill holes. Outline of study area mapped shown.

record was filed with the Ontario Department of Mines and Northern Affairs, now the Ministry of Northern Development and Mines. No further exploration was undertaken in the area until Wasabi Resources Ltd. conducted a large scale exploration program from January 1980 to October 1981 that consisted of geophysical surveys, geological mapping, geochemical soil sampling and diamond drilling. Following up on the results of Wasabi Resources Ltd.'s exploration program, additional diamond drilling was undertaken by Locator Exploration Ltd./Duration Minerals Ltd. in 1988, while Joutel Resources Ltd. completed additional ground geophysics in 1990. East West Resource Corporation began exploration in 2000, continuing to present, involving ground and airborne geophysics, soil sampling, and diamond drilling.

3.2.1 Summary of Field Mapping

The map area is dominated by massive to pillowed basalts with occasional sedimentary layers and pyroxenitic/gabbroic bodies (Figure 3.2). A large antiformal fold with an east plunging axis dominates the area. There is an overall east-west trend to the lineations within the area that is expressed on topographic maps and aerial photographs of the region, consistent with the observations of Thurston and Carter (1970) and Hill (1981a, 1981b).

Outcrop exposure tends to be restricted to low, poorly exposed hummocks and ridges that parallel the regional lineations and are often separated by swampy topographic lows. Relief in the area is low, averaging 1 – 5 m, resulting in little outcrop exposure (approximately 2 to 5 %).

In the southern portion of the map area lineation planes and bedding tend to dip

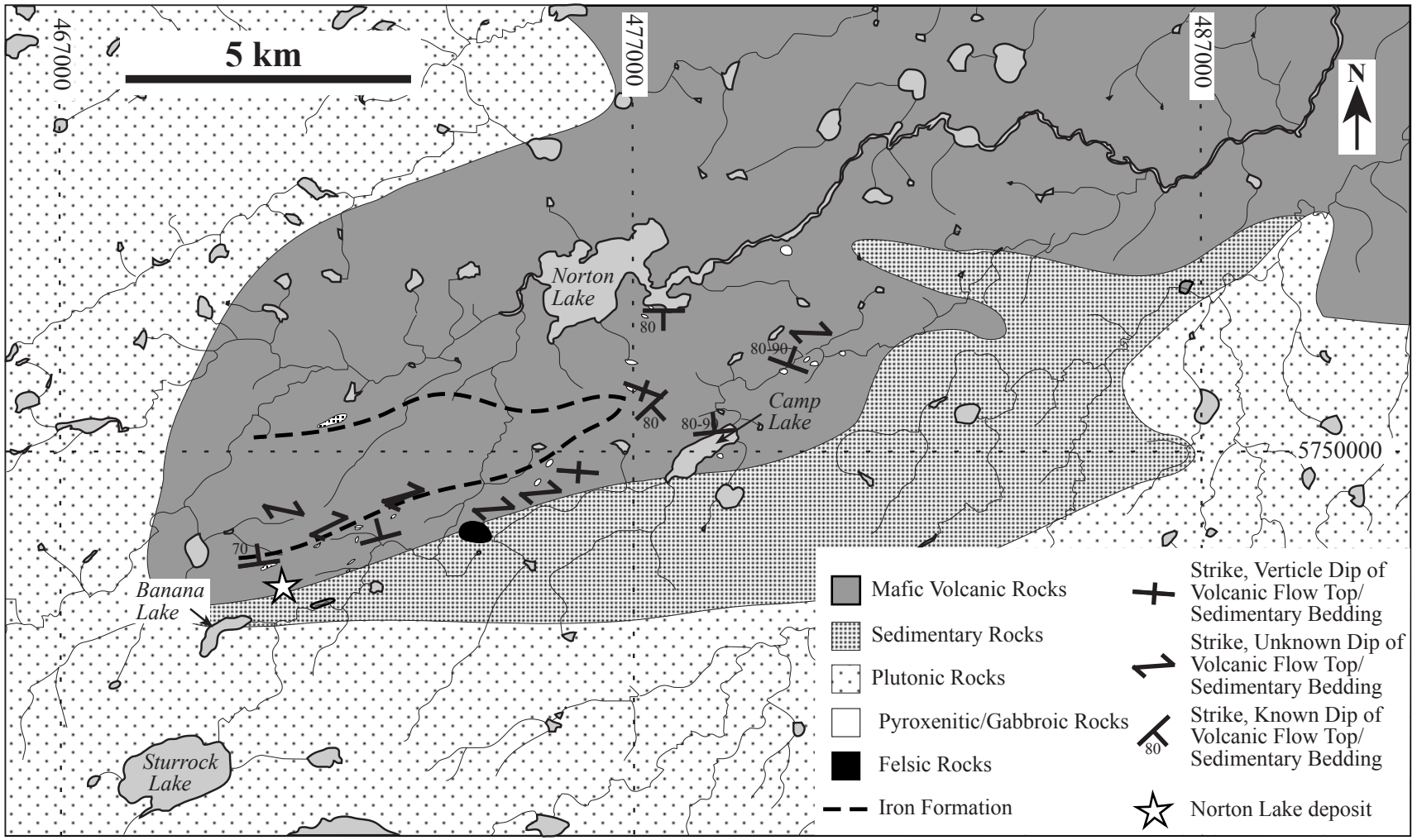

Figure 3.2: Geolological compilation map of the Norton Lake region based on mapping of surficial geology (this study; Thurston and Carter, 1970), and use of diamond drill logs. Pyroxenite/gabbroic, sedimentary, and felsic units shown are smaller than illustrated, exageration is for clarity.

steeply to sub-vertically north. North of the synclinal fold axis (as interpreted from aeromagnetic data) the dips change to steeply south and sub-vertically north. Foliation and pillow top determinations parallel the structure of the interpreted fold nose. Sedimentary units are uncommon and poorly exposed within the area. Numerous poorly exposed pyroxenitic/gabbroic outcrops were noted throughout the mapped area.

3.2.2 Mafic Volcanic Rocks

The mafic volcanic rocks in the area are pillowed, massive to foliated with rare volcaniclastic units present. In outcrop, pillows generally varied in size from 0.2 – 0.8 m, only rarely exceeding 1 m. The classic pillow shape is rarely preserved in outcrop with the majority of outcrops deformed, making top determinations impossible. Furthermore it is difficult to differentiate potential pillows from potential flow-top breccias (Figure 3.3C). Amygdaloidal pillows were rare but were most frequently encountered northeast of Camp Lake (Figure 3.2).

The outcrops of mafic volcanic rocks vary from light grey/green (Figure 3.3B) to nearly black (Figure 3.3D) on weathered surfaces depending on composition and degree of glacial polishing. Samples are commonly aphanitic to fine-grained but can be medium to coarse-grained with euhedral pyroxenes. Quartz ± carbonate veining commonly occurs in outcrop but varies in amount. In rare locations pink feldspar and quartz phenocrysts or breccia clasts were identified. Phenocryst vary in size from 0.3 – 5.0 cm while clasts are larger in size, varying from 6 – 18 cm. The volcanics are variably altered, varying from relatively pristine samples to samples that have undergone strong to weak chloritization with variable amounts of silicification and occasional carbonatization.

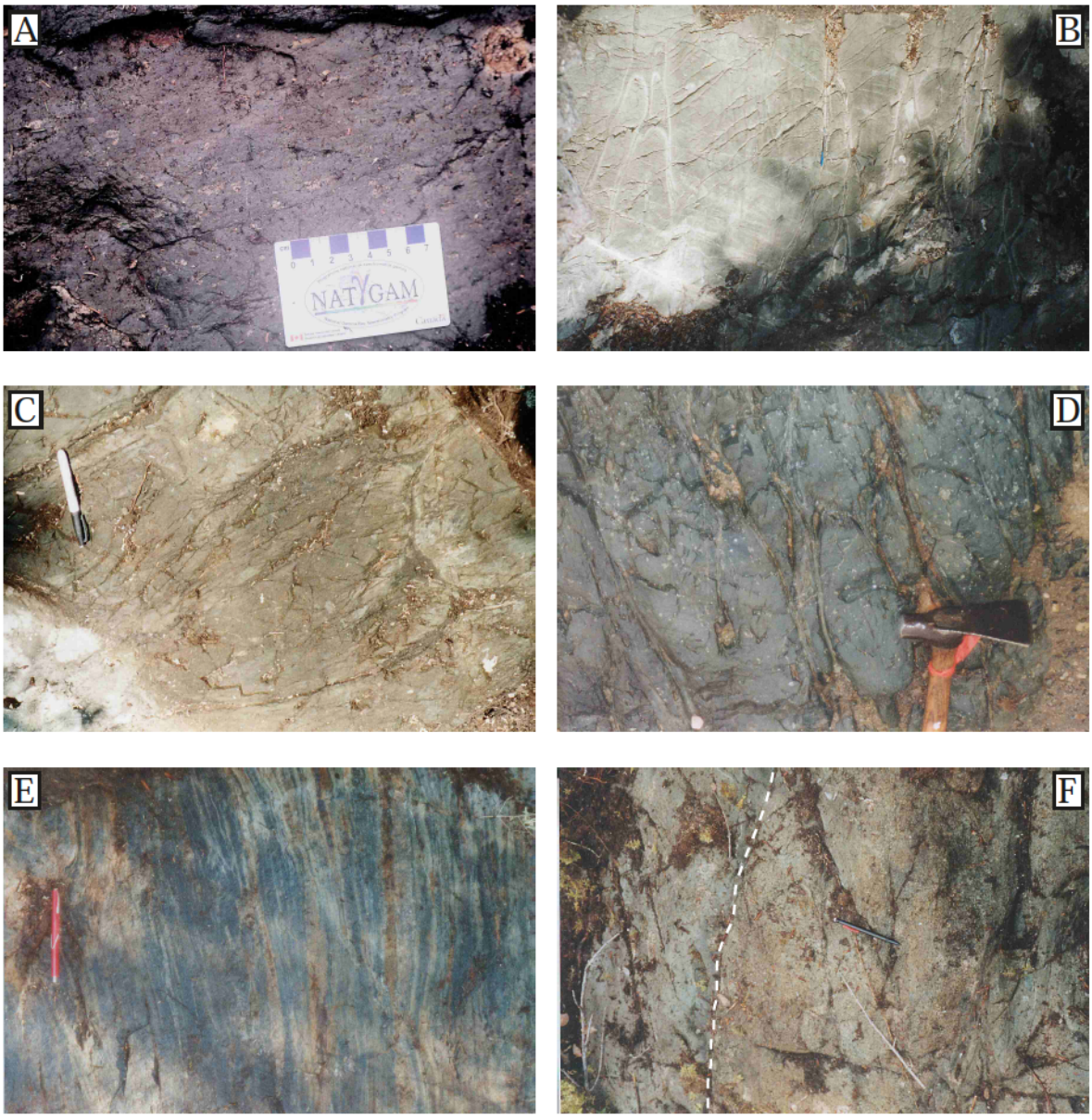

Figure 3.3: Photographs of outcrop exposure within Norton Lake region. A) feldspar phenocrysts within mafic flow, B) stretched pillows (select pillows outline by dashed line), C) strongly sheared pillow basalts, D) amygdaloidal pillow basalts, E) banded iron formation, F) contact (dashed line) between mafic volcanics (left) and sedimentary rocks (right).

Volcaniclastic units were encountered throughout the map area, most notably to the east of Camp Lake and in the area between Camp Lake and Banana Lake (Figure 3.2), and consist of lapilli tuffs. The lapilli tuff units typically contained fragments from 0.5 – 2.0 cm in size with their long axes roughly parallel to the lineation in the area (strike of 80° – 90°). The units found vary in composition from being dominantly clast supported to matrix supported. Rare larger clasts, up to 15 cm, were noted but poor exposure made them difficult to distinguish from selvages of severely deformed and sheared pillowed basalts. The volcaniclastic units were generally found in close proximity to the sedimentary units.

3.2.3 Sedimentary Units

Sedimentary units were uncommon within the mapped area. Due to the scarcity of outcrops and the generally poor exposure none of the units could be laterally traced for more than five metres. Where present the sedimentary units were normally found interbedded within the mafic volcanics with sharp contacts between the two units conformable to the foliation within the area. In rare cases the sedimentary units were found in contact with volcaniclastic units. The sedimentary units varied in thickness from 2 cm to more than 1 m often with one or both contacts inferred.

In addition to the sedimentary rocks and lapilli tuffs (see section 3.2.2), high grade metamorphosed sedimentary rocks were also recognized. Rare biotite gneisses were observed in the field, to the west and northeast of Banana Lake (Figure 3.2). Where present, the gneisses were near or in direct contact with granitic or pyroxenitic intrusions and are interpreted to represent contact metamorphic zones.

3.2.4 Iron Formation

Iron formation was recognized at three locations, all located to the north of Banana Lake. The iron formation within the area consists of thin (less than 4 cm) bands of magnetite and sugary quartz with disseminated sulphides and rare, thin (less than 8 mm) sulphide layers (Figure 3.3E). The formations varied in width from 30 cm to 1 m, with their exposure being limited by overburden. The undulating nature of the iron formations' bedding resulted in a variation of up to ±20° in their strike resulting in an overall east-west orientation.

3.2.5 Granite

Two distinct types of granite were encountered within the area. The first crops out on Sturrock Lake and within the southern portion of Banana Lake (Figure 3.2). This granite consists of coarse crystals (up to 25 mm) of quartz, feldspar, muscovite and biotite. The second type of granite is located to the west of Banana Lake and south of the Norton Lake deposit where it is in contact with a biotite gneiss. Here the granites are pegmatoidal, consisting of coarse crystals (up to 45mm) of quartz, pink feldspar and biotite, with large crystals of labradorite noted in the western occurrence. Samples of the second granite are similar to samples of pegmatitic granites encountered within drill holes at the Norton Lake deposit and likely represent a surface exposure of the same unit.

3.2.6 Gabbroic/Pyroxenitic Units

Numerous outcrops of pyroxenite and occasionally gabbro were identified throughout the area. The majority of outcrops are dark grey to black on surface with

medium to coarse grained pyroxene and amphibole crystals visible. Fresh surfaces revealed the crystals to be randomly orientated with rare samples containing a distinct foliation. Due to differential weathering and alteration, grain size noted on the weathered surface was not always consistent with the grains size observed on a fresh surface. The units could only be traced for 10 – 15 m due to poor exposure making it difficult to determine if the outcrops are a series of discrete lenses or if they are part of a larger series of sills and dykes. Examination of airborne and ground geophysics available (Hill, 1981a; Hill 1981b; East West Resource Corporation internal files, 2004) does not reveal a lateral continuance of the geophysical characteristics of the units, suggesting the units are lenses and pods, ranging from 10 – 200 m in diameter, rather than continuous planar sills or dykes. In addition, the ultramafic intrusion hosting the Norton Lake deposit is considered to be a pyroxenite lens of limited strike length based on current delineation by drilling (East West Resource Corporation, 2004).

3.2.8 Structure

The general structure of the Norton Lake area is readily visible on airborne geophysical maps. A magnetic anomaly suggests the presence of a west opening syncline fold to the north of the Norton Lake deposit with several additional fold noses seen expressed further to the east. These folds are highlighted on the total field magnetic airborne geophysics (East West Resource Corporation internal report, 2004) by the iron formation within them. Mapping indicates that the folds are overturned synclines.

Strike and dip determinations of sedimentary beds and volcanic flow tops indicate a general east-west strike (075° – 095°) with a steep (70° to vertical) north dip (Figure

3.4). The strike of the flow tops and bedding change as the nose of the fold is reached, rotating to parallel the structure of the fold nose. The dip of the rocks changes from 70° north to vertical along the southern limb of the fold to 80° south to vertical in the northern limb once the interpreted axis of the fold is crossed.

There are numerous pillowed outcrops throughout the area; unfortunately top determination was only possible at a select few locations. Pillow top determinations are in agreement except within an area about 1.5 km west of Camp Lake, south of the interpreted fold nose (Figure 3.4). Within the space of approximately 200 m, a reversal of pillow top directions occurs. The reversal can be explained by the change in dip of the rocks at this location. The flows within this area are vertical in orientation. A small increase in the rotation of the units would result in an overturning of the flows, giving top determinations to the south. It should be noted that the south facing pillows have been mildly deformed and stretched.

3.3 Petrography

Mafic rocks (basaltic to andesitic in composition) examined in thin section are fine grained and have low quartz and plagioclase contents (5 - 20 % combined) with pyroxenes and amphiboles, in various stages of alteration, being the dominant minerals. The samples have undergone strong to weak chloritization, carbonatization, silicification and talc/tremolite replacement of the ferromagnesium minerals. Several thin sections examined had indications of shearing, indicated by the lineation of minerals and rare pressure shadows.

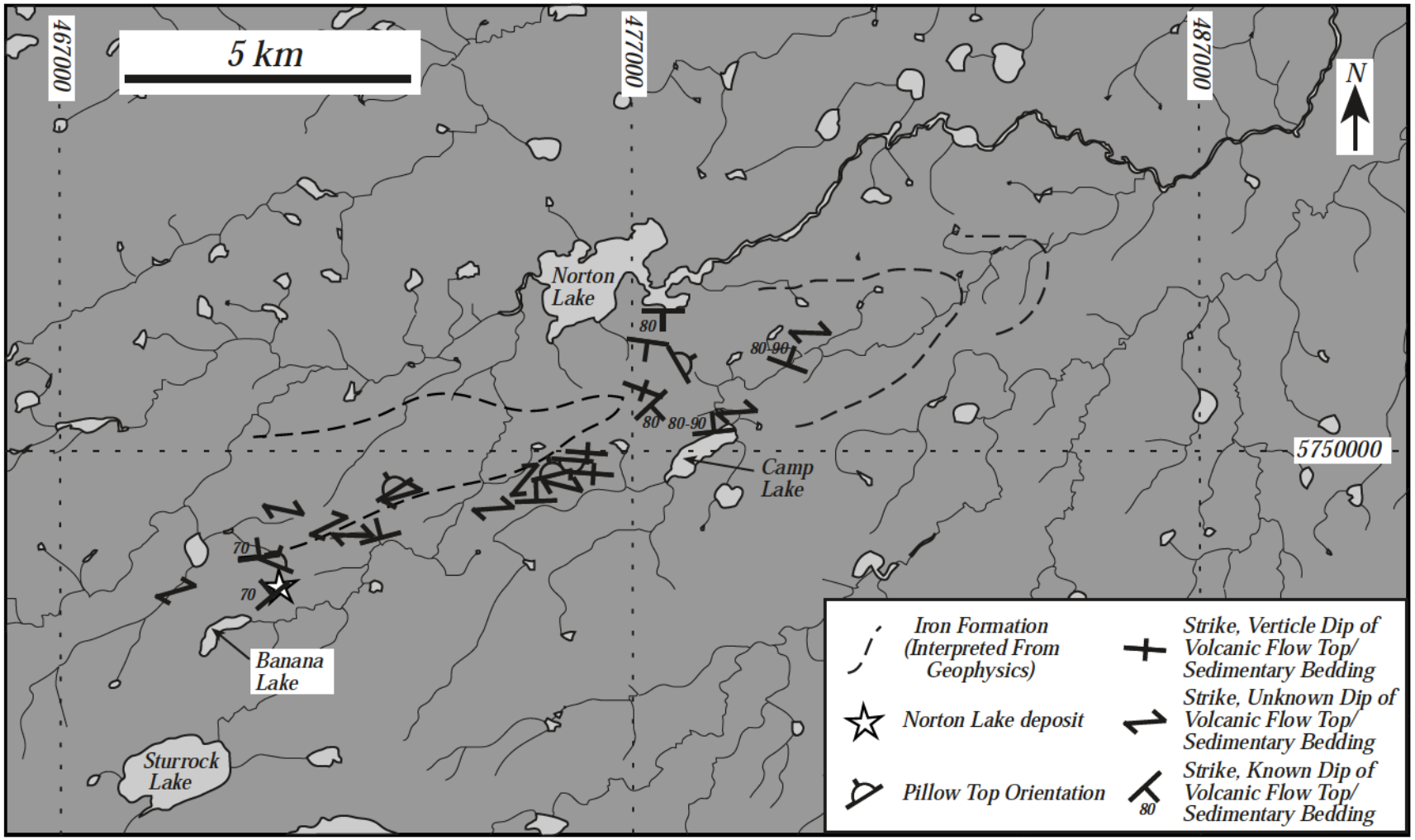

Figure 3.4: Summary of structural features identified during mapping.

In thin section the gneiss samples examined had a strong mineral lineation. They consisted of interlocking grains of quartz (60-70%) and biotite (40-30%) with trace amounts of chlorite.

The pyroxenites examined were medium to coarse grained and highly variable in composition with a range of 70 – 90 % combined pyroxene and amphibole, 0 – 20 % plagioclase, 0 – 20 % quartz, 5 – 15 % opaque minerals (pyrite, pyrrhotite and magnetite), and 0 – 5 % biotite. In general, samples were severely to moderately altered with the majority of the samples having near total replacement of pyroxene by amphibole.

3.4 Summary

The division of the region into distinct lithological units is difficult due to the absence of laterally continuous outcrops and the lack of distinct marker horizons. The following summary is based on available outcrop exposure, examination of diamond drill core left in the region by Wasabi Resources Ltd., Locator Resources Ltd. and the available government data.

The mafic volcanics of the region, consisting of pillowed to massive basalts, are the dominant rock type within the study area. Interspersed within the volcanics are rare sedimentary beds of undetermined thickness and extent as well as numerous small intrusions of pyroxenites and gabbros. The intrusions are interpreted to be small pods or lenses that vary in size from four to five metres to less than four hundred metres, based on outcrop exposure, interpretation of geophysics and examination of the Norton Lake deposit host ultramafic unit.

A thick sedimentary unit is interpreted to the south and east of the volcanic unit based on limited outcrop exposure found during geological mapping (this study; Thurston and Carter, 1970), geophysics and limited diamond drill holes (Wasabi Resources Ltd and Locator Resources Ltd.). The contact between the sedimentary unit and the mafic volcanics has not been observed in outcrop. The sedimentary unit is cross cut by occasional granitic dikes and has interbedded mafic volcanics (encountered in drill core and rare outcrop exposure). The sedimentary rocks observed in the abandoned drill core and outcrop consist of low grade argillites and sandstones with rare gneiss units. Poor outcrop exposure and limited diamond drill coverage makes it impossible to determine whether the gneisses represent localized changes in metamorphic grade due to the presence of granitic or mafic to ultramafic intrusions, or if they are the result of a large scale change in metamorphic or geological conditions.

CHAPTER 4

Whole Rock and Radiogenic Isotope Geochemistry

4.1 Introduction

A geochemical study of the rocks within the northern part of the Miminiska-Fort Hope Greenstone Belt (MFGB) was undertaken to evaluate the tectonic setting in which the rocks formed, and to investigate potential geochemical correlations with other assemblages in greenstone belts to the west-southwest that have previously only been correlated based on geophysical data. A suite of samples was selected from those collected during regional mapping of the area and from the drill core abandoned in the area. Thirty least altered samples (defined as samples with less than 5 vol% of alteration minerals and no observed carbonate minerals or serpentine) were selected on the basis of location, to ensure coverage of the widest area (Figure 4.1). The selected samples were analyzed at the University of Saskatchewan by Inductively Coupled Plasma Emission Mass Spectrometer (ICP-MS) and at XRAL labs by X-ray fluorescence (XRF) to determine the trace and major elements, respectively (see Section 1.2.1 for detection limits and detailed methodologies). The samples were separated into three suites on the basis of their rare earth element (REE) patterns and characteristics (see Section 4.2.2). A subset of eight samples, spanning the three suites, was sent to Carleton University for analysis of rubidium, strontium, neodymium and samarium isotopes. The data set was

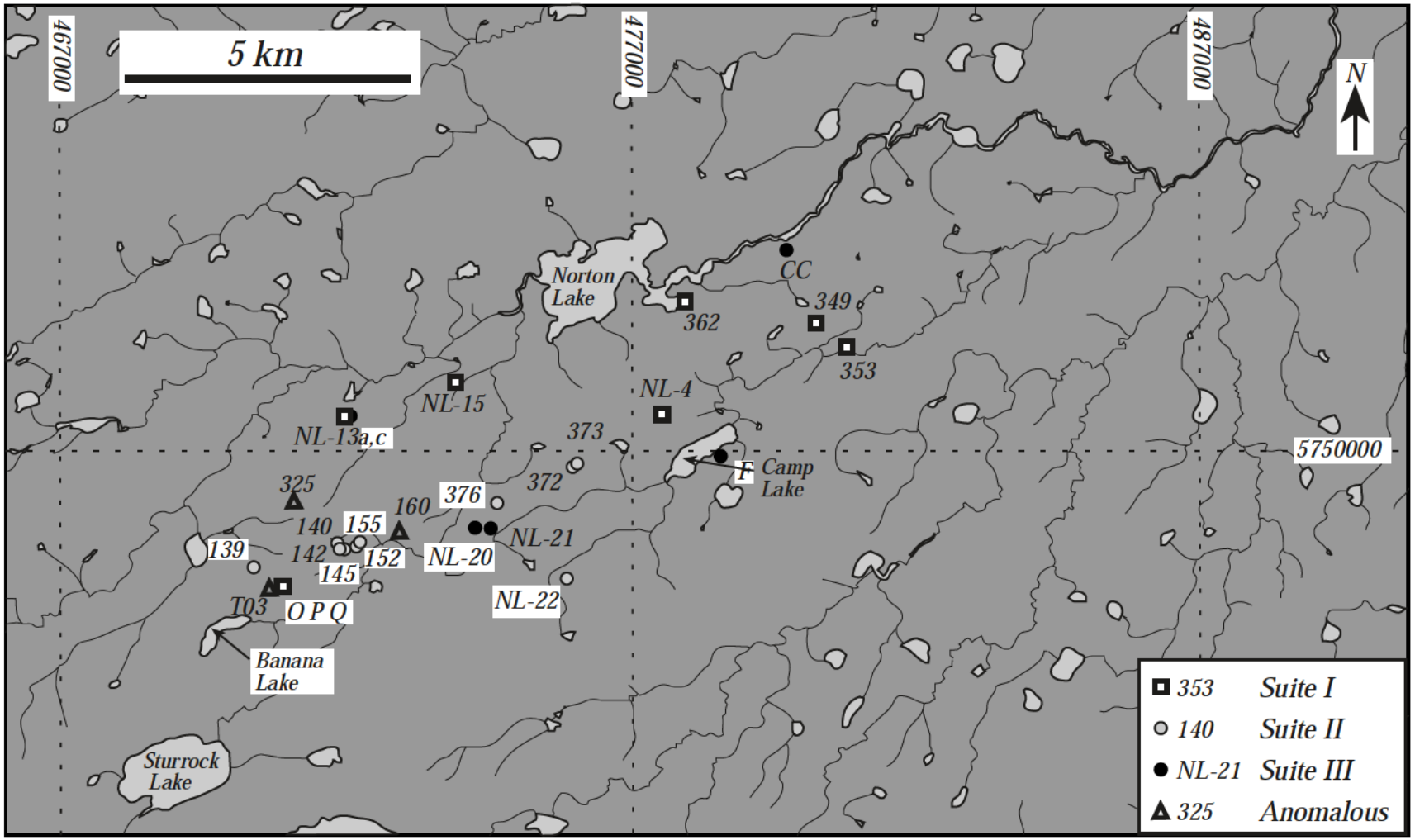

Figure 4.1: Samples selected for whole rock geochemistry and radiogenic isotope analysis within the Norton Lake area.

supplemented with whole rock and select trace elements (analyses by ALS Chemex, see Section 1.2.6 for details) from East West Resource Corporation, confined to samples of drill core from near the mineralized zone (see Appendix B for data).

4.2.1 Whole Rock and Rare Earth Element Geochemistry of the Norton Lake Area

There has been limited geochemical work done within the MFGB. Prior to this study, geochemical data was limited to major element analyses of samples collected as part of the government mapping programs (refer to Figure 2.3 for limits of government mapping; Thurston and Carter, 1970; Wallace, 1978; Wallace, 1981a, b). Additional whole rock analyses were conducted by East West Resource Corporation but this was restricted to the area surrounding the Norton Lake deposit, with only the major elements and select trace elements determined. Geochemical data from East West Resource Corporation confirmed the petrographic classifications of drill core and outcrop exposure, supporting the presence of mafic rocks (basalt to andesites), and ultramafic rocks including possible komatiites identified during field work undertaken by East West Resource Corporation field work (J. Halle, personal communication 2002; Figure 4.2).

Samples used for this study cover an area of approximately twelve kilometres by six kilometres (Figure 4.1). The high concentration of samples around the Norton Lake deposit reflects the focus of the first mapping season.

In the Uchi Subprovince rocks have undergone varying degrees of alteration and greenschist to amphibolite facies metamorphism. It is widely considered that aluminium, titanium, the high field strength elements (HFSE; thorium, niobium, tantalum, zircon and hafnium), the rare earth elements (REE; except cerium and europium), yttrium, scandium

and vanadium are the least susceptible to disturbance by alteration and metamorphism, while calcium, sodium, potassium, and barium are recognized as mobile (Ludden et al., 1982; Lafleche et al., 1992; Jochum et al., 1991; Arndt, 1994; Pearce, 1996). Figure 4.3 illustrates a greater range of values for the mobile elements (calcium, sodium and potassium) within individual suites than the immobile elements (lanthanum, niobium and thorium). The high detection limits for the EWR data (see Appendix B) gives the false impression of scatter. This is illustrated by lanthanum values (Figure 4.3) where much of the analyses are clustered around the detection limit of 5 or 10 ppm, dependant on the method of analyses used (see Appendix B).

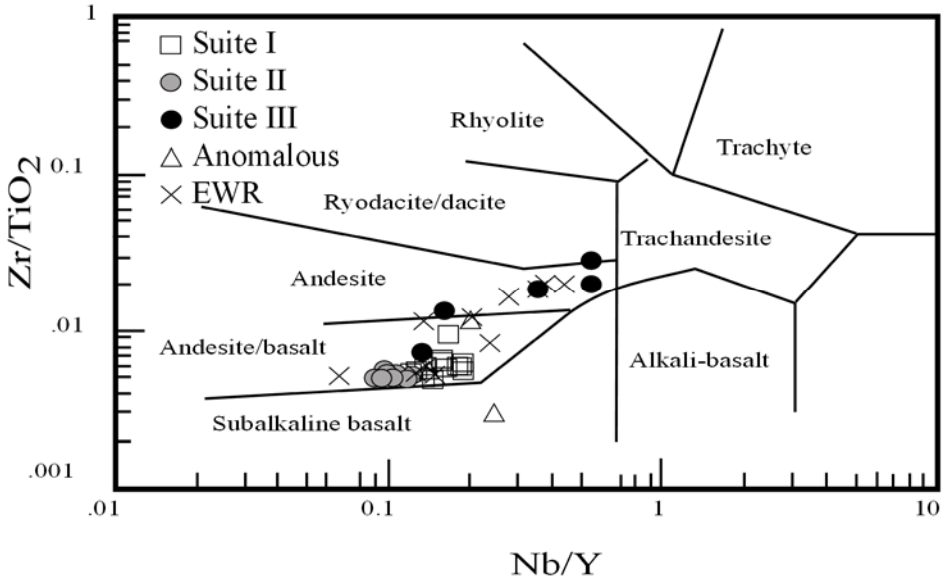

Figure 4.2: Discrimination diagram for whole rock analysis with additional data from East West Resource Corporation. After Winchester and Floyd (1977).

All samples used for this study have been metamorphosed to a minimum of greenschist facies. To minimise the effect of alteration on the analyses and interpretations the generally immobile major elements (MgO, Al_2O_3 and TiO_2),

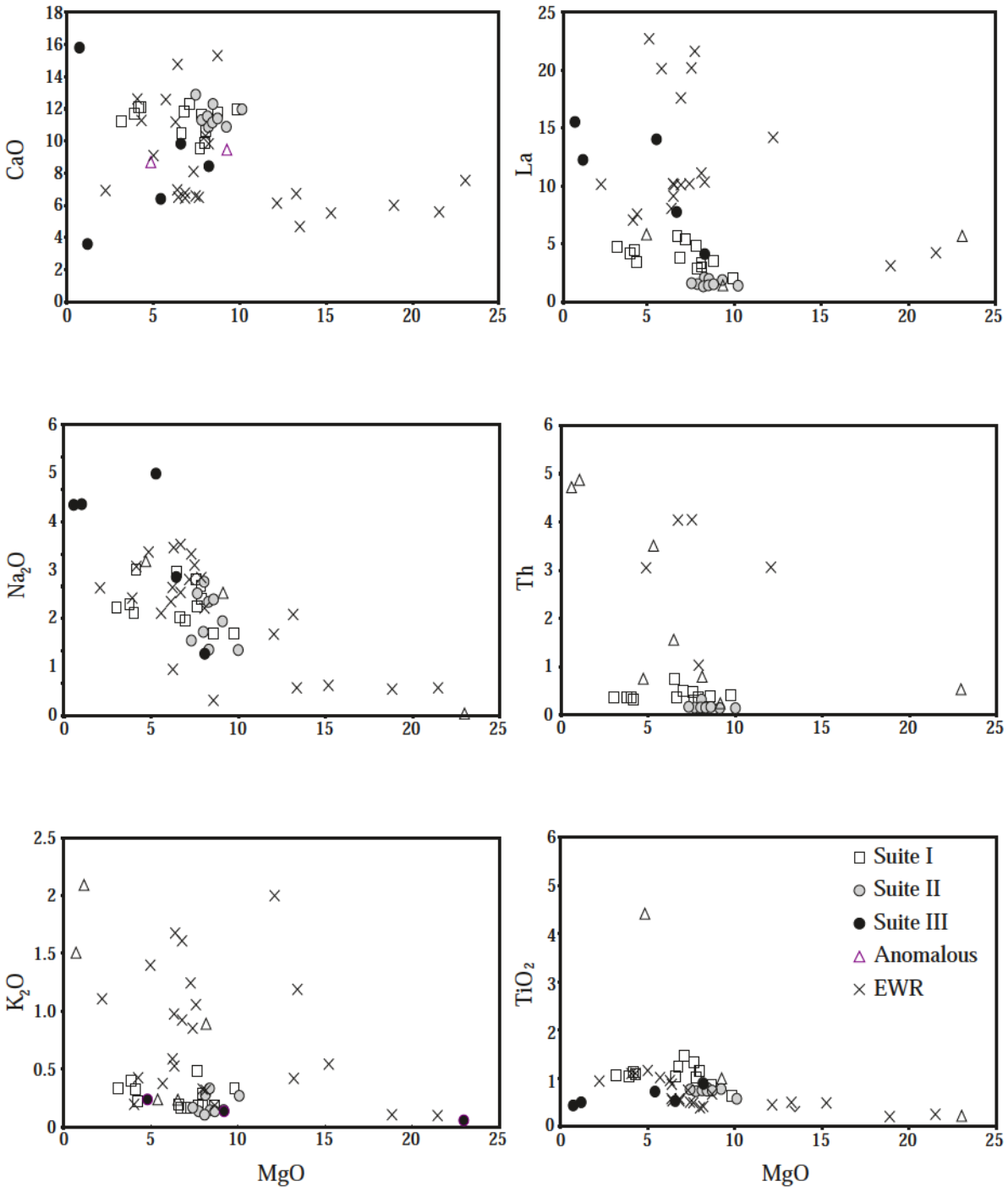

Figure 4.3: MgO vs mobile (left) and immobile (right) elements, oxides in wt%, elements in ppm. EWR-East West Resource Corporation data, see Appendix B.

incompatible trace elements (nickel and chromium), HFSE and REE are used (Ludden et al., 1982; Lafleche et al., 1992; Jochum et al., 1991; Arndt, 1994; Pearce, 1996). Sodium and potassium, typically used for the distinction between tholeiitic and calc-alkaline volcanic rocks, are avoided in favour of using trace element data for classification. Elevated La/Sm_{cn} ratios (greater than 2) combined with negative HFSE anomalies are characteristics generally associated with calc-alkaline rocks, while tholeiites will typically display flat LREE signatures that lack any significant HFSE anomalies (Hollings, 1998).

4.2.2 Results

The multi-element patterns of the thirty samples analyzed have been used to identify three suites as well as a small number of anomalous samples that do not fit any of these suites (Figure 4.4). The samples were grouped into suites on the basis of similarities in REE patterns (see Table 4.1 for summary of characteristics).

Suite I consists of thirteen samples of which four are surface samples and the remainder are taken from drill core. The samples consist of tholeiitic basalts to andesites (Figure 4.2). Samples, in general, have low loss on ignitions (0.2 to 2.5 wt%) with two samples, H5a and H5b, having higher loss on ignition values of 7.5 wt% and 8.4 wt% respectively. These two samples are included within the suite despite their high loss on ignition because they display coherent, smooth REE plots that are consistent with the other samples of Suite I. Alteration effects would likely have resulted in light rare earth element (LREE) depletion and a jagged, irregular REE plot (Jenner, 1996; Kerrich and Wyman, 1996). In addition, thin section examination did not reveal any change in the

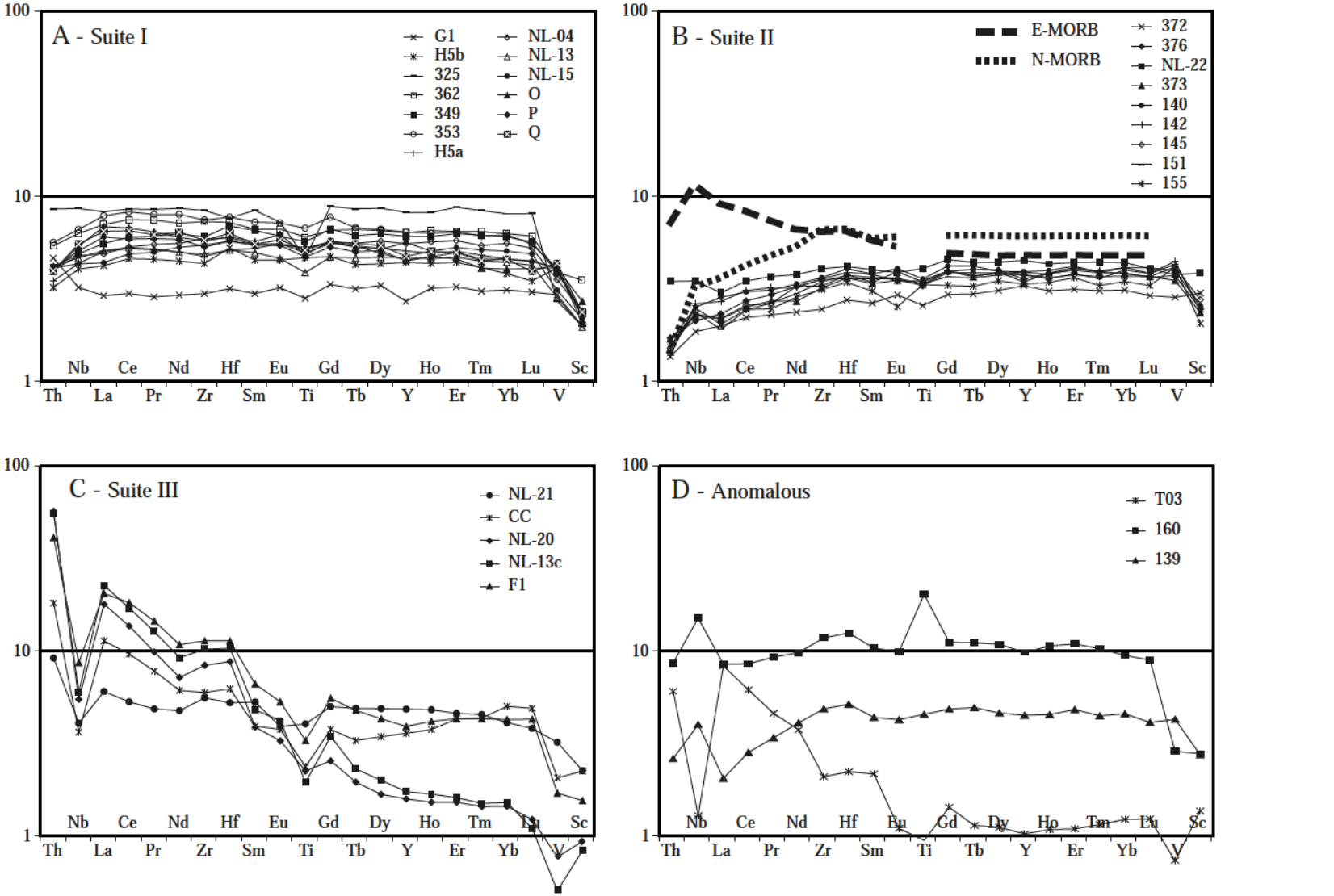
A - Suite I
G1
H5b
325
362
349
353
H5a
NL-04
NL-13
NL-15
O
P
Q
B - Suite II
E-MORB
N-MORB
372
376
NL-22
373
140
142
145
151
155
C - Suite III
NL-21
CC
NL-20
NL-13c
F1
D - Anomalous
T03
160
139
100
10
1
Th La Pr Zr Sm Ti Tb Y Er Yb V
Nb Ce Nd Hf Eu Gd Dy Ho Tm Lu Sc

(continued)

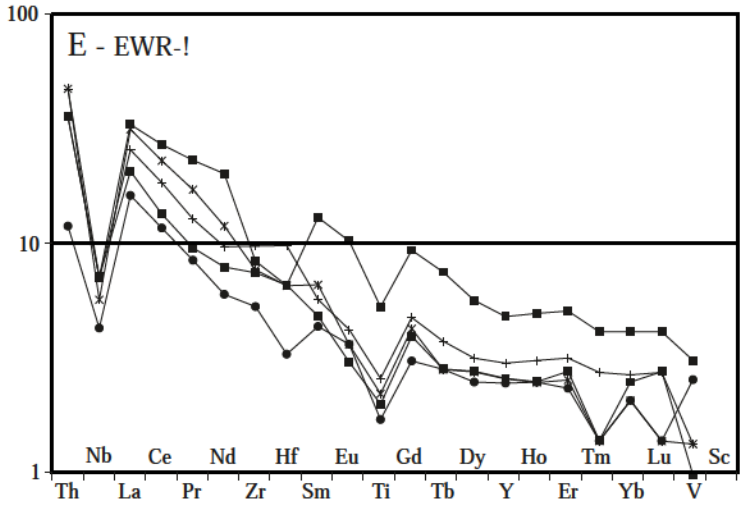

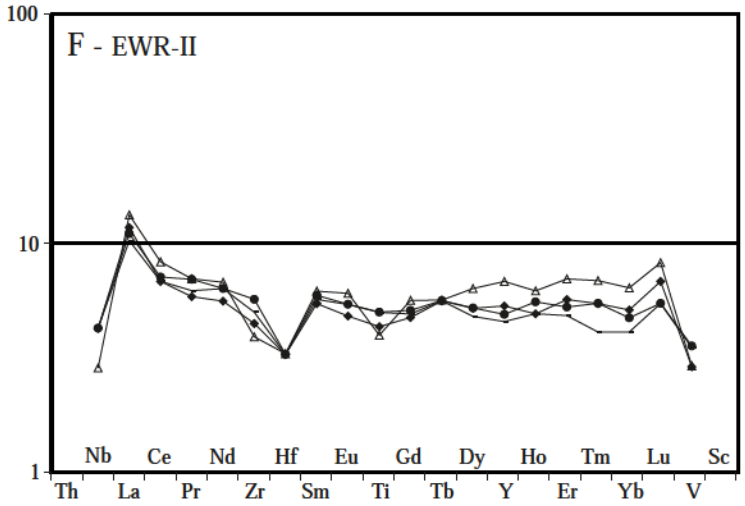

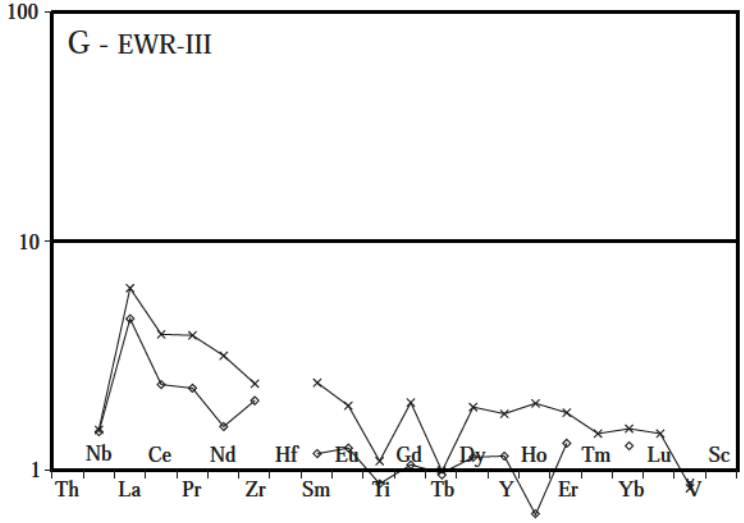

Figure 4.4: Primitive mantle normalized diagram for samples, A) Suite I, B) Suite II, C) Suite III, D) Anomalous Samples, E) EWR-I, F) EWR-II, and G) EWR-III. Stippled area on A represents Ontong Java plateau data from Mahoney et al. (1993), E-MORB and N-MORB from Sun and McDonough (1989). Normalization values from McDonough and Sun (1995).

Table 4.1: Summary of geochemical characteristics of samples. Values are in wt%.

Sample	Suite I	Suite II	Suite IIIa	Suite IIIb	EWR-I	EWR-II	EWR-III
SiO2	45.2 - 56.0	48.3 - 49.9	60.4, 68.9	50.6 - 58.1	52.2 - 53.9	45.5 - 53.8	47.1, 45.5
MgO	3.1 - 9.8	7.4 - 10.1	0.7, 1.1	5.4 - 8.1	5.0 - 12.1	4.0 - 6.3	18.9, 21.5
Ni	116 - 187	164 - 296	18, 24	90 - 159	116 - 401	151 - 206	940, 1238
Cr	311 - 469	353 - 445	62, 106	158 - 464	334 - 751	294 - 414	653, 1299
Co	50 - 70	60 - 70	12, 14	38 - 58	29 - 48	60 - 104	59, 129
La/Sm	0.8 - 1.2	0.5 - 0.8	4.8, 4.7	1.1 - 3.1	2.6 -4.8	1.8 - 2.2	2.6, 3.9
Gd/Yb	1.0 - 1.4	0.9 - 1.0	2.3, 1.8	0.8 - 1.3	1.5 -2.2	0.9 -1.2	0.8, 1.3
Nb/Nb*	0.8 - 1.1	1.0 - 1.6	0.2	0.3 - 0.6	0.1 - 0.2	0.1 - 0.3	0.2

mineralogy or significant presence of carbonate minerals that can indicate mobilization or loss of REE (Wyman, 1999).

SiO_2 contents of Suite I range from 45 to 56 wt% with a range of MgO values that vary from 3 to 10 wt% and Fe_2O_3 values between 8 and 15 wt%. Rocks of Suite I have moderate to high nickel (116 to 187 ppm) and chromium (311 to 469 ppm) values with high cobalt (50 to 70 ppm) values that are characteristic of Archean tholeiites (Nesbitt and Sun, 1976; Arndt, 1991; Lesher and Arndt, 1995).

The Suite I samples have weakly depleted to slightly enriched LREE (La/Sm_{cn} = 0.8 to 1.2) and minor heavy rare earth elements (HREE) fractionation (Gd/Yb_{cn} = 1.0 to 1.4; Figure 4.4A). The samples have niobium anomalies that vary from slightly negative to slightly positive, with Nb/Nb* values ranging from 0.8 to 1.1.

Suite II consists of nine samples, one from drill core and eight from outcrop. The samples are tholeiitic basalts (based on the Nb/Y vs Zr/TiO_2 classification of Winchester and Floyd, 1977; Figure 4.2) and have low loss on ignitions (0.4 to 1.7 wt%). SiO_2 values vary less than 2 wt% (48 to 50 wt%) with MgO values of 7 to 10 wt%. Rocks of Suite II have nickel, chromium and cobalt abundances that are comparable to those of Suite I with nickel ranging from 164 to 296 ppm, chromium varying from 353 to 445 ppm, and cobalt values of 60 to 70 ppm. As with Suite I these values are typical of Archean tholeiites (Nesbitt and Sun, 1976; Arndt, 1991; Lesher and Arndt, 1995). The samples from Suite II are characterized by depleted LREE (La/Sm_{cn} = 0.5 to 0.7) and unfractionated HREE (Gd/Yb_{cn} = 0.9 to 1.0). Suite II samples have flat to positive Nb anomalies with Nb/Nb* ratios of 1.0 to 1.6.

Suite III represents more fractionated rocks, consisting of basalts to dacites. It is divided into two subsets, with the five samples all taken from drill core. Suite IIIa (n = 2) has widely different loss on ignition values with sample NL-13c having 10.4 wt% and sample NL20 having 1.5 wt%. Sample NL-13c, despite its high loss on ignition, has a coherent, smooth REE pattern, which lacks any europium anomaly that closely approximates sample NL20. In addition, values of immobile elements plot near sample NL20 (Figure 4.4C). Suite IIIa samples are classified as calc-alkaline dacites (Figure 4.2) with SiO_2 values of 60 wt% and 68 wt% and correspondingly low MgO values of 0.7 wt% and 1.1 wt%, respectively. Suite IIIa also has dramatically lower Fe_2O_3 values of 2 wt% and 3 wt% compared to an average of 11 wt% for Suite I and 12 wt% for Suite II. Samples from Suite IIIa have much higher Zr/Y ratios (15 and 13) than the other suites with average values of 2.7 for Suite I and 2.2 for Suite II.

Calc-alkaline basalts to dacites (Figure 4.2) of Suite IIIb (n = 3) have low loss on ignitions, ranging from 0.7 to 1.6 wt% with SiO_2 values of 51 to 58 wt% and MgO values of 5 to 8 wt%. All of Suite III samples are strongly enriched in LREE with La/Sm_{cn} ratios of 4.8 and 4.7 for Suite IIIa and 1.1 to 3.1 for Suite IIIb. In addition, all of the samples from Suite III display pronounced negative niobium and titanium anomalies. Suite IIIa samples are characterized by highly fractioned HREE (Gd/Yb_{cn} = 1.8 and 2.3) compared to Suite IIIb's (Gd/Yb_{cn} = 0.8 to 1.3).

Three samples, two from outcrop exposure and one from drill core, cannot be assigned to any of the three suites and are characterized by distinct REE patterns. These samples form the anomalous data set. The loss on ignition of these samples is highly variable with samples 139 and 160, a pyroxenite collected from outcrop, having very low

values consisting of 0.4 wt% and below detection limit respectively. Sample T03, an ultramafic fragment collected from within the mineralized zone, has a moderate loss on ignition value of 4.6 wt%.

Despite careful selection of the portion of T03 to be used for analysis, in order to minimize the possible inclusion of altered host rock, including avoiding any portion near the edge of the fragment or any portion containing veining, sample T03 contained a minor amount of alteration minerals. Examination of T03 revealed the presence of small amounts of serpentine, which may account for its higher loss on ignition value.

Sample 160 has SiO_2 of 46 wt% and MgO of 5 wt%. Sample 139 has a SiO_2 value of 50 wt% and MgO of 9 wt% while sample T03 has SiO_2 of 48 wt% and MgO of 23 wt%. The samples vary from strongly enriched in LREE (T03; $La/Sm_{cn} = 3.9$) to depleted with 139 and 160 having La/Sm_{cn} ratios of 0.5 and 0.8 respectively. The three samples have unfractionated to slightly fractionated HREE ($Gd/Yb_{cn} = 1.1 – 1.2$). Sample 160 displays a pronounced positive titanium and niobium anomaly (Figure 4.4D) that can be attributed to an accumulation of oxides, such as ilmenite, within the rock.

From the East West Resource Corporation data set of twenty-three drill core analyses approximately half of the analysed samples (n = 11) had the necessary trace elements to be classified on REE plots. This discussion focuses on those eleven samples. Due to the lack of control on the sampling, preparation and method of analysis of the East West Resource Corporation samples they are not used to define the characteristics of the suites. Instead they provide additional data that helps to support the existence of the proposed suites.

The analysed samples can be divided into three sample sets. Suite EWR-I is composed of samples of the amphibolite tuff that underlie the Norton Lake deposit, while EWR-II samples consist of mafic rocks taken from various drill core intersections and EWR-III is composed of samples taken from the ultramafic intrusion that is found hosting the mineralization of the Norton Lake deposit. These additional samples can be related to the other suites with EWR-I (n = 5) and EWR-II (n = 4) potentially representing a less evolved, more mafic equivalent of Suite IIIa and IIIb while EWR-III (n = 2) displays characteristics that are similar to the anomalous sample T03.

Geochemically EWR-I comprises calc-alkaline andesites to basalts. SiO_2 values vary from 52 to 59 wt% with corresponding MgO values of 5 to 12 wt%. EWR-II's samples are classified as calc-alkaline basalts with SiO_2 values of 46 to 54 wt% and MgO values between 4 and 6 wt%. EWR-III's two samples are geochemically classified as calc-alkaline basalts (Figure 4.2) with SiO_2 values of 47 wt% and 45 wt% and MgO values of 19 wt% and 22 wt% respectively. Suites for EWR-I and EWR-II have low loss on ignitions (0.7 to 1.4 wt%) while samples from EWR-III have moderate values of 3.5 wt% and 5.2 wt% (comparable to sample T03's value of 4.7).

The samples in EWR-I and EWR-II, like Suite III's samples, are highly to moderately LREE enriched with La/Sm_{cn} ratios of 2.6 to 4.8 for EWR-I and 1.8 to 2.2 for EWR-II. The sample sets have highly variable HREE fractionation, with EWR-I being highly fractionated (Gd/Yb_{cn} = 1.5 to 2.2, comparable to Suite IIIa) while EWR-II has minor to unfractionated HREEs (Gd/Yb_{cn} = 0.9 to 1.2, values comparable to Suite IIIb). There are pronounced niobium anomalies within all of the EWR samples (Nb/Nb* = 0.1 to 0.3; Figure 4.4).

The characteristics of EWR-III's samples are likely the result of the samples being taken proximal to and within the Norton Lake deposit. The samples are enriched in LREE (La/Sm_{cn} = 2.6 and 3.9) with minor to unfractionated HREE (Gd/Yb_{cn} = 0.8 and 1.3), values comparable to anomalous sample T03 (La/Sm_{cn} = 3.9; Gd/Yb_{cn} = 1.2). The mineralized zone is highly deformed and brecciated in addition to having undergone a secondary hydrothermal enrichment stage (see Chapter 5). The irregular saw-tooth REE patterns of these samples combined with the moderate values for the loss on ignitions may be the result of alteration. The irregular pattern may also be due, in part, to the low abundances of the elements. At these levels some of the elements are near or even below the analytical detection limits. It is possible that the EWR-III samples are ultramafic rocks that have been serpentinized to some degree, as has sample T03, but hand samples or thin sections were not available for examination.

4.2.3 Interpretation

To interpret the tectonic settings of Archean volcanic rocks, correlations with modern geological settings can be made. Samples obtained in this study vary from calc-alkaline (Suite III, EWR-I, EWR-II and EWR-III) to tholeiitic (Suites I and II) (Figure 4.5). The tholeiites of Suite I have characteristics similar to samples found throughout the Superior Province that have been attributed to ocean plateaus (Desrochers, et al., 1993; Xie et al, 1991; Hollings et al., 1999) (Figure 4.5). Ratios of Nb/Nb* and La/Yb_{cn} for Suite I fall within Archean plateau and Ontong Java plateau fields as defined in Figure 4.5.

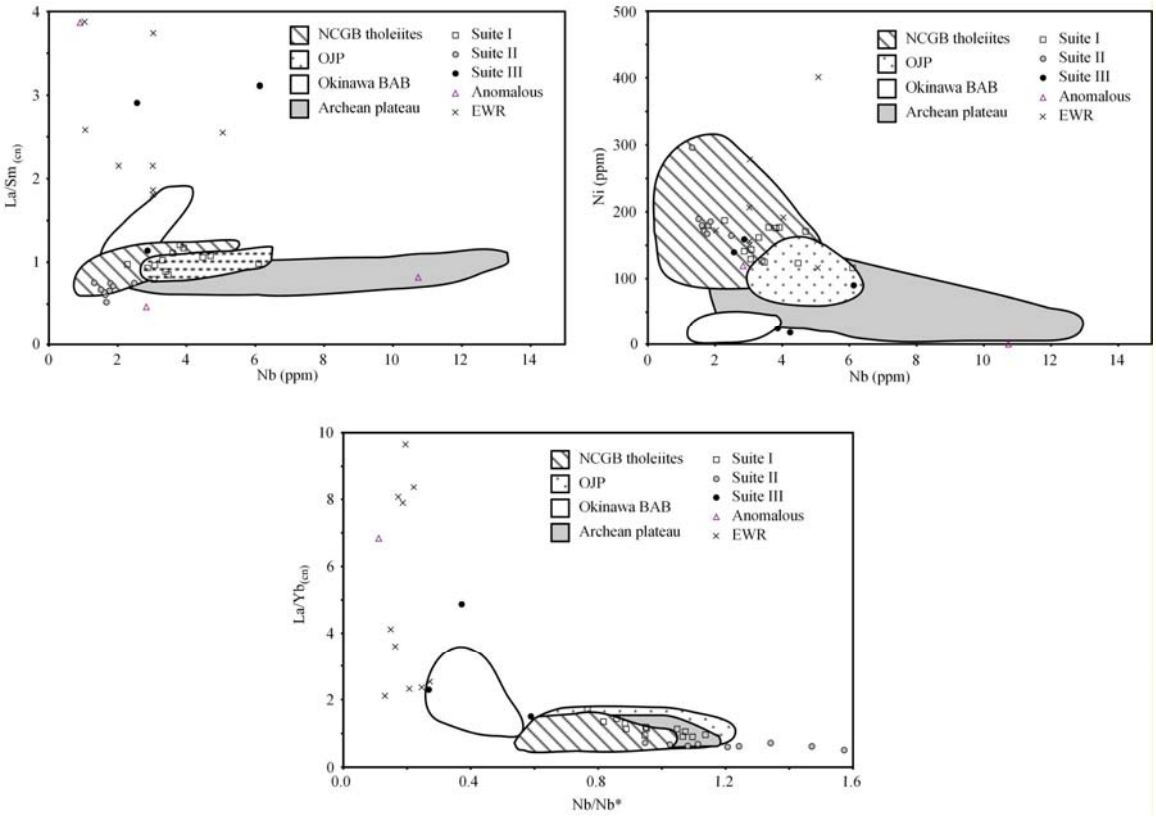

Figure 4.5: Variation plots for samples of the Norton Lake area, East West Resource Corporation (EWR) data is included. Fields are defined as: NCGB- North Caribou greenstone belt (Hollings et al., 2000), OJP-Ontong Java plateau (Mahoney et al., 1993), Okinawa BAB-Okinawa back arc basalts (Shinjo, 1998), Archean plateau (Kerrich et al., 1999).

Comparison of incompatible element ratios, shown in Figure 4.6, shows good correlation between Suite I samples and primitive mantle values. Ocean plateau basalts are thought to be the result of a large degree of melting from high temperature mantle plumes interacting with the upper mantle (Arndt, 1991; Campbell et al., 1989). This relationship has been backed by thermodynamic models and experimental petrology in addition to analogies with post Archean hotspots and plateaus (Storey et al., 1991; Herzberg, 1992; McDonough and Ireland, 1993; Stern et al., 1995; Kerr et al., 1996).

The mantle plume could also account for the komatiites (as these are typically found associated with Archean plateaus; Hollings, 2002) reported by East West Resource Corporation (J. Halle, personal communication 2002) but not seen during the course of this study.

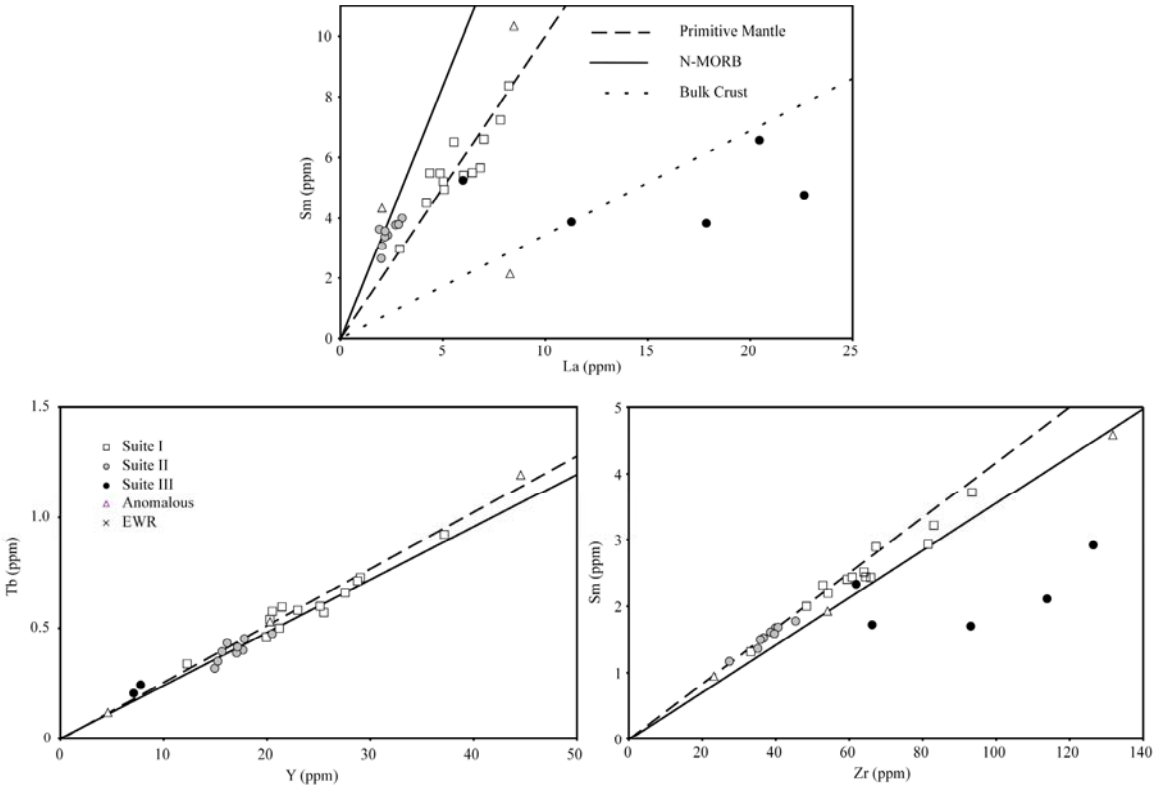

Figure 4.6: Variation diagrams showing incompatible element abundances for samples from this study. Ratios of primitive mantle and bulk crust from Taylor and McLennan (1985) and N-MORB from Sun and McDonough (1989) are shown for comparison. Values are normalized to primitive mantle.

The LREE depletion of the tholeiites from Suite II is similar to that associated with modern N-MORB volcanism (Figure 4.4, 4.5 and 4.6). MOR volcanism is believed to be the result of a large degree partial melting of a depleted mantle source (Stern et al.,

1995). It is important to determine if the samples represent primary compositions or have undergone contamination. To investigate this their LILE/HFSE and LILE/REE ratios were examined. The Th/Nb ratio may be used as a proxy for the LILE/HFSE ratio in greenschist facies basalts because the two elements are considered relatively immobile and the upper continental crust is highly enriched in Th when compared to MORB (Stern et al., 1995). Consequently any contamination by continental crust will produce anomalously high Th/Nb ratios. Modern, uncontaminated N-MORBs have a Th/Nb ratio of less than 0.07 (Saunders et al., 1988; Sun and McDonough, 1989). Suite II's Th/Nb range from 0.06 to 0.12 (average 0.08), values that are slightly enriched and possibly indicating minor contamination by continental crust. A second possibility is that the basalts were produced in an intra-oceanic arc or a back-arc setting (Pearce, 1983; Falloon et al., 1992; Stern et al., 1995). In such instances the sub-arc mantle wedge can develop elevated LILE/HFSE values from the addition of LILEs derived from the subducted slab.

The calc-alkaline samples of Suite III are comparable to volcanic rocks associated with modern subduction-related arc volcanism. The pronounced niobium anomaly combined with LREE enrichment is typical of subduction-related volcanism. Dehydration of the subducted slab results in fluids that are enriched in LILE compared to the HFSE (Pearce and Peate, 1995). The fluids and magma, derived from partial melting of the mantle wedge, mix giving rise to the negative niobium anomaly characteristic of this setting. Two similar but distinct sources can be inferred on the basis of the two subsets. The Suite IIIa rocks likely originated from a deeper source melt than those associated with Suite IIIb, which is reflected by their HREE patterns. Suite IIIa's magma is proposed to have originated at a depth where the partial melting occurred in the

presence of residual garnet (Lesher et al., 1986; Laflèche et al., 1992). The garnet concentrates the HREE relative to LREE resulting in a HREE depleted magma (Lesher et al., 1986; Laflèche et al., 1992). The Suite IIIa samples reflect this partial melting at a high pressure with little to no fractionation during ascent, similar to the source proposed for Lesher et al.'s (1986) FI type volcanics, while Lesher et al.'s (1986) FII volcanics can be interpreted to represent shallower melts similar to Suite IIIb.

The anomalous sample 160 displays pronounced positive niobium and titanium anomalies. These enrichments maybe due to the high abundance, 2 to 5 vol %, of opaque minerals (inferred to be magnetite and ilmenite) compared to the trace abundances, less than 1 vol%, present in other pyroxenites. The REE pattern displayed by sample 160 is similar to those first noted by Wyman (1997) within the Crater Island area of the Flin Flon region. These samples may represent a "sink" or reservoir that contains the upper mantle and/or crust's excess niobium, resulting from the formation of niobium depleted arc volcanism, and believed to exist based on trace element systematics of OIB and E-MORB (Wilson, 1989). Such a source results from the fractionation of niobium rich reservoir from the slab residue within the mantle which is then removed from the subduction zone environment to the deeper mantle. Wyman (1997) speculated that the disruption of a subduction zone during back arc spreading may access this reservoir before it is removed to the deep mantle.

Sample 139 has a very similar REE pattern to Suite I except for its depleted LREE values. Thin section examination of sample 139 indicates the presence of trace amounts of carbonate. The carbonate alteration has likely resulted in the mobilization of the LREE relative to the HFSE and HREE (Wyman, 1997).

The REE patterns of T03 and EWR-III resemble those of Suite III and EWR-I & II but have a more irregular, saw tooth pattern. These samples are from within or are adjacent to the mineralized zone and are thought to have undergone hydrothermal alteration, resulting in the loss of REE. This alteration may account for their overall lower abundances and saw tooth pattern.

4.3 Radiogenic Isotopes

Seven samples, spanning the three suites and the two subsets, in addition to one sample of the anomalous samples were selected for rubidium, strontium, samarium and neodymium radiogenic isotope analysis. An assumed age of 2900 Ma was used to calculate ε_{Nd} for all samples. This is the assumed age of the unnamed assemblage that contains the study area and is based on correlations with tectonic assemblages located to the west.

The rubidium and strontium data obtained are not addressed in this study; only the samarium and neodymium radiogenic isotopes will be used. Rubidium and strontium are relatively mobile elements and may be readily disturbed by the influx of fluids or by a later thermal event (Faure, 1986; Rollinson, 1993).

The ε_{Nd} value can be used to assess crustal contamination and provide additional insight into the possible sources of the volcanism. The ε_{Nd} value for depleted Archean mantle at 2900 Ma is +2.3 (DePaolo, 1981). The positive ε_{Nd} of Suite I rocks (ε_{Nd} = 1.32 – 2.89; Table 4.2) are consistent with them representing melts of Archean mantle that have undergone little to no contamination. Contamination of mantle melts by significantly older crustal material will result in a lower ε_{Nd} values. Older crustal

material has a lower original samarium-neodymium ratio which, when assimilated into a younger melt, results in a lower calculated ε_{Nd}. The absence of contamination in Suite I samples is supported by the trace element chemistry that displays a lack of negative niobium anomalies and LREE enrichment that is typically associated with contamination by older felsic continental crust. Contamination by tholeiites of similar age with similar REE patterns to Suite I cannot be ruled out, as this would not be resolved by these methods.

Table 4.2: Summary of isotope data, see Appendix B for full data set.

Sample	NL13A	P	353	142	155	NL20	CC	160
Suite	I	I	I	II	II	IIIa	IIIb	
$\varepsilon_{Nd\ (2900)}$	2.89	1.51	1.32	0.10	0.10	2.31	-2.49	0.95
T_{dm} (Ma)	2896	3259	3313	436	1563	2939	3501	-1249
$^{87}Rb/^{86}Sr$	0.1718	0.1214	0.0128	0.5548	0.4909	0.6971	0.0714	0.0546
$^{87}Sr/^{86}Sr$	0.7047	0.7086	0.7014	0.7321	0.7184	0.7299	0.7024	0.7033

The calculated T_{dm} values of Suite I are near to slightly older than the 2900 Ma assumed age for the assemblage. The highest value for ε_{Nd} (2.89 for NL13a) correlates closely to the assumed age with a value of 2896 Ma. The slightly lower ε_{Nd} values for samples P and 353 of 1.51 and 1.32 result in older estimated ages of 3259 Ma and 3313 Ma, respectively. It is quite common for samarium-neodymium age determinations to be higher than the assumed or actual age (Smith and Ludden, 1989; Henry et al., 2000). Contamination by upper continental crust, even to a small degree, results in a rotation of the isochrons to a lower intercept, lowering the $^{143}Nd/^{144}Nd$ to a value that is intermediate between the mantle source and the crustal contaminate (Smith and Ludden, 1989; Henry et al., 2000).

The lower ε_{Nd} values for samples from Suite II (values of 0.10) indicate that they may have undergone minor contamination, resulting in an isotopically enriched source, but the multi-element plots indicate LREE depletion. This contradiction can be explained if an isotopically enriched mantle source was melted, resulting in a LREE depleted but isotopically enriched residue (Tomlinson et al., 1998). It is this residue that generates the final magma. An alternate explanation for the generation of an isotopically enriched but LREE depleted source is mixing of a MORB source asthenosphere with a metasomatized arc lithosphere within a back arc setting (Stern et al., 1995).

Samples from Suite III display dramatically different ε_{Nd} values dependant on which subset they are from (Figure 4.7). Suite IIIa, which displays the highest enrichment in LREE has an ε_{Nd} value (2.31), comparable to those of Suite I, which indicates little to no crustal contamination of the magma. In addition the T_{dm} of sample NL20 (2939 Ma) is in close agreement with the assumed age of 2900 Ma. Suite IIIb has the lowest ε_{Nd} value (-2.49) and highest T_{dm} (3501 Ma) observed in this study, suggesting a high degree of contamination. The increased contamination associated with Suite IIIb is consistent with its origin within a shallower melt than Suite IIIa.

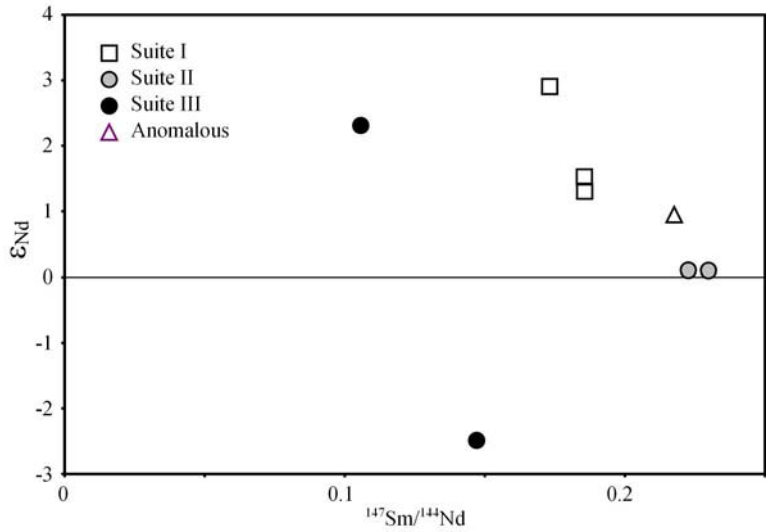

Figure 4.7: ε_{Nd} vs $^{147}Sm/^{144}Nd$ variation plot of isotope samples.

4.4 Summary

Three distinct suites of rocks have been identified within the Norton Lake region. Suite I consists of uncontaminated rocks with ocean plateau-like characteristics while Suite II is composed of uncontaminated to slightly contaminated N-MORB-like rocks. Suite III represents subduction-influenced arc rocks with Suite IIIa likely representing melting at a greater depth than Suite IIIb.

Figure 4.8 shows interpreted trends for the samples based on sample location and known structures. It is important to realize that these are only interpreted trends. The limited outcrop exposures and sparse samples in the northern and eastern extent of the area combined with the absence of exposed contacts and only limited availability of the abandoned drill core makes all interpretations tentative.

The sequence illustrated, in terms of its tectonic setting (Figure 4.8), is that of MORB type rocks (Suite II) overlain by subduction related rocks (Suite III) followed by a plateau-like sequence (Suite I) then further MORB volcanism. Such a complex

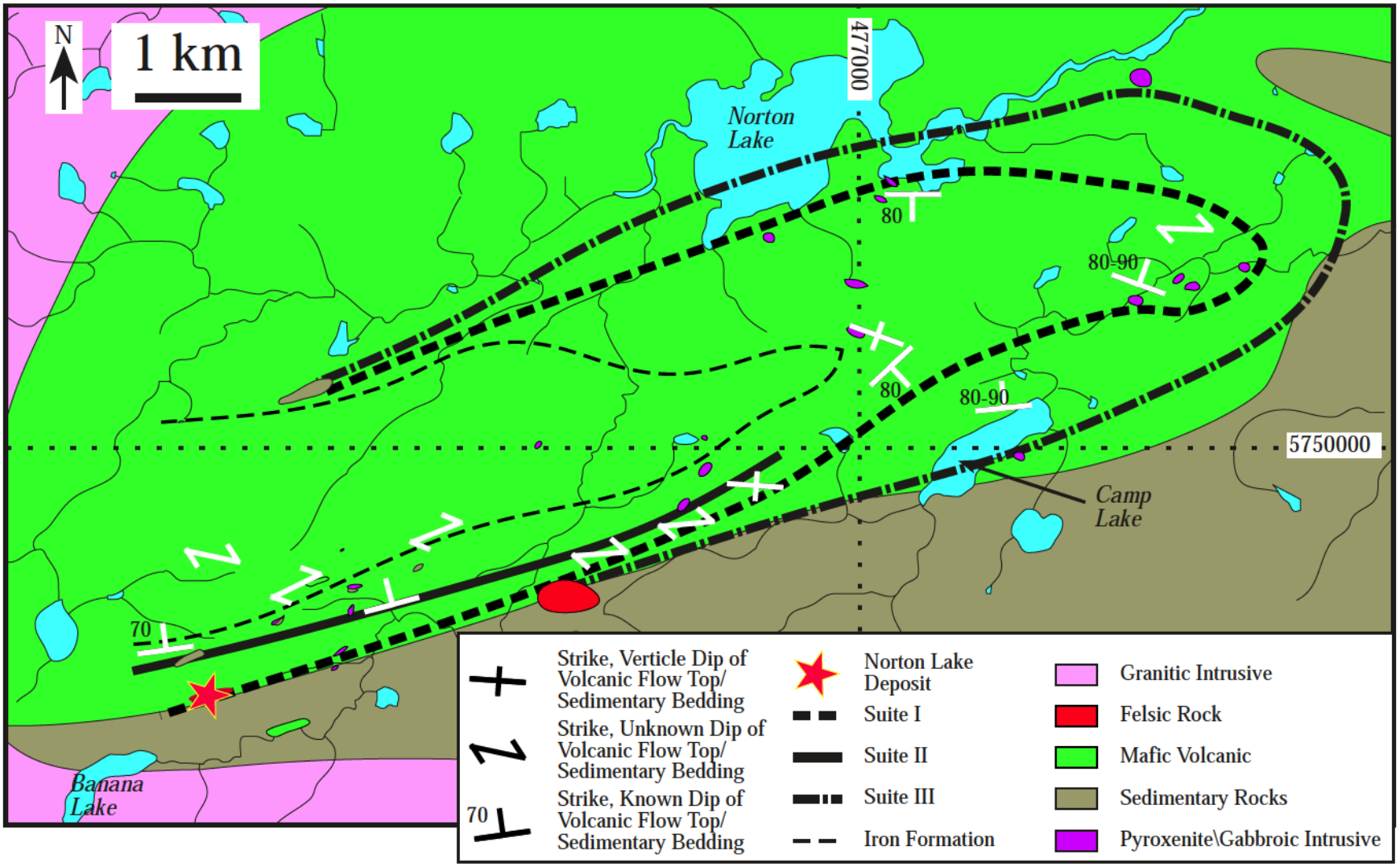

Figure 4.8: Interpreted trends of sample suites within the Norton Lake region.

arrangement of tectonic assemblages can be explained by either a complex set of thrust faults or possibly a back arc environment.

It is not thought likely that there is a system of extensive, unidentified faults within the study area. There is no evidence of a strong tectonic fabric in samples examined. In addition airborne geophysics within the area have not revealed the presence of any features that may represent a complex set of faults.

The second environment, that of a back arc basin, is more plausible as studies of modern back arc basins have demonstrated that they comprise a complex mix of rock types including MORB, ocean island basalts, niobium-enriched basalts, komatiites and arc-like rocks (Lafleche et al., 1992; Stern et al., 1995; Tomlinson et al., 1998; Kerrich et al., 1999; Hollings et al., 2000; Hollings and Kerrich, 2000; Hollings, 2002; Wang et al., 2004). Back arc basins have been identified in other greenstone belts of the Uchi Subprovince including the Northern Pickle assemblage of the Pickle Lake greenstone belt (Hollings, 2002), the Birch-Uchi greenstone belt (Hollings and Kerrich, 2000), and the Meen-Dempster greenstone belt (Hollings et al., 2000).

Although a back arc basin setting may be more plausible explanation than that of tectonic thrusting, it is not without its own problems. The presence of arc-influenced volcanics beneath the plateau-like rocks suggests that the plateau may have been obducted onto a pre-established subduction zone. The potential problem with this is the debate over whether or not plate tectonics occurred during the Archean. Despite strong geochronological (Corfu and Ayres, 1991; Corfu and Stott, 1993a; Beakhouse et al., 1999), geochemical (Hollings, 1998; Beakhouse et al., 1999), stratigraphic and structural (Percival and Williams, 1989; Kusky, 1990; Kusky, 1991; Descrochers et al., 1993;

Young, 2003) evidence there are proponents that argue plate tectonics did not occur in the Archean (Bickle et al., 1995; Hamilton, 1998). It should be noted that those that argue against plate tectonics rely heavily on their own observations and interpretations, not on scientific data.

An addition problem is that ocean plateau sequences normally comprise a greater thickness (kilometres) than that observed (hundreds of meters: Storey et al., 1991). The occurrence of the various rock types, presumably, as thin slivers is more indicative of thrusting than of a back arc environment.

The whole rock and radiogenic isotope geochemistry of this study supports the previous inference by Stott and Corfu (1991) that the northern most unnamed assemblage of the MFGB correlates with the Northern Pickle assemblage of the Pickle Lake greenstone belt. Although no geochemically distinct marker units were encountered in this study, such as the niobium enriched basalts identified in drill core from the Northern Pickle assemblage by Hollings (1998; 2002), this may have been due to the sample population. A back arc basin setting for the unnamed assemblage and the Northern Pickle assemblage together with the interpreted aeromagnetic trend extending between the two assemblages, a tentative correlation in age (T_{DM} 2896 and 2939, samarium-neodymium, this study; ca. 2860-2890, U-Pb, Stott and Corfu, 1993b; Young, 2003) and similarities in rock types (Stott and Corfu, 1991) support the correlation between the two assemblages.

CHAPTER 5

Economic Mineralogy of the Norton Lake Deposit

5.1 Introduction

A detailed study of the Norton Lake Deposit was undertaken to classify the precious metal minerals (PMMs), their occurrences and to examine the nature of a change in the ratio of platinum to palladium observed in bulk assays of drill core. SEM analysis of platinum group minerals (PGMs) indicated a deficiency in platinum when compared to bulk assays analyzed at ALS Chemex. Consequently sulphide grains were analyzed by electron microprobe to determine if platinum was contained in the minerals, either as micro inclusions or as substitutions within the crystal structure. Initial investigation of the mineralogy of the Norton Lake deposit involved visual inspection of the drill core, followed by reflected light microscopy, scanning electron microscopy at Lakehead University and electron microprobe studies at the University of Saskatchewan (refer to Section 1.2.4 and Section 1.2.5 for methods).

5.2 Norton Lake Ni-Cu-Co-PGE Deposit

The original Norton Lake nickel-copper deposit was defined in 1980 by Prospection Inc. as a 944,500 tonne deposit grading 0.72% nickel and 0.56% copper. No cobalt or platinum group element (PGE) assays were conducted at this time. The mineralized zone was traced by twenty drill holes totalling 2,708 m at 50 foot spacing along strike for 225m and down dip for 150m with an average thickness of 7.1m but was believed to thin with depth (Hill, 1981b). Work by East West Resource Corporation (2000-2004) indicates the deposit consists of two lenses that have total strike length of ~300 m and extend down dip to the 200 m level with the sulphide lenses projected to continue to depth (Figure 5.1).

The mineralized massive sulphide zone is located within an ultramafic intrusion at the contact between an underlying, sheared, amphibolite tuff and overlying mafic volcanic unit. The sulphide zone is often brecciated with the breccia composed of mafic, ultramafic and gabbroic fragments in addition to highly siliceous fragments that represent potential iron formation, within a highly deformed sulphide matrix. The texture of the deformed sulphide matrix surrounding fragments is often referred to as durchbewegung texture (Figure 5.2). Hill (1981b) identified the mineralization as consisting of massive pyrrhotite in irregular stringers, veins and patches forming 10 to 75 vol% and averaging 30 to 35 vol% with erratically distributed chalcopyrite as grains, patches and seams. Pyrite was locally recognized, as was pentlandite and violarite.

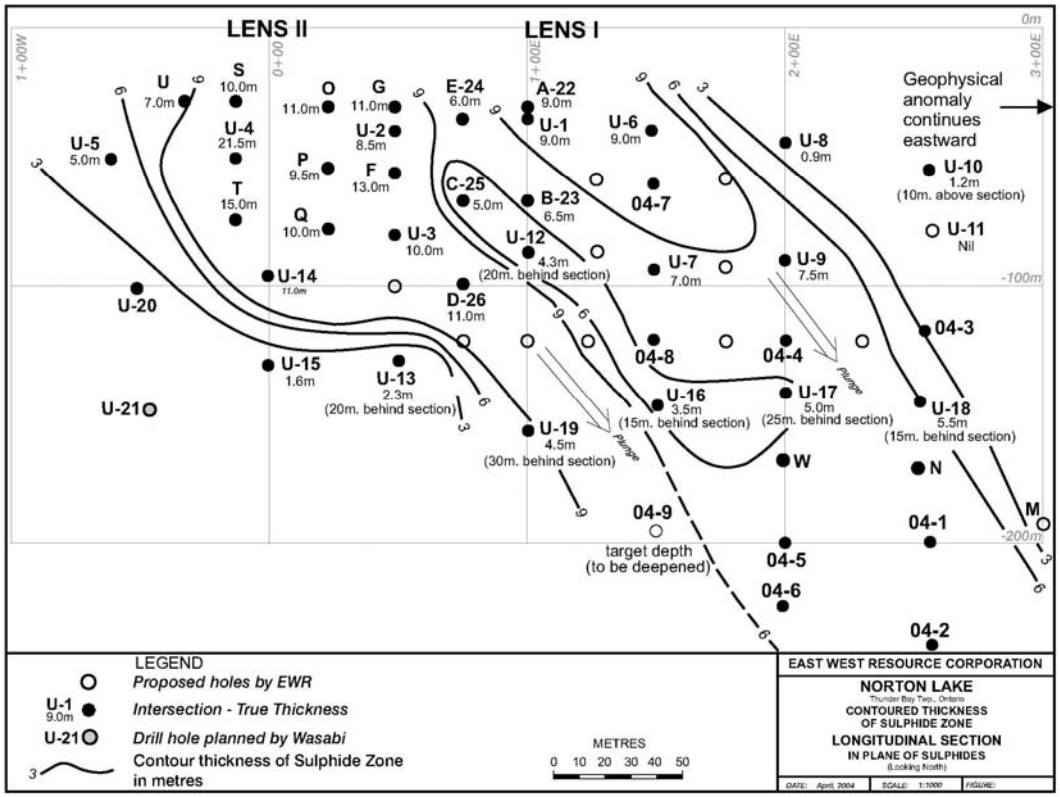

Figure 5.1: Longitudinal section of the mineralized zone (East West Resource Corporation, 2004).

This study has shown the mineralized zone to be dominated by pyrrhotite with lesser amounts of pentlandite, chalcopyrite and pyrite. Minor amounts of magnetite and a manganese-rich ilmenite are also present, in addition to trace amounts of violarite, molybdenite, galena, sphalerite and skutterudite. Volumetrically minor but economically significant amounts of precious metal minerals (PMMs), including assorted platinum group and silver minerals, have been identified.

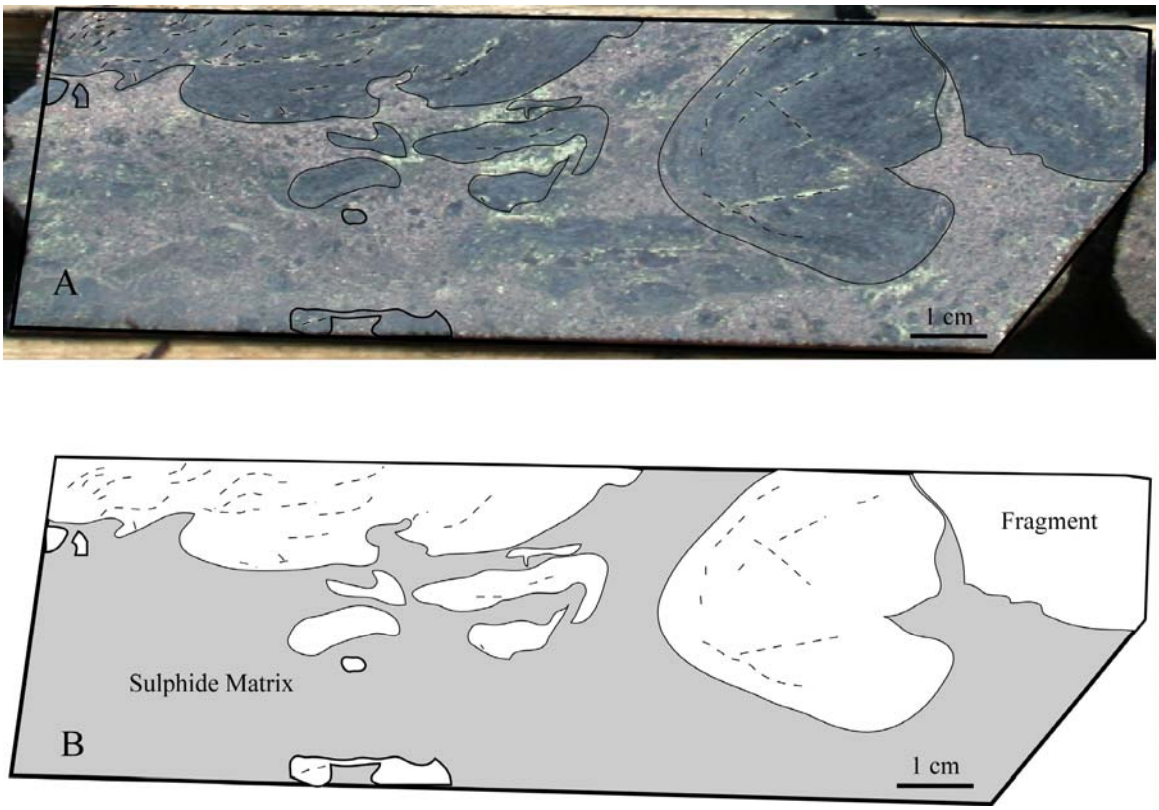

Figure 5.2: A) Durchbewegung texture in drill core. B) Cartoon of drill core with select fragments highlighted. Dashed lines indicate foliation.

5.2.1 Sulphides

Analytical data, unless otherwise specified, are from microprobe analyses with supporting data from SEM analyses. A complete data set is presented in Appendices C and D. Spot analyses for the microprobe were selected, when possible, from the centre of large (>15 μm) sulphide grains. Locations near sulphide-gangue boundaries were avoided when possible. Lead, rhenium, ruthenium, palladium, cadmium, osmium, iridium, gold and silver were detected in many of the grains analyzed at or slightly above the detection limits (see Appendix D for values and detection limits). These elements are not discussed below. Analyses from the SEM gave results that agreed with the microprobe data except in instances of low concentrations. For elements with low

concentrations the SEM could not detect the elements in question with any reliability due to higher detection limits (i.e. platinum; see Appendixes C and D for detection limits).

A representative sub-set of samples were selected for microprobe analysis. The samples were chosen to represent a range of platinum and palladium values as determined by bulk rock assays (see Table 5.1) and contained only minor variations in sulphide proportions and one noticeable exception involving PGMs. The PGM sperrylite was identified in samples G-01 and O-02 while the other samples investigated did not include any PGMs with platinum as a primary constituent.

Table 5.1: Bulk assays by ALS Chemex of ~1 m of drill core for samples studied by microprobe (East West Resource Corporation).

Sample	Pt ppb	Pd ppb	Ag ppm	Co ppm	Cu ppm	Ni ppm	S %
D-03	90	800	0.80	507	2970	15000	5.13
F-01	676	460	6.00	371	13700	5880	8.51
G-01	1790	1020	2.00	554	5160	15900	7.45
M-01	145	328	2.00	615	1125	3910	>10.00
O-01	166	1330	2.40	440	9130	11600	6.83
T-01	200	766	1.00	398	3650	13900	4.95
W-01	230	340	2.80	400	5140	7320	6.37
U12-04	3690	690	5.60	895	16400	9270	7.17

Pyrrhotite ($Fe_{(1-x)}S$) is the dominant sulphide species, occurring as masses of anhedral to subhedral grains and rarely as isolated subhedral grains (Figure 5.3). Microprobe analyses indicated that trace amounts of cobalt (0.02 - 0.12 wt%) exist in all samples (Table 5.2). Nickel is present in variable amounts in all samples, with thirty of the samples containing between 0.43 and 0.70 wt% and the remaining two samples containing more significant amount of nickel, between 1.54 and 4.60 wt%. SEM

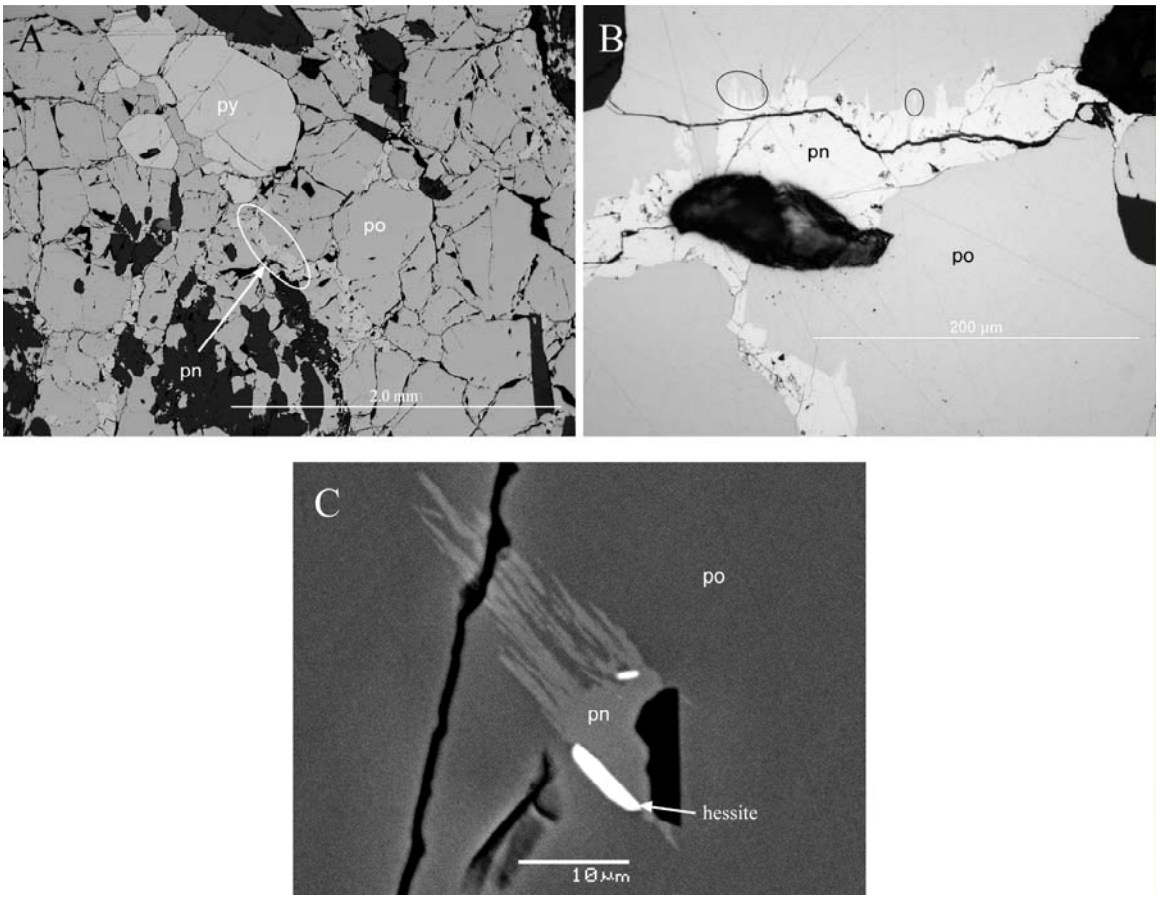

Figure 5.3: Reflected light photomicrographs illustrating the various habits of pyrrhotite. (A) Subhedral to anhedral pyrrhotite (po) with pyrite (py), and pentlandite (pn) chains. (B) Massive pyrrhotite with pentlandite chain and small exsolution flames (circled). (C) Pyrrhotite with pentlandite exsolution flames, hessite at the contact between pyrrhotite and pentlandite.

analyses of pyrrhotite (n = 45) detected no cobalt, as expected given the higher (0.2 wt%) detection limit of the SEM, with only 90% (forty-nine) of the samples having detectable nickel values (0.35 – 1.23 wt%). When the microprobe analyses are projected onto a Fe-Co-Ni composition diagram, two clusters are seen (Figure 5.4). Of the thirty-two samples analyzed by microprobe only two were determined to be hexagonal pyrrhotite.

Table 5.2: Summary table of sulphide compositions for platinium and cobalt (in wt%) as determined by microprobe analysis. No. Samples refers to samples with values greater than detection limit/total samples analyzed (detection limit of 0.05 wt% and 0.02 wt% for platinum and cobalt respectively).

Mineral	Ideal Formula	Platinium		Cobalt	
		No. Samples	Range	No. Samples	Range
Pyrrhotite	$Fe_{1-X}S$	7/32	0.05-0.11	32/32	0.02-0.12
Pyrite	FeS_2	5/26	0.05-0.08	26/26	0.05-3.0
Pentlandite	$(Ni,Fe)_9S_8$	4/30	0.06-0.14	27/30	1.10-1.82
Chalcopyrite	$CuFeS_2$	0/13	-	8/13	0.02-0.06
Violarite	$(Ni,Fe)_3S_4$	0/5	-	5/5	1.12-2.09
Galena	PbS	0/1	-	1/1	0.03
Sphalerite	ZnS	1/2	0.07	2/2	0.03-0.06
Molybdenite	MoS_2	-	-	-	-

Monoclinic pyrrhotite plots near the iron apex of the ternary diagram, whereas hexagonal pyrrhotite trends away from the iron apex with the additional incorporation of nickel into the structure (Vaughan et al., 1971; Carter et al., 2001). Determination of monoclinic and hexagonal pyrrhotite, based on composition, was not possible using the SEM analysis.

Pentlandite $(Fe,Ni)_9S_8$ was typically found as massive, broken chains or as exsolution lamellae (Figure 5.3) that form from nickeliferous pyrrhotite at temperatures below 610°C (Vaughan and Craig, 1978). Pentlandite also occurs as rare anhedral clusters of grains and occasionally as isolated euhedral grains or as crystals replacing or being replaced by pyrite and/or chalcopyrite.

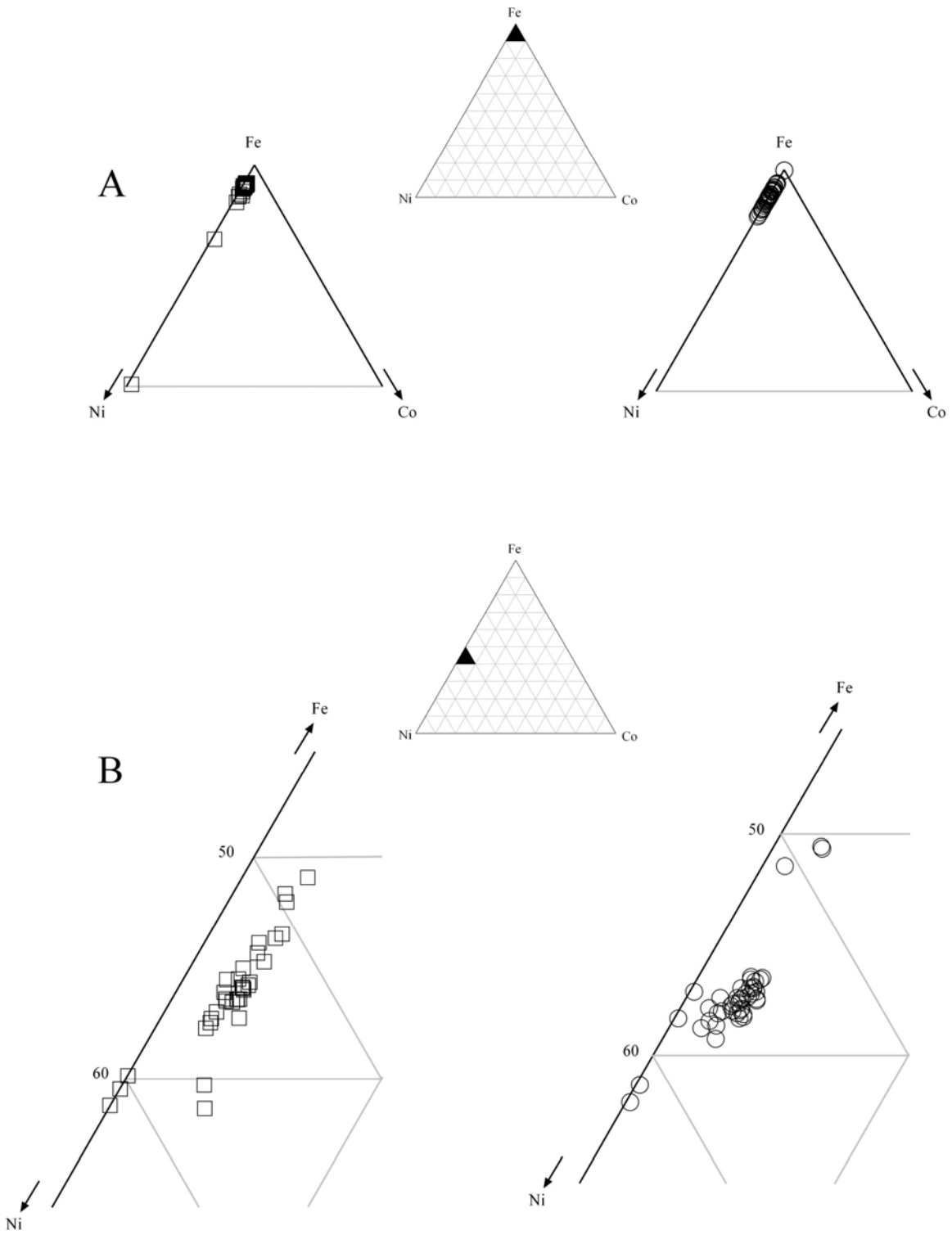

Figure 5.4: Fe-Ni-Co composition diagrams illustrating (A) pyrrhotite compositions and (B) pentlandite compositions. Open squares represent microprobe analyses and open circles represent SEM analyses.

Pentlandite compositions were variable $(Fe,Ni\pm Co)_{7.24\text{-}9.34}S_{7.66\text{-}9.76}$. Analysis indicated two populations in terms of their cobalt-nickel values. The majority of the samples carried minor amounts of cobalt, between 1.10 and 1.82 wt%, while a smaller subset contained values at or below the detection limit (200 ppm). The second population consists of analyses from a single slide (M-01) and was determined to have elevated nickel values (40.50 - 41.19 wt% compared to an average of 34.59 wt%; Appendix D). SEM analyses closely followed the results of the microprobe analyses with the majority of the samples (n = 41) containing minor cobalt, between 0.52 – 1.78 wt%, while a smaller set (n = 2) carried no cobalt but elevated nickel (41.38 and 41.58 wt% compared to an average of 36.87 wt%; Appendix C). The pentlandite analyses, with below detection limits of cobalt, as determined by SEM came from the same slide as the microprobe analysis (M-01).

Violarite $[(Ni,Fe)_3S_4]$ had a limited range of compositions $[(Ni,Fe,Co)_{2.98\text{-}3.05}S_{4.02\text{-}3.95}]$. Violarite was differentiated from pentlandite solely on the basis of stoichemetry. The two minerals are indistinguishable by SEM and microprobe observation (back scattered electron imaging) due to their similarity in composition. A minor amount of cobalt was determined to be carried by violarite (1.12 – 2.09 wt% by microprobe; 0.50 – 2.94 wt% by SEM). The rarity of violarite may be more apparent than real due to the difficulty involved in distinguishing between it and pentlandite by use of the SEM and microprobe.

Pyrite (FeS_2) within the mineralized zone occurs as anhedral masses to euhedral grains (Figure 5.5). Numerous grains are partially replaced by chalcopyrite, pentlandite or pyrrhotite, while other grains replace chalcopyrite. Inclusions of other sulphides

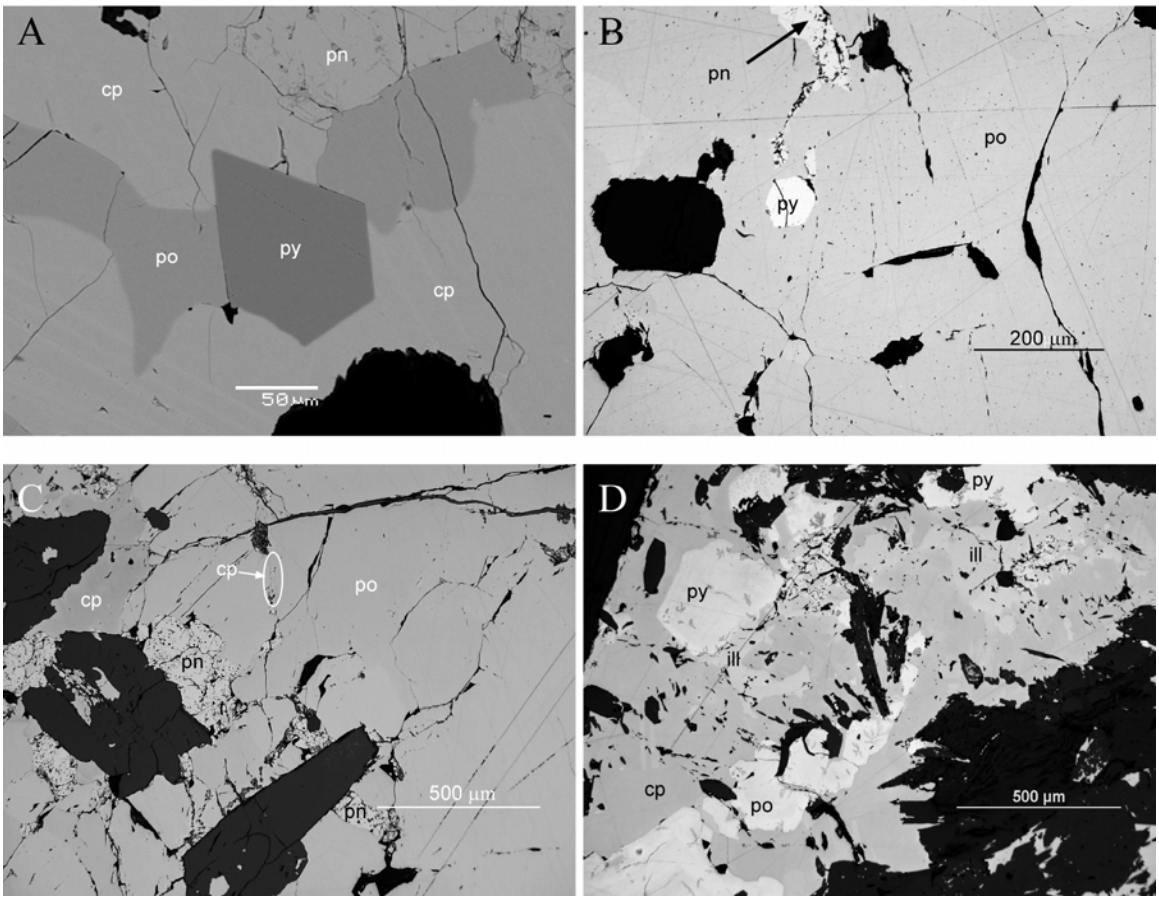

Figure 5.5: (A) SEM backscattered image of euhedral pyrite (py) cutting a pyrrhotite (po) vein within chalcopyrite (cp); pentlandite (pn) is present in upper right corner. (B) Photomicrograph of euhedral pyrite fully enclosed within massive pyrrhotite, pentlandite. (C) SEM backscattered image of chalcopyrite and pentlandite after pyrrhotite. (D) SEM backscattered image of pyrite, pyrrhotite and ilmenite (ill) being replaced by chalcopyrite.

(pyrrhotite, pentlandite and chalcopyrite) within pyrite were observed in several slides. It was not possible to determine if the inclusions were primary in nature, formed by the intergrowth of the sulphides, exsolution of the sulphides, or the result of near complete replacement of the sulphides by pyrite. Annealing textures were noted in several slides,

most commonly located in slides taken from or adjacent to cross-cutting chalcopyrite veins.

Pyrite was compositionally close to the ideal stoichemetric value, $(Fe\pm Co\pm Ni)_{0.99-1.09}S_{2.01-1.91}$ with analysis indicating two sample populations. The first contained minor amounts of cobalt (0.95 - 3.0 wt% by microprobe; 0.61 – 2.23 wt% by SEM) with no appreciable amounts of nickel (0.00 - 0.09 wt%) while the second contained no or minor amounts of nickel (0.00 wt%, 0.76 - 4.11 wt% by microprobe; 0.16 – 4.88 wt% by SEM) with no significant amounts of cobalt (0.05 - 0.09 wt%).

Chalcopyrite ($CuFeS_2$) has a highly variable frequency and mode of occurrence within the deposit. It occurs both as isolated grains and as small aggregates of grains to massive blebs, as a partial replacement of other sulphides or as irregular crosscutting veinlets. Compositionally, it has only slight deviations from stoichemetric values ($Fe_{1.05-0.96}Cu_{1.02-0.96}S_{1.92-2.07}$) and contains no appreciable amounts of minor elements.

Additional sulphides that were observed include molybdenite, galena and sphalerite. These sulphides account for less than 1 vol% (combined) of the total sulphides, varied in size from less than 2 μm to 45 μm and in form from anhedral to euhedral. Samples where these sulphides were present did not display anomalous molybdenum, lead or zinc values. This is explained if the bulk rock analyses done by ALS Chemex did not have sufficiently low detection limits for these elements and therefore was unable to detect the potential variation caused by these sulphides.

Palladium was determined to be present at or near detection limits within nine of the one hundred, ten microprobe analyses of the sulphides (sphalerite, 0.05 wt%; pyrite

(n=4) 0.03 – 0.04 wt%; pyrrhotite (n=3), 0.02 – 0.03 wt%; pentlandite 0.03 wt%: Appendix D).

Detectable levels of platinum were observed in pyrrhotite, pyrite and pentlandite (Table 5.2; Appendix D). Within pyrrhotite seven of the thirty-two samples analyzed had platinum vales ranging from 0.05 - 0.11 wt%. Pentlandite grains displayed platinum abundances of 0.06 - 0.14 wt% in four of the thirty-five grains analyzed, all from the sample population that contained cobalt. Five out of the twenty-five pyrite analyses returned values slightly above detection limits (0.06 - 0.08 wt%). Microprobe analysis could not identify how the platinum was contained within the sulphides. Single point analyses were unable to determine if there were inclusions of PGMs below the level of resolution of the microprobe or if there was an even distribution of PGEs, resulting from the PGEs being in solid solution of the sulphides, as new work in South Africa is finding (Kozyrev et al., 2002; A.J. Naldrett, personal communication 2004). There is no correlation between the distribution of the sulphide grains that contain platinum and the location of the known PGMs or to the bulk assay.

5.2.2 Precious Metal Minerals

A variety of PMMs were identified by SEM, since they were too small to be readily identified by optical microscopy. They ranged in size from less than 1 μm up to 40 μm and in shape from euhedral to anhedral, often consisting of composite grains. Quantitative chemical analyses were carried out on grains greater than 3 μm in size, while smaller grains were analyzed qualitatively to identify the dominant elements present.

Analyses on grains less that 3 μm in size would only indicate the presence of an element (i.e. platinum, silver, palladium). It was not possible to determine the amount of these elements due to the resolution of the SEM. Minor contamination was determined to occur in grains up to 5μm in size due to fluorescence from the surrounding minerals (see Section 1.2.4 for details). The minerals identified and their compositional ranges are listed in Table 5.3 (see Appendix C for complete analytical results).

Table 5.3: Summary of precious metal minerals identified. Ideal Formula is as given by Cabri (2002).

Mineral	**Ideal Formula**
Acanthite	Ag_2S
Hessite	Ag_2Te
Kotulskite	PdTe
Merenskyite	$PdTe_2$
Michenerite	PdBiTe
Sperrylite	$PtAs_2$
Testibiopalladite	PdSbTe
Unidentified Au-Ag Telluride	$Au_{3.17}Ag_{0.79}Te_{1.04}$

The PMMs have five different occurrences. The vast majority of minerals were found along either sulphide-sulphide or sulphide-silicate grain boundaries with a small proportion found along fractures within the silicates or along silicate-silicate grain boundaries. Small, euhedral crystals fully enclosed by sulphide grains rarely occurred.

Silver was almost exclusively found as hessite. Hessite dominantly occurred as subhedral grains along silicate-silicate grain boundaries or along fractures within the silicates (see Figure 5.3 and 5.6). It also was also often found as part of composite PMM grains. The only other silver mineral identified was a single occurrence of acanthite. The

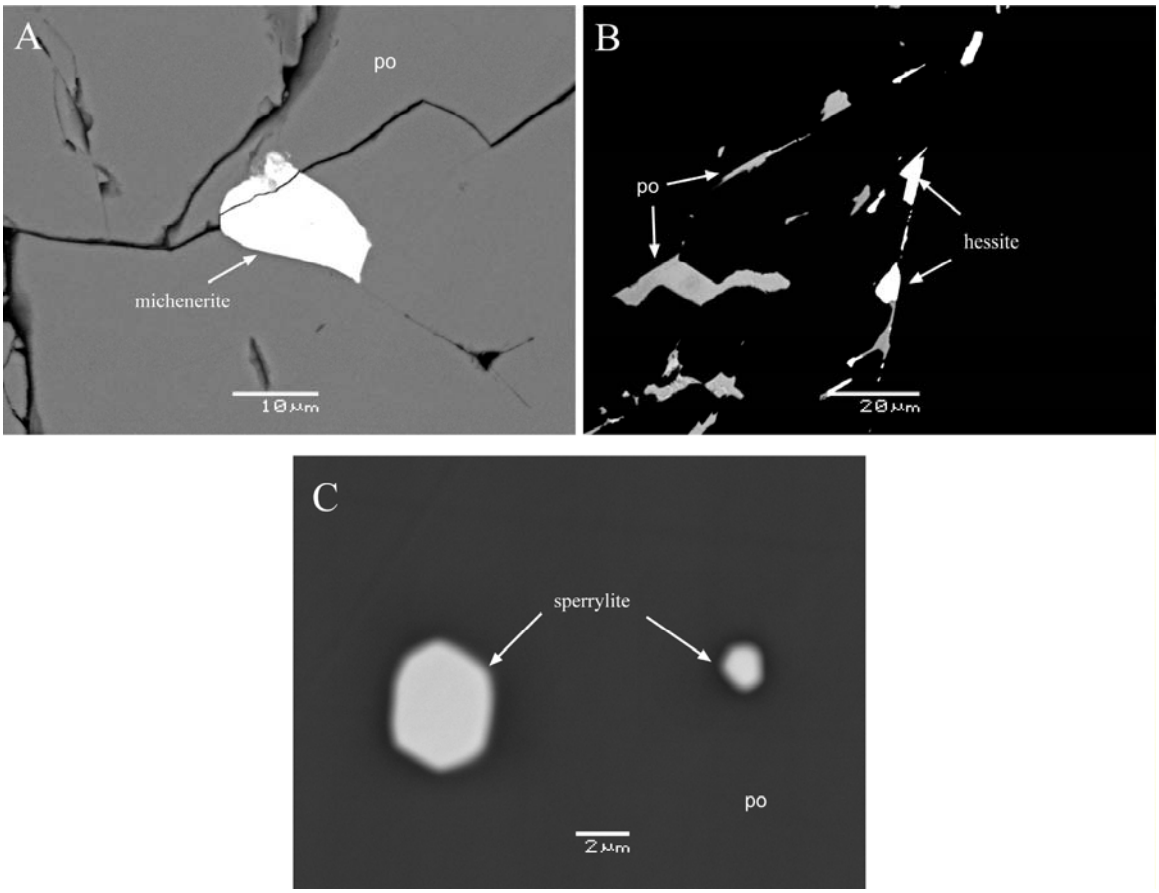

Figure 5.6: SEM back-scattered images illustrating the occurrences of PMMs. (A) Michenerite grain along pyrrhotite (po) grain boundaries, fractures in image are the result of slide preparation. (B) Hessite along a linear fracture within silicates. (C) Sperrylite grains fully enclosed within pyrrhotite.

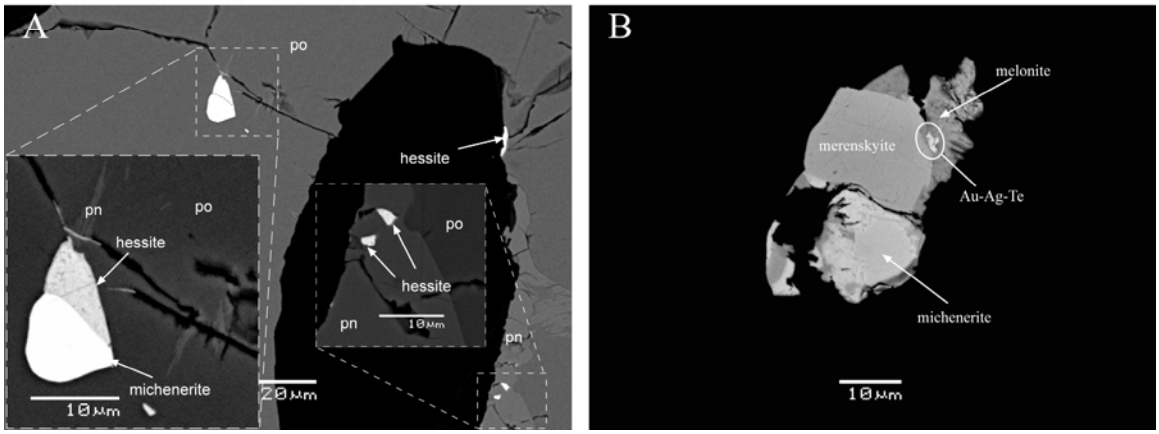

Figure 5.7: SEM back-scattered images of composite PMM grains.

acanthite was located within silicates along a grain boundary. In addition an unidentified gold-silver telluride was identified within a complex multi-mineral assemblage (Figure 5.7).

Many of the PGMs identified form a complete solid solution with one another. Michenerite and testibiopalladite, along with maslovite (PtBiTe), display a complete solid solution with platinum, palladium and bismuth substituting while antimony, bismuth and nickel substitute for each other (see Figure 5.8). Merenskyite forms a complete solid solution with moncheite ($PtTe_2$) and melonite ($NiTe_2$) where palladium, platinum and nickel substitute for one another (see Figure 5.9). Kotulskite forms a solid solution with sudburite (PdSb) and sobolevskite [Pd(Bi,Te)] (Cabri, 2002; Figure 5.10).

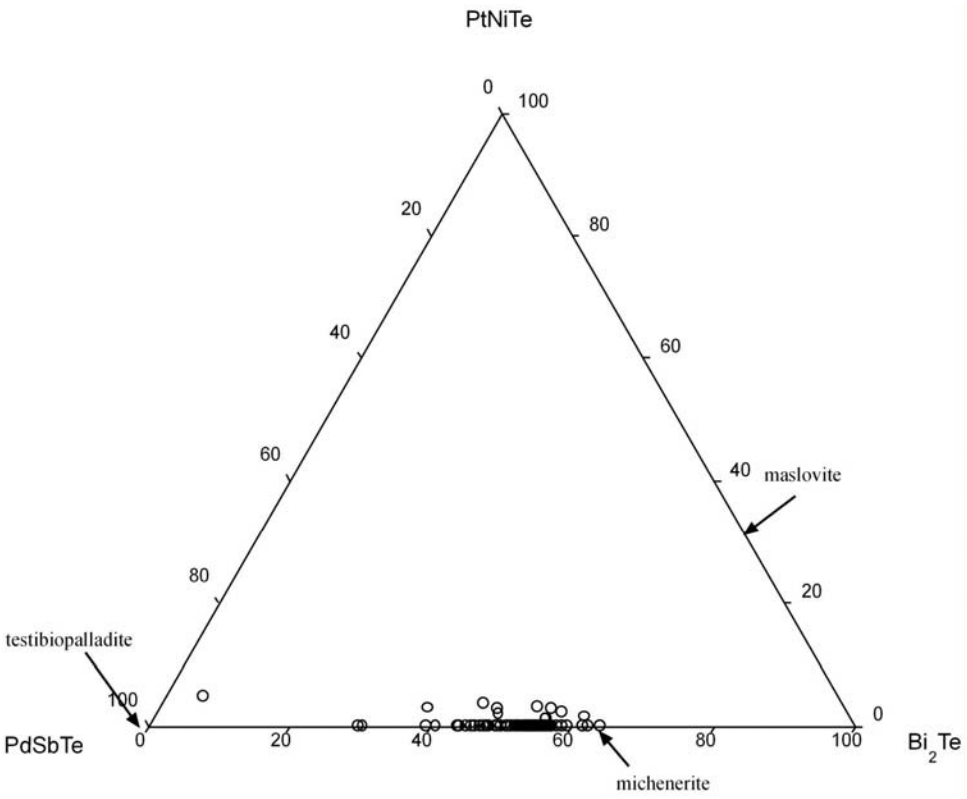

Figure 5.8: Ternary diagram of SEM analyses illustrating the solid solution between michenerite and testibiopalladite.

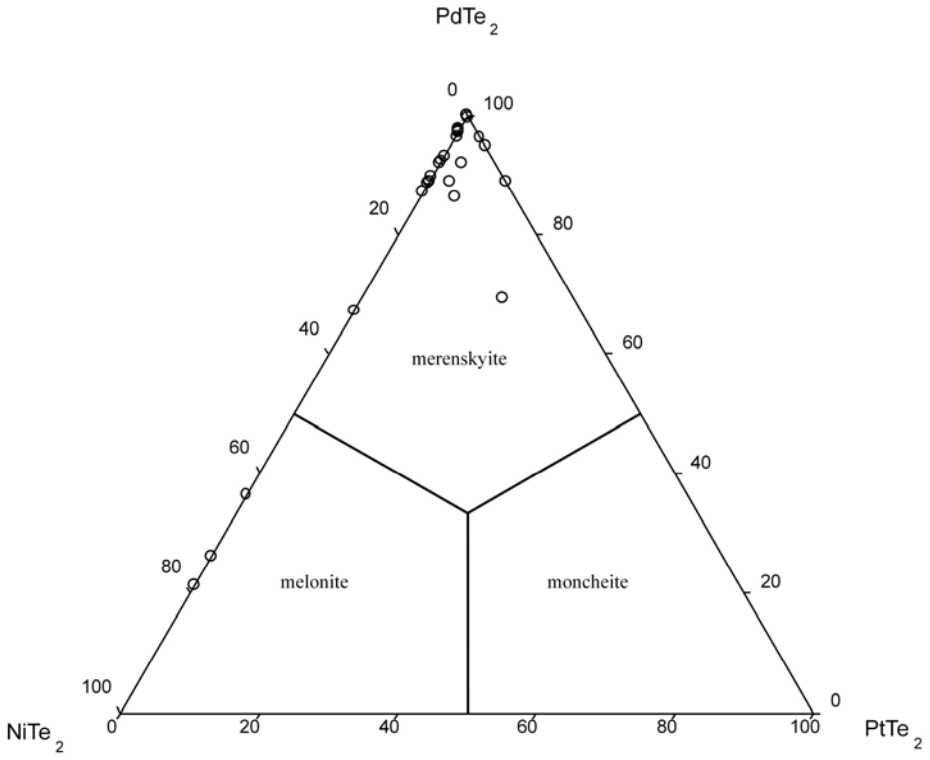

Figure 5.9: Ternary diagram of SEM analysis of the melonite – merenskyite – moncheite solid solution.

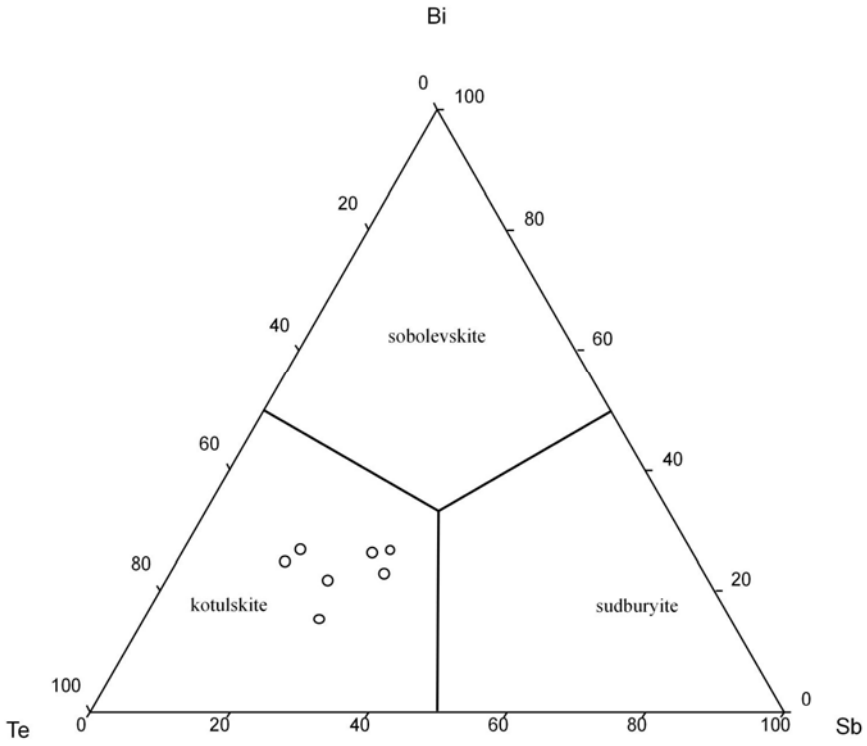

Figure 5.10: SEM analyses of kotulskite plotted on the ternary Sb – Bi – Te diagram.

5.2.3 Oxides and Arsenides

Skutterudite [$(Co,Ni,Fe)As_{3-x}$] was observed in two separate sections and is the only significant cobalt-bearing mineral. The sections where skutterudite was found do not contain abnormal bulk assay values for cobalt or arsenic. This suggests that the majority of the cobalt found by bulk assays is carried within the sulphides, not as discrete cobalt-bearing minerals.

Magnetite (Fe_3O_4) and a mixture of manganese-rich ilmenite ($FeTiO_3$ to pyrophanite $MnTiO_3$) were found in varying abundances in all sections. The two minerals occurred both as complex intergrowths and as distinct grains (Figure 5.11B).

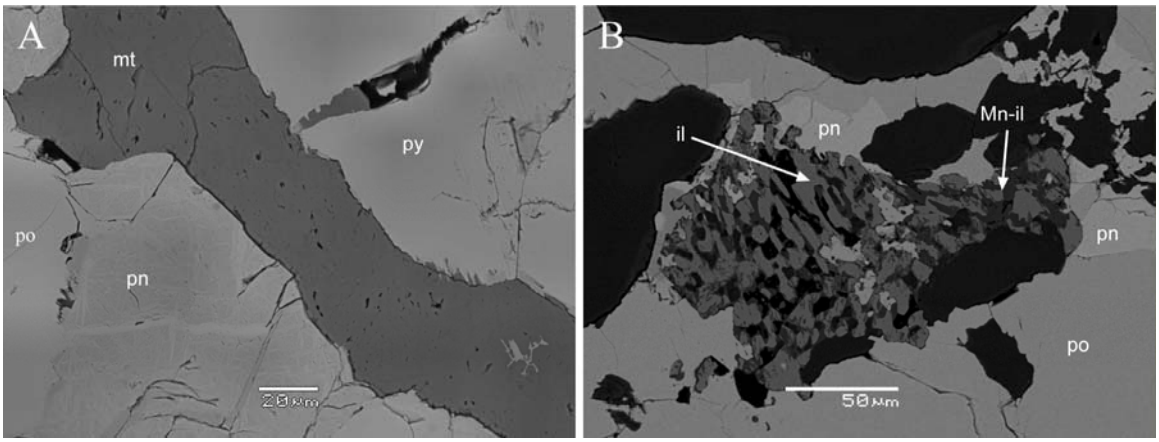

Figure 5.11: SEM backscattered images: (A) magnetite (mt) veinlet within pyrite (py) and pyrrhotite (po) being replaced by pentlandite (pn); (B) complex intergrowth of ilmenite (il), manganese rich ilmenite and pyrophanite (Mn-il).

5.3 Mineral Occurrences and Relationships

Three different styles of PGM mineralization are present. PGMs can be found as: (1) well formed, euhedral crystals totally enclosed within sulphides, as round grains commonly enclosed within sulphides but also rarely enclosed by silicates; (2) subhedral

to anhedral grains that occur along fractures within sulphides, along sulphide – sulphide, sulphide – silicate or silicate – silicate grain boundaries; or (3) they may be totally enclosed within silicates. Multi-mineral, composite grains are only found within the third style of mineralization.

The euhedral crystals and round grains are dominantly sperrylite with a lesser number of galena and palladium telleruides identified. The crystals enclosed within sulphides represent a primary magmatic mineralization of the PGMs. A PGE-rich phase would be exsolved from a sulphide melt that was enriched in PGEs as a result of fractionation, concentrating the chalcophile elements, or as the result of an enriched parent magma (Evans, 1993; Li et al., 2001). The PGEs would crystallize into euhedral PGMs or form immiscible droplets (i.e. round grains in cross section). Once formed the PGMs would be enclosed by the sulphide solid solution surrounding them, preventing an additional influx of PGEs and thus limiting their size and growth. It is unlikely that these PGMs formed independently of their enclosing sulphides. In all cases the enclosing sulphide was massive pyrrhotite and the PGMs were located well away from the edges of the pyrrhotite. The vast majority of the surrounding pyrrhotite contained small exsolution lamellae of pentlandite.

The composite grains of PGMs can be the result of either a primary mineralization or a secondary mineralization event. Many of the PGMs found as composite grains, are constituents of the same solid solution series. In these cases it is possible they are a result of primary magmatic mineralization resulting in simple and complex intergrowths of minerals due to potential changes in the conditions of formation (Markovicky, 2002). It is also possible that the outer mineral may have been precipitated from a hydrothermal

fluid. In numerous instances one or both of the minerals are hessite or michenerite both of which are readily mobile by hydrothermal fluids (Magyarosi et al., 2002).

The two styles of mineralization suggest that there was more than one mineralizing event. PGMs found along fractures may represent a second stage of mineralization. This is supported by the common occurrence of hessite and Pd-tellurides along the fractures. Hydrothermal fluids can remobilize PMMs as exemplified by the New Rambler Mine, Wyoming; Rathbun Lake, northeastern Ontario; the Roby Zone at Lac de Iles; and areas of the Sudbury Basin (McCallum et al., 1976; Rowell and Edgar, 1986; Watkinson and Melling, 1992; Farrow and Watkinson, 1997). Molnár and Watkinson (2001) have found that platinum and palladium may both be transported by chloride complexes under acidic and relatively oxidizing, low-temperature (<300°C) conditions. Under such conditions the remobilization of palladium is higher than platinum resulting in a greater chance for the remobilization and deposition of additional palladium minerals.

Chalcopyrite can be found as cross-cutting veinlets and replacing the other sulphide minerals. As later hydrothermal fluids moved through the mineralized zone they would form minerals, such as chalcopyrite, along fractures. This also suggests a secondary phase of mineralization occurred. Pyrite is normally found in close association with chalcopyrite and, like chalcopyrite, could be found both replacing and being replaced by the various other sulphides. Pyrite also occurs displaying approximately 120° dihedral angles characteristic of annealing. This indicates that those areas of the deposit have either undergone slow cooling or a later period of high temperature after its initial formation (Craig, 1990).

Assay results provided by East West Resource Corporation were filtered to include only samples from the mineralized zone, excluding samples from offshoot veinlets and stringers (a threshold of greater than 1000 ppm copper or nickel was used). Nickel values display a relative increase in relationship to cobalt values, but with a scattering of values at higher abundances (Figure 5.12). This correlation occurs because the majority of the cobalt is contained within pentlandite, the dominant nickel species. The scatter and outliers likely reflect the presence of additional cobalt carried by other sulphides, most notably pyrite, in areas with unusual pyrrhotite:pentlandite:pyrite ratios. Nickel values display a weak covariation with palladium (Figure 5.12). This covariation may be the result of nickel indicating of the extent of pentlandite mineralization, which in turn is an indicator of the amount of total mineralization. Areas with increased nickel values represent areas of increased primary magmatic mineralization (i.e. massive sulphides vs. stringer to disseminated sulphides) and consequently areas of increased palladium mineralization.

Copper values display no correlation with the distribution of nickel or cobalt within the deposit (Figure 5.12). There is also no correlation between copper and platinum or palladium. A relationship between copper and the PGEs would be expected if there were no secondary remobilization within the mineralized zone. Formation of an immiscible sulphide liquid results in the depletion of the chalcophile elements from the residual magma (Barnes et al., 1987). Due to the high partition coefficient for the PGEs they are concentrated within the sulphide liquid (Li et al., 2001). As the sulphides begin crystallization the chalcophile elements are concentrated until they reach their saturation

point at which time they begin to crystallize. Remobilization by hydrothermal fluids or a second stage mineralization will disrupt the primary relationship between these elements.

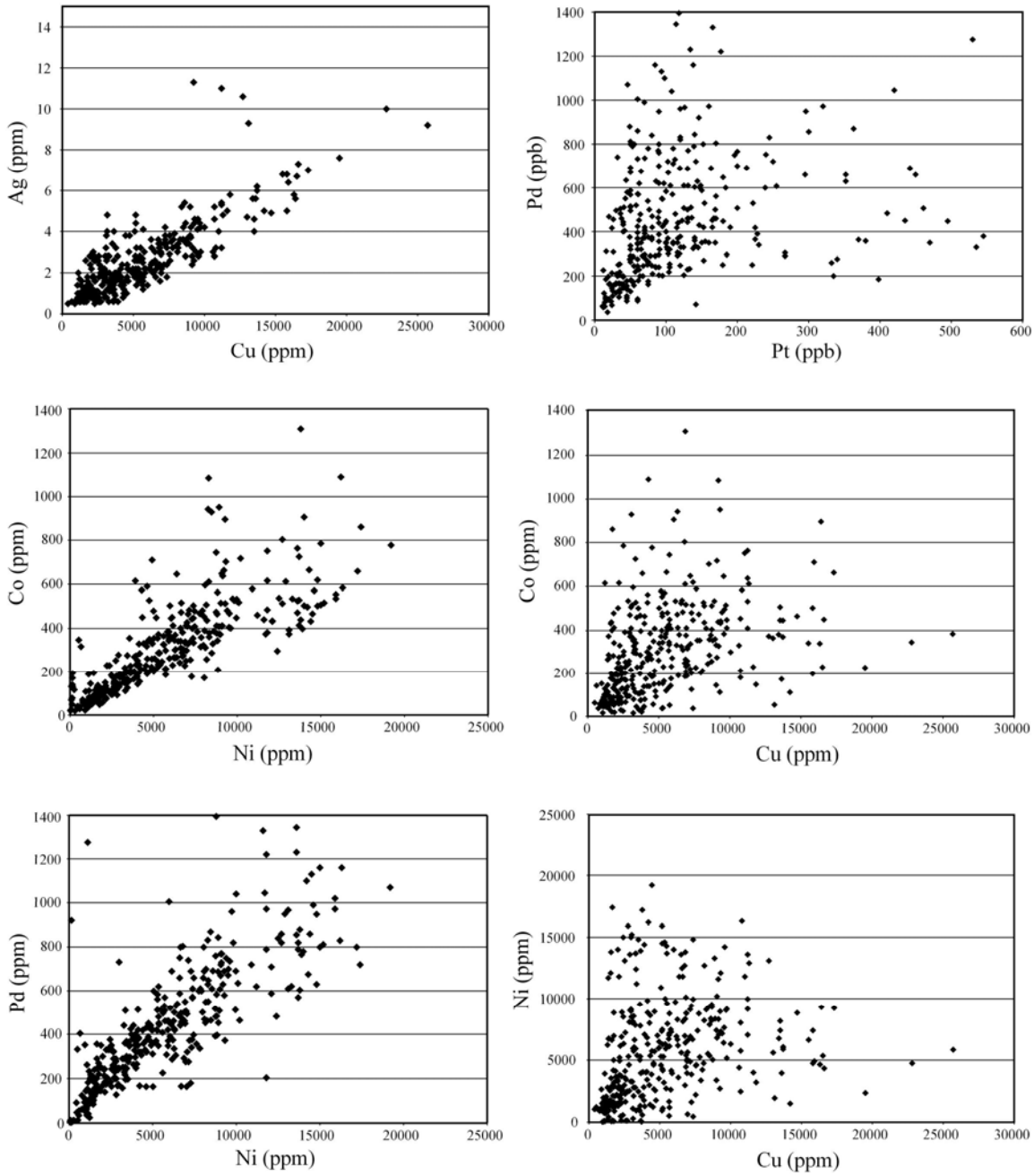

Figure 5.12**:** Element abundances diagrams, data from East West Resource Corporation drill core assays (2002-2004).

There is a general increase in copper values corresponding to a general increase in silver assays (Figure 5.12). Both copper and silver can be highly mobile within a hydrothermal system (McCallum et al., 1976). A general increase between the two without a corresponding increase in nickel values points to a secondary remobilization event in which copper, silver and, to a smaller extent, palladium tellurides were concentrated.

Platinum and palladium display no correlation in Figure 5.12, supporting a later remobilization event. The platinum:palladium ratio for the deposit averages 1:3 (310 analyses, East West Resource Corporation). In a small number of samples, twelve assays from East West Resource Corporation drill program and seven of sixty-four assays on select Wasabi Resources Ltd. core (provided by East West Resource Corporation), the platinum:palladium ratio increases to as high as 9:1. The assays of the drill core with the high ratio also tended to have one or more elevated values of nickel, copper and cobalt. Thin sections examined from these areas indicated the presence of sperrylite. These intersections contained the only identified sperrylite grains found in the course of this study indicating that the elevated platinum values are due to an increase in the amount of platinum-bearing PGMs.

5.3.1 Constraints on Formation

Conditions of the formation for the sulphides, tellurides and most PMMs in terms of the prevailing fugacities, equivalent to partial pressures in this study, are inferred. Mulja (1989) used derived predominance diagrams for the Pb-PbS-PbTe, Ag-Ag_2S-Ag_2Te-Ag_5Te_3, Pd-PdS-PdTe-$PdTe_2$, Ni-NiS-NiTe-$NiTe_2$ and the Cu-sulphide systems to constrain the fugacities for sulphur and tellurium. This study follows his techniques. Kotulskite (PdTe) and merenskyite ($PdTe_2$) are assumed to be representative of the other PGM and the $P(O_2)$ is considered negligible due to the common oxides being unstable with respect to either sulphides or tellurides (Mulja, 1989). In addition, for construction of the predominance diagrams, non-solid phases are suppressed, and it is assumed that all solid phases have an activity of one (Mulja, 1989). The effects of the second mineralizing event has to be accounted for before the initial conditions of formation can be determined.

Initial conditions of formation were determined using a stable mineral assemblage of pyrrhotite, chalcopyrite, galena and acanthite (Ag_2S; Figure 5.13). Pyrite was not used due to textural evidence indicating replacement of pyrrhotite by pyrite. The palladium tellurides and silver telluride were not used due to the uncertainty of their initial composition and whether they represent primary mineralization (see Section 5.3) or a secondary mineralization event that is believed to have remobilized and concentrated the tellurides. In addition, the stability fields for deposition (Figures 5.13 and 5.14) of hessite and the palladium tellurides do not overlap those of acanthite. Initial conditions of deposition are defined to be less than 557°C, the upper temperature of stability for chalcopyrite (Craig, 1982).

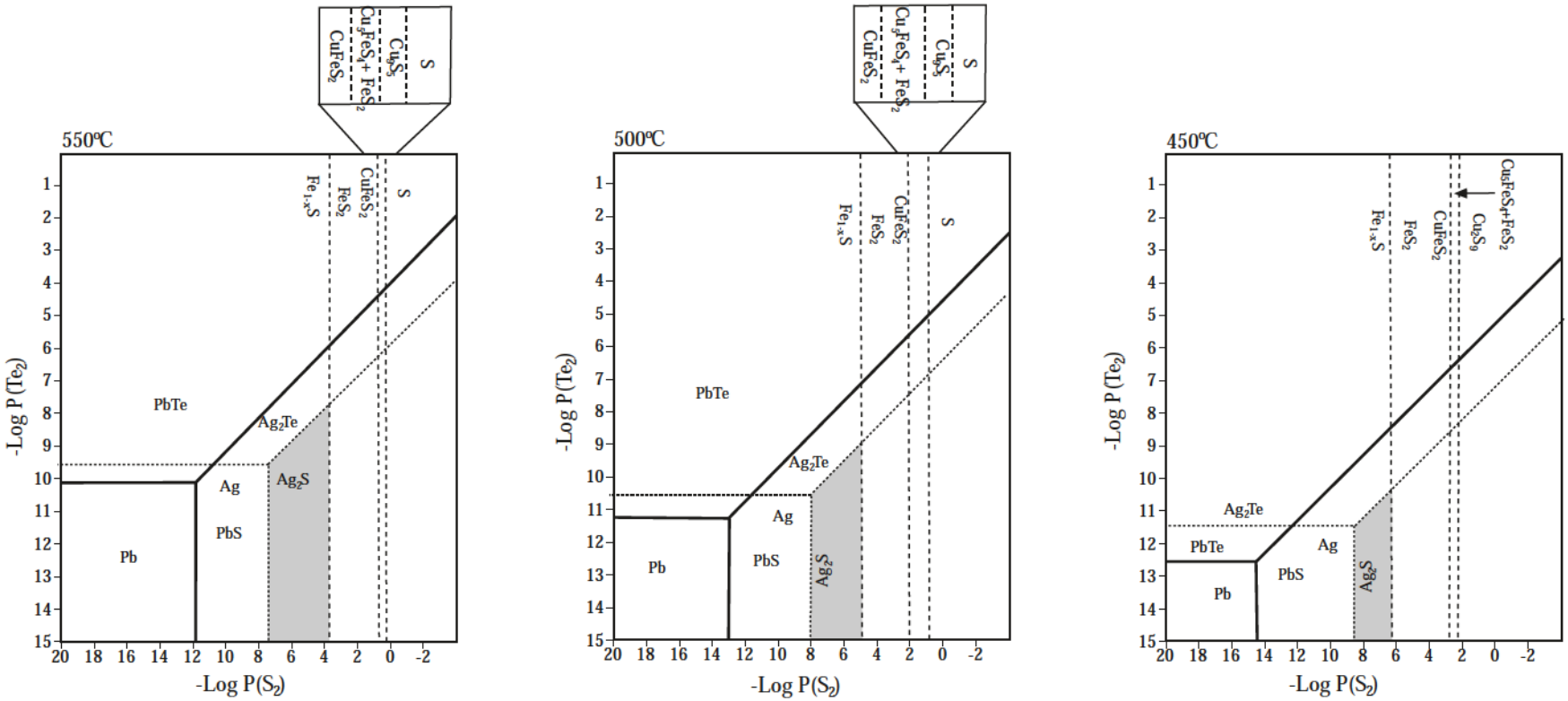

Figure 5.13: Superimposed predominance diagrams of the sulphides at 550°C, 500°C and 450°C. Shaded areas are depositional conditions (after Mulja, 1989).

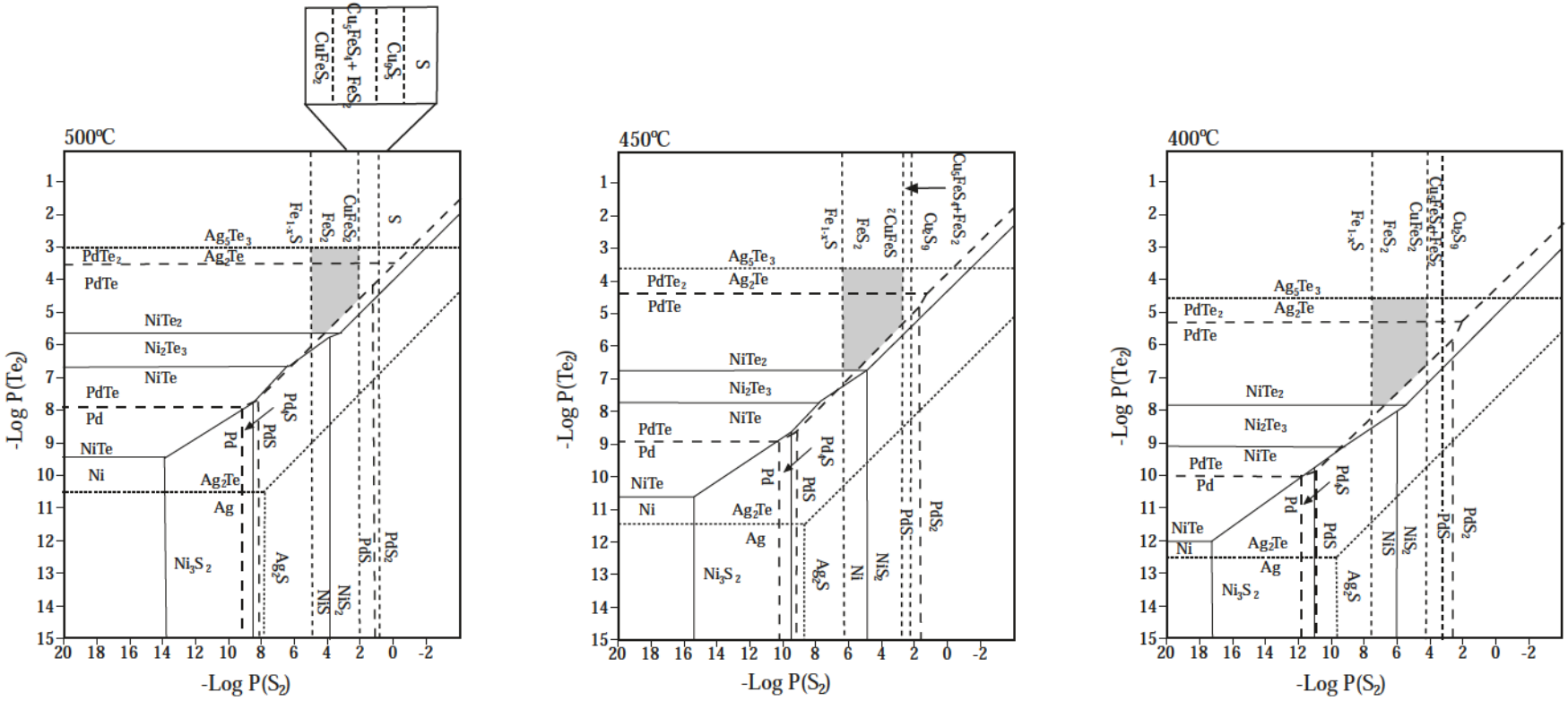

Figure 5.14: The superimposed predominance diagrams of the tellurides and PGM at 500°C, 450°C and 400°C. The shaded areas represent depositional conditions (after Mulja, 1989).

The stability fields illustrated in Figure 5.14 (determined using the mineral assemblage pyrite, chalcopyrite, melonite and hessite) indicate the conditions of secondary mineralization. The temperature range of 400°C to 500°C is illustrated to cover the upper temperature range at which bismuth-rich (489°C) and telluride-rich (501°C) michenerite form from bismuth-rich kotulskite (Hoffman and MacLean, 1976). In addition, this temperature range is consistent with upper greenschist and lower amphibolite grade metamorphism, the interpreted metamorphic grade of the host rocks.

In Figure 5.13, the primary mineral assemblage's $P(S_2)$ and $P(Te_2)$ are bound by the stability fields of pyrrhotite and acanthite. The $\log P(S_2)$ changed from –7.1 to –3.8 bar at 550°C to –8.4 to –6.2 bar as the temperature decreased to 450°C. The $\log P(Te_2)$ is less well constrained with the lower limit defined by the limit of the diagram and upper limit defined by the stability of acanthite (-9.6 to –8.1 bar at 550°C to –11.5 to –10.8 bar at 450°C).

The conditions of deposition for the secondary mineral assemblage illustrated in Figure 5.14 are fairly well constrained. The diagrams indicate that the sulphur fugacity increased from between –2 to -5 bars at 500°C to –4.2 to -7.8 bars at 400°C while the $\log P(Te_2)$, defined by the stability field of hessite and melonite changed from –3.0 to –5.6 bars at 500°C to –4.5 to –7.8 bars at 400°C.

5.4 Summary

The mineralized zone of the Norton Lake deposit consists of 72% pyrrhotite, 14% chalcopyrite and 14% pentlandite (as calculated to 100% sulphides). In addition, it contains minor amounts of pyrite and violarite with trace amounts of molybdenite, galena, sphalerite, ilmenite, magnetite, manganese rich ilmenite, skutterudite and a variety of PMMs, all typical of magmatic nickel – copper deposits. There is also evidence of a second mineralization or hydrothermal enrichment of the deposit. This is suggested by the presence of chalcopyrite as cross cutting veinlets often associated with pyrrhotite being replaced by secondary pyrite. In addition, palladium and silver tellurides, which are mobile under moderate hydrothermal conditions, are found along grain boundaries and within fractures.

CHAPTER 6

Discussion and Conclusion

The geology of the Norton Lake region displays considerable complexity over a relatively small area. The area is dominated by massive to pillowed mafic volcanic rocks with scattered intrusions of pyroxenite and gabbro. In addition, sedimentary beds of undetermined thickness sporadically occur. Trace element geochemistry of the intermediate to mafic volcanic strata has revealed that the potential tectonic environment is quite complex, with considerable diversity now recognised within the mafic volcanics.

The apparent sequence (from supposed oldest to youngest) of MORB (Suite I), subduction related volcanism (Suite III), ocean plateau (Suite II) and MORB (Suite I) is difficult to explain. Obduction of an oceanic plateau onto an immature island arc followed by formation of a back arc basin can account for the distribution of the volcanic rocks but is difficult to reconcile with the limited outcrop exposure. An alternative explanation, that the sequences have been thrust together, is not supported by structural evidence in the field. Further work will be required to resolve this issue.

Study of the Norton Lake Cu-Ni-Co-PGE deposit, located at an unknown stratigraphic position within Suite I, was (initially) undertaken to determine the minerals that host the economic metals (copper, nickel, cobalt and the PGEs) present within the deposit. Examination of the mineralogy indicated that pyrrhotite, chalcopyrite,

pentlandite and pyrite (in order of decreasing abundance) are the primary sulphide phases within the deposit and carry the economic base metals.

Copper is exclusively carried by chalcopyrite, which occurs as discrete grains, masses and veins, except for trace amounts found in rare analyses of other sulphides. Nickel is dominantly found within pentlandite and violarite (violarite was only determined by stoicheometry, refer to Chapter 5) although nickel-bearing pyrite and pyrrhotite (1 to 4 wt% nickel) do occur in minor amounts. Cobalt minerals, with the exception of rare occurrences of skudderite, did not occur within the deposit. Instead cobalt was consistently found at elevated levels (1 to 3 wt%) within select sulphides of the deposit (pentlandite/violarite and pyrite).

The PGEs located by bulk assay (platinum and palladium) were found to have a variable occurrence. Palladium is dominantly found as tellurides and bismuth-tellurides (see Table 5.4 and Section 5.2.2 for details). Platinum occurs as a minor substitution within select palladium minerals and also, rarely, as discrete grains of sperrylite. A substantial amount of the platinum was determined to be contained within the sulphides, notably pyrrhotite and pentlandite with a smaller proportion contained within the pyrite. However it was not possible to resolve whether the platinum is in solid solution with the sulphides or is contained within microinclusions.

During this study, insight into the mineralization history of the deposit was also gained. Two mineralization events were determined to occur. The first, a primary magmatic mineralization, is the result of sulphur saturation being reached within the intruding magma while the second represents a later hydrothermal remobilization and enrichment event.

The first event, responsible for the majority of the sulphides, is related to primary magmatic mineralization. The ultramafic intrusion that hosts the deposit is located at, but not restricted to, a contact between overlying mafic volcanics and an underlying, sheared amphibolite tuff. It is possible that the intrusion assimilated part of a banded iron formation located at this contact and seen in drill core further to the east of the deposit where a thin, 1 – 2 m, ultramafic intrusion is located. The intrusion would have preferentially intruded along this plane of weakness. Assimilation of the iron formation would have caused sulphide saturation in the intrusion and initiated the precipitation of the sulphides where they would accumulate within topographic irregularities in the intrusion. Sulphide saturation would have been reached by either assimilation of sulphur from the sulphides within the iron formation (2 to 6 l % sulphides by volume) or due to the assimilation of silica which would result in a decrease in the sulphide saturation point (Barnes et al., 1987).

The second mineralization event is a hydrothermal remobilization and concentration of copper, palladium and silver. Evidence for this comes from the presence of chalcopyrite in crosscutting veins and fractures that often contain silver and palladium tellurides along with the mineral overgrowths of the palladium tellurides and/or silver tellurides. Additional evidence comes from the presence of incompatible minerals (as shown by the mineral stability fields in Section 5.3.1) within the deposit.

There are strong similarities between the Thierry Mine (for detailed information on the Thierry Mine refer to Patterson, 1980; Patterson and Watkinson 1984a and 1984b; Curtis, 2001), located within the Northern Pickle assemblage of the Pickle Lake greenstone belt, and the Norton Lake deposit. Tectonically, both are considered to be

located within a back arc environment. In addition both are hosted by ultramafic intrusions, believed to have intruded along and to have assimilated an iron formation. The Thierry Mine area consists of several mineralized lenses of pyroxenite while the Norton Lake deposit consists of two joined lenses with the potential for recognition of additional lenses along strike.

The two deposits have similar mineralogies with palladium tellurides being the dominant PGMs in both cases (Norton Lake deposit see Chapter 5; Curtis, 2001). In addition, the two deposits have similar copper:nickel ratios that are nearly 1:1 (Patterson and Watkinson, 1984a). This ratio, similar to the Shebandowan deposit near Thunder Bay, Ontario, indicate that the mineralization may not simply be the result of magmatic processes but may have been remobilized and altered (Abel et al., 1979; Morton, 1982; Patterson and Watkinson, 1984a; Carter et al., 2001). At the Thierry Mine the secondary remobilization was more intensive resulting in a zonation of the ore body that is related to the presence of strong shear zones near the mine.

The similarities between the mineralization of the Thierry mine and the Norton Lake deposit, together with the geochemistry of the Norton Lake area supports the correlation of the Northern Pickle assemblage of the Pickle Lake greenstone belt, with the northern most unnamed assemblage of the Miminiska-Fort Hope greenstone belt, proposed by this study and earlier by Stott and Corfu (1991).

Outstanding questions that need to be resolved are: 1) determination of how the platinum is carried by the sulphide phases; 2) constraining the changes in depositional conditions that are responsible for the increase in platinum mineralization indicated by

the inversion of the platinum:palladium ratio; and 3) refinement of the tectonic setting of the Norton Lake region.

Additional microprobe work would be valuable to determine if the platinum detected within the sulphides is contained as microinclusions or is present in solid solution within the sulphide itself. Along the same line there is the question of why platinum mineralization occurs only in select areas within the mineralized zone. Identifying what potential changes in depositional conditions were responsible for this phenomenon, through supplementary examination of the mineralogy and mineral chemistry of these areas, would be useful. Additional diamond drilling would provide additional material that would help to resolve this.

The relationship of the tectonic settings within the study area requires additional clarification. The absence of any field contacts makes accurate determination of the limits of the mapped units impossible. Additional trace element geochemistry with detailed sampling is needed to determine the potential extent of the mapped units defined and the tectonic environment they represent. This is complicated by difficulties in access to the area and the scarcity of outcrop exposure. Complicating any future detailed study of the area are the large expanses containing no outcrop. Further drilling of untested areas would provide much needed samples that would help to resolve these issues.

References

Abel, M.K., Buchan, R., Coats, C.J.A., and Penstone, M.E., 1979. Copper mineralization in the footwall comples, Stratcona mine, Sudbury, Ontario. Canadian Mineralogist, v. 17, pp. 275-285.

Arndt, N.T., 1991. High Ni in Archean tholeiites. Tectonophysics, v. 187, pp. 411-419.

Arndt, N.T., 1994. Archean komatiites, *In* Archean Crustal Evolution. *Edited by* K.C. Condie, Elsevier, pp. 11-44.

Barnes, S.J., Boyd, R., Korneliussen, A., Nilsson, L.P., Often, M., Pedersen, R.B. and Robins, B., 1987. The use of mantle normalization and metal ratios in discriminating between the effects of partial melting, crystal fractionation and sulphide segregation on platinum-group elements, gold, nickel and copper: examples from Norway. Geo-Platinum 87, pp. 113-143.

Beakhouse, G.P., Heaman, L.M. and Creaser, R.A., 1999. Geochemical and U-Pb zircon geochronological constraints on the development of a late Archean greenstone belt at Birch Lake, Superior Province, Canada. Precambrian Research, v. 97, pp. 77-79.

Bickle, M.J., Nisbet, E.G., and Martin, A., 1995. Archean greenstone belts are not oceanic crust. Journal of Geology, v. 102, pp. 121-138.

Cabri, L.J., 2002. The platinum-group minerals, *In* The Geology, Geochemisty, Mineralogy and Mineral Beneficiation of Platium-Group Elements. *Edited by* L.J. Cabri. Canadian Institute of Mining, Metallurgy and Petroleum, Special Volume 54, pp. 13-130.

Campbell, I.H., Griffiths, R.W. and Hill, R.I., 1989. Melting in an Archean mantle plume; heads it's basalts, tails it's komatiites. Nature, v. 339, pp. 697-698.

Card, K.D. and Ciesielski, A., 1986. DNAG#1, Subdivisions of the Superior Province of the Canadian Shield. Geoscience Canada, v. 13, pp. 5-13.

Carter, W.M., Watkinson, D.H. and Jones, P.C., 2001. Post-magmatic remobilization of platinum-group elements in the Kelly Lake Ni-Cu sulfide deposit, Copper Cliff Offset, Sudbury. Exploration Mining Geology, v. 10, pp. 95-110.

Cousens, B.L., 1996. Magmatic evolution of Quaternary mafic magmas at Long Valley Caldera and the Devils Postpile, California: effects of crustal contamination on lithospheric mantle-derived magmas. Journal of Geophysical Research, v. 101, pp. 673-689.

Corfu, F. and Ayres, L.D., 1991. Unscrambling the stratigraphy of an Archean greenstone belt: a U-Pb geochronological study of the Favourable Lake belt, northwstern Ontario, Canada. Precambrian Research, v. 50, pp. 201-220.

Corfu, F. and Stott, G.M., 1993a. Age and petrogenesis of two late Archean magmatic suites, northwestern Superior Province, Canada, inferred from zircon U-Pb and Lu-Hf isotopic systematics. Journal of Petrology, v. 34, pp. 817-838.

Corfu, F. and Stott, G.M., 1993b. U-Pb Geochronology of the Central Uchi Subprovince, Superior Province. Canadian Journal of Earth Science, v. 30, p 1179-1196.

Corfu, F. and Stott, G.M., 1996. Hf Isotopic composition and age constraints on the evolution of the Archean Central Uchi Subprovince, Ontario, Canada. Precambrian Research, v. 78, p 53-63.

Craig, J.R., 1982. The Cu-Fe-S System, *In* Sulfide Phase Equilibria: Sulfide Mineralogy, Reviews in Mineralogy Volume 1. *Edited by* P.H. Ribbe, MSA, pp. 64-76.

Craig, J.R., 1990. Textures of the ore minerals, *In* Mineralogical Association of Canada Short Course on Advanced Microscopic studies of Ore Minerals. *Edited by* J.L. Jambor and D.J. Vaughan. Mineralogical Association of Canada, Short Course Handbook Volume 17, p. 213-256.

Curtis, L., 2001. Thierry Mine Property Thunder Bay, Ontario for PGM Ventures Corporation. www.pgm-ventures.com.

DePaolo, D.J., 1981. Neodymium isotopes in the Colorado Front Range and crust-mantle evolution in the Proterozoic. Nature, v. 291, p. 193.

Desrochers, J.P., Hubert, C.H., Ludden, J.N. and Pilote, P., 1993. Accretion of Archean oceanic plateau fragments in the Abitibi greenstone belt, Canada. Geology, v. 21, pp. 451-454.

East West Resource Corporation, 2004. Annual Report.

Ellingham, E., 1988. Locator Explorations Ltd. (Duration Mines Ltd.) Norton Lake property OMEP OM87-4-L-112 geological report. Ministry of Northern Development and Mines assessment files.

Evans, A.M., 1993. Ore Geology and Industrial Minerals 3rd edition. Blackwell Science Ltd., Malden, MA.

Falloon, T.J., Malahoff, A., Zonenshain, L.P., and Bogdanov Y., 1992. Petrology and geochemistry of back-arc basin and basalts from Lau Basin spreading ridges at 15°, 18° and 19°S. Mineralogy and Petrology, v. 45, pp. 1-35.

Fan, J. and Kerrich, R., 1997. Geochemical characteristics of aluminum depleted and undepleted komatiites and HREE-enriched low Ti tholeiites, western Abitibi greenstone belt: A heterogeneous mantle plume-convergent margin environment. Geochemica et Cosmochimica Acta, v. 61, pp. 4723-4744.

Farrow, C.E.G. and Watkinson, D.H., 1997. Diversity of precious-metal mineralization in footwall Cu-Ni-PGE deposits, Sudbury, Ontairo: Implications for hydrothermal models of formation. The Canadian Mineralogist, v. 35, pp. 817-839.
Faure, G., 1986. Principles of Isotope Geology, Second Edition. John Wiley & Sons, Toronto.

Hall, L.A.F., 2004. Project Unit 04-006. Precambrian Geology and Mineral Potential of the Opikeigen Lake Area, *In* Summary of Field Work and Other Activities 2004, Ontario Geological Survey, Open File Report 6125, p 8-1 to 8-11.

Hamilton, W.B., 1998. Archean magmatism and deformation were not products of plate tectonics. Precambrian Research, v. 91, pp. 143-179.

Henry, P., Stevenson, R.K., Larbi, Y. and Gariepy, C., 2000. Nd isotopic evidence for early to late Archean (3.4-2.7 Ga) crustal growth in the Western Superior Province (Ontario, Canada). Tectonophysics, v. 322, pp. 135-151.

Herzberg, D., 1992. Depth and degree of melting of komatiites. Journal of Geophysical Research, v. 97, pp. 4521-4540.

Hill, G., 1981a. Interim report on the Norton Lake area for Wasabi Resources Ltd. Ministry of Northern Development and Mines assessment files.

Hill, G., 1981b. Report on anomaly U nickel-copper deposit Norton Lake area for Wasabi Resources Ltd. Ministry of Northern Development and Mines assessment files.

Hoffman, L.M. and MacLean, W.H., 1976. Phase relations of michenerite and Merenskyite in the Pd-Bi-Te system. Economic Geology, v. 71, pp. 1461-1468.

Hollings, P., 1998. Geochemistry of the Uchi Subprovince, northern Superior Province: and evaluation of the geodynamic evolution of the northern margin of the Superior Province ocean basin. Ph.D. thesis, University of Saskatchewan, Saskatoon, Saskatchewan.

Hollings, P., 2002. Archean Nb-enriched basalts in the northern Superior Province. Lithos, v. 64, pp. 1-14.

Hollings, P. and Kerrich, R., 2000. An Archean arc basalt-Nb-enriched basalt-adakite association: the 2.7 Ga Confederation assemblage of the Birch-Uchi greenstone belt, Superior Province. Contributions to Mineralogy and Petrology, v. 139, pp. 208-226.

Hollings, P., Stott G., and Wyman D., 2000. Trace element geochemistry of the Meen-Dempster greenstone belt, Uchi subprovince Superior Province, Canada: back-arc development on the margins of an Archean protocontinent. Cananadian Journel of Earth Science, v. 37, p 1021-1038.

Hollings, P., Wyman, D.A., and Kerrich, R.,1999. Komatiite-basalt-rhyolite volcanic associations in Northern Superior Province greenstone belts: significance of plume-arc interaction in the generation of the proto-continental Superior Province. Lithos, v. 46, pp. 137-161.

Jenner G. A., Longerich H. P., Jackson S. E., and Fryer B. J., 1990. ICP-MS- A powerful tool for high precision trace-element analysis in earth sciences: Evidence from analysis of selected USGS reference samples. Chemical Geology, v., pp. 133-148.

Jenner, G.A., 1996. Trace element geochemistry of igneous rocks: geochemical nomenclature and analytical geochemistry, *In* Trace Element Geochemistry of Volcanic Rocks: Applications For Massive Sulphide Exploration: Geological Association of Canada, Short Course Notes. *Edited by* D.A. Wyman, v. 12, pp. 51-77.

Jochum, K.P., Arndt, N.T. and Hofman, A.W. 1991. Nb-Th-La in komatiites and basalts: constraints on komatiites petrogenesis and mantle evolution. Earth and Planetary Science Letters, v. 107, pp. 272-289.

Kerr, A.C., Marriner, G.F., Arndt, N.T., Tarney, J., Nivia, A., Saunders, A.D., and Duncan, R.A., 1996. The petrogenesis of Gorgona komatiites, picrites and basalts: new field, petrographic and geochemical constraints. Lithos, v. 37, pp. 245-260.

Kerrich, R., Polat, A., Wyman, D., and Hollings, P., 1999. Trace element systematics of Mg-, to Fe-tholeiitic basalt suites of the Superior Province: implications for Archean mantle reservoirs and greenstone belt genesis. Lithos, v. 46, pp. 163-187.

Kerrich, R. and Wyman, D.A., 1996. The trace element systematics of igneous rocks in mineral exploration: an overview, *In* Trace Element Geochemistry of Volcanic Rocks: Applications for Massive Sulphide Exploration: Geological Association of Canada, Short Course Notes. *Edited by* D.A. Wyman, v. 12, pp. 1-50.

Kozyrev, S.M., Komarova, M.Z., Emilina, L.N., Oleshkevich, O.I., Yakovleva, O.A., Lyzlinov, D.V. and Maximov, V.I., 2002. The mineralogy and behaviour of PGM during processing of the Noril'sk-Talnakh PGE-Cu-Ni ores. *In* The Geology, Geochemisty, Mineralogy and Mineral Beneficiation of Platium-Group Elements. *Edited by* L.J. Cabri. Canadian Institute of Mining, Metallurgy and Petroleum, Special Volume 54, pp. 757-791.

Kusky, T.M., 1990. Evidence for Archean ocean opening and closing in the southern Slave Province. Tectonics, v. 9, pp. 1533-1563.

Kusky, T.M., 1991. Structural development of an Archean orogen, western Point Lake, Northwest Territories. Tectonics, v. 10, pp. 820-841.

Lafleche, M.R., Dupuy, C. and Dostal, J., 1992. Tholeiitic volcanic rocks of the Late Archean Blacke River Group, southern Abitibi greenstone belt: Origin and geodynamic implications. Canadian Journal of Earth Sciences, v. 29, pp. 1448-1358.

Lesher, .M. and Arndt, N.T., 1995. REE and Nd isotope geochemistry, petrogenesis and volcanic evolution of contaminated komatiiites at Kambalda, Western Australia. Lithos, v. 34, pp. 127-157.

Lesher, C.M., Goodwin, I.H., Campbell, H. and Gorton, M.P., 1986. Trace-element geochemistry of ore-associated and barren, felsic metavolcanic rocks in the Superior Province, Canada. Canadian Journal of Earth Science, v. 23, pp. 222-237.

Li, C., Maier, W.D., de-Waal, S.A., 2001. Magmatic Ni-Cu versus PGE deposits; contrasting genetic controls and exploration implications. South African Journal of Geology, v. 104; 4, pp. 309-318.

Ludden, J., Gelinas, L. and Trudel, P., 1982. Archean metavolcanics from the Rouyn-Noranda District, Abitibi greenstone belt, Quebec; 2, Mobility of trace elements and petrogenetic constraints. Canadian Journal of Earth Sciences, v. 19, pp. 2276-2287.

Magyarosi, Z., Watkinson, D.H. and Jones, P.C., 2002. Mineralogy of Ni-Cu-Platinum-Group element Sulfide Ore in the 800 and 810 Orebodies, Copper Cliff South Mine, and P-T-X Conditions during the Formation of Platinum-Group Minerals. Economic Geology, v. 97, pp. 1471-1486.

Mahoney, J.J., Storey, M., Duncan, R.A., Spencer, K.J. and Pringle, M., 1993. 1. Geochemistry and geochronology of leg 130 basement lavas: nature and origin of the Ontong-Java Plateau. Proceed of Ocean Drilling Program, Science Research, v. 130, pp.3-22.

Markovicky, E., 2002. Ternary and quaternary phase systems with PGE. *In* The Geology, Geochemistry, Mineralogy and Mineral Beneficiation of Platinum-Group Elements. *Edited by* L.J. Cabri. Canadian Institute of Mining, Metallurgy and Petroleum, Special Volums 54, pp.131-175.

McCallum, M.E., Loucks, R.R, Carlson, R.R., Cooley, E.F. and Doerge, T.A., 1976. Platinum Metals Associated with Hydrothermal Copper Ores of the New Rambler Mine, Medicine Bow Mountains, Wyoming. Economic Geology, v. 71, pp. 1429-1450.

McDonough, M.F. and Ireland, T.R., 1993. Intraplate origin of komatiites inferred from trace elements in glass inclusions. Nature, v. 365, pp. 432-434.

Molnár, F., Watkinson, D.H., 2001. Fluid-inclusion data for vein-type Cu-Ni-PGE footwqll ores, Sudbury Igneous Complex and their use in establishing an exploration model for hydrothermal PGE-enrichment around mafic-ultramafic intrusions. Exploration and Mining Geology, v. 10, pp. 125-141.

Morton, P., 1982. Archean volcanic stratigraphy and petrology and chemistry of mafic and ultramafic rocks, chromite and the Shebandowan Ni-Cu Mine, Shebandowan, northwestern Ontario. Ph.D. thesis, Carleton University, Ottawa, Ontario.

Mulja, T., 1989. Petrology, geochemistry, sulphide and platinum-group element mineralization of the Geordie Lake Intrusion, Coldwell Complex, Ontario. M.Sc. thesis, Lakehead University, Thunder Bay, Ontario.

Nesbitt, R.W. and Sun, S.S., 1976. Geochemistry of Archean spinifex-textured peridotites and magnesian and low magnesian tholeiites. Earth and Planetary Science Letters, v. 31, pp. 433-453.

Patterson, G., 1980. The geology of the Kapkichi Lake ultramafic-mafic bodies and related Cu-Ni mineralization Pickle Lake, Ontario. Ph.D thesis, Carleton University.

Patterson, G.C. and Watkinson, D.H., 1984a. The geology of the Thierry Cu-Ni mine, northwestern Ontario. Canadian Mineralogist, v.22, p3-11.

Patterson, G.C. and Watkinson, D.H., 1984b. Metamorphism and supergene alteration of Cu-Ni sulfides, Thierry mine, nowthwestern Ontario. Canadian Mineralogist, v.22, p.13-21.

Pearce, J.A., 1983. Role of sub-continental lithosphere in magma genesis at active continental margins. *In* Continental Basalts and Mantle Xenoliths. *Edited by* C.J. Hawkesworth and M.J. Norry, pp. 230-249.

Pearce, J.A., 1996. A user's guide to basalt discrimination diagrams. *In* Trace Element Geochemistry of Volcanic Rocks: Applications for Massive Sulphide Exploration: Geological Association of Canada, Short Course Notes, v. 12. *Edited by* D.A. Wyman, pp. 79-113.

Pearce, J.A. and Peate, D.W., 1995. Tectonic implications of the composition of volcanic arc magmas. Annual Review Earth and Planetary Science, v. 23, pp. 251-285.

Percival, J.A. and Williams, H.R., 1989. Late Archean Quetico accretionary complex, Superior province, Canada. Geology, v. 17, pp. 23-25.

Prest, K.V., 1944. Geology of the Fort Hope Area. Ontario Department of Mines, Annual Report, v. 51, pt 3, 28 p.

Richard, P., Shimizu, N., and Allegre, C.J., 1976. $^{143}Nd/^{146}Nd$, a natural tracer; and application to oceanic basalts. Earth and Planetary Science Letters, v. 31, pp. 269-278.

Rogers, N., 2002. Whole-rock chemical analyses from the Birch-Uchi Greenstone Belt, Superior Province, Geological Survey of Canada. Open File Report, 4271, pp. 1-29.

Rogers, N., McNicoll, V., van Staal, C.R., and Tomlinson, K.Y., 2000. Lithogeochemical studies in the Uchi-Confederation greestone belt, northwestern Ontario: Implications for Archean tectonics. Current Research – Geological Survey of Canada, Geological Survey of Canada, Ottawa, Ontario, 11p.

Rollinson, H., 1993. Using Geochemical Data: Evaluation, Presentation, Interpretation. Pearson Education Limited, Essex, England.

Rowell, W.F. and Edgar. A.D., 1986. Platinum-group element mineralization in a hydrothermal Cu-Ni sulfide occurrence, Rathbun Lake, Northeastern Ontario. Economic Geology, v. 81, pp. 1272-1277.

Saunders, A.D., Norry, M.J., and Tarney J., 1988. Origin of MORB and chemically-depleted mantle reservoirs: trace element constraints. Journal of Petrology, pp. 415-445.

Shinjo, R., 1998. Petrochemistry and tectonic significance of the emerged late Cenozoic basalts behind the Okinawa Troughs Ryukyu arc system. Journal of Volcanology and Geothermal Research, v. 80, pp. 39-53.

Smith, A.D. and Ludden, J.N., 1989. Nd isotopic evolution of the Precambiran mantle. Earth and Planetary Science Letters, v. 93, pp. 14-22.

Stern, R.A., Syme, E.C. and Lucas, S.B., 1995. Geochemistry of 1.9 Ga MORB- and OIB-like basalts from the Amisk collage, Flin Flon Belt, Canada: Evidence for an intra-oceanic origin. Geochemica et Cosmochimica Acta, v. 59, pp. 3131-3154.

Storey, M., Mahoney, J.J., Kroenke, L.W. and Saunders, A.D., 1991. Are oceanic plateaus sites of komatiites formation. Geology, v. 19, pp. 376-379.

Stott, G.M., 1996. The geology and tectonic history of the Central Uchi Subprovince; Ontario Geological Survey, Open File Report 5952, 178 p.

Stott, G.M., 1997. The Superior Province, Canada. *In* The tectonic evolution of greenstone belts. *Edited by* M.J. deWit and L.D. Ashwal, Oxford University Press, pp. 480-507.

Stott, G. M. and Corfu F., 1991. Uchi Subprovince, *In* Geology of Ontario, Ontario Geological Survey, Special Volume 4, Part 1, pp. 145-236.

Sun, S.S., and McDonough, W.F., 1989. Chemical and isotopic systematics of oceanic basalts: implications for mantle composition and processes. *In* Magmatism in the Ocean Basans. Geological Society Special Publication. *Edited by* A.D. Saunders and M.J. Norry, pp. 313-345.

Taylor, S.R., and McLennan, S.M., 1985. The Continental Crust: Its Composition and Evolution. Blackwell Scientific Publications, U.K.

Thurston, P.C., 1991. Archean geology of Ontario: Introduction. *In* Geology of Ontario, Ontario Geological Survey, Special Volume 4, Part 1, pp. 73-78.

Thurston, P.C., Osmani, I.A. and Stone, D., 1991. Northwestern Superior Province: Review and Terrane Analysis. *In* Geology of Ontario, Ontario Geological Survey, Special Volume 4, Part 1, pp. 81-142.

Thurston, P.C., 2002. Autochthonous development of Superior Province greenstone belts? Precambrian Research, v. 115, pp. 11-36.

Thurston, P.C. and Carter, M.W., 1969. Operation Fort Hope, Lansdowne House-Fort Hope Sheet; Ontario Department of Mines, Preliminary Geological Map P.562, scale 1 inch to 2 miles. Geology 1969.

Thurston, P.C. and Carter, M. W., 1970, Operation Fort Hope; Ontario Department of Mines and Northern Affairs, Miscellaneous Paper 42, 64 p.

Tomlinson, K.Y., Stevenson, R.K., Hughes, D.J., Hall, R.P., Thurston, P.C. and Henry, P., 1998. The Red Lake greenstone belt, Superior Province: evidence of plume-related magmatism at 3 Ga and evidence of an older enriched source. Precambrian Research, v. 89, pp. 59-76.

Vaughan, D.J. and Craig, J.R., 1978. Mineral Chemistry of Metal Sulfides. Cambridge University Press, New York.

Vaughan, D.J., Schwarz, E.J. and Owens, D.R., 1971. Pyrrhotites from the Strathcona mine Sudbury, Canada: A thermomagnetic and mineralogic study. Economic Geology v. 66, pp. 1131-1144.

Wallace, H. 1978. Geology of the Opikeigen Lake Area; Ontario Geological Survey, Report 185, 56 p.

Wallace, H. 1981a. Geology of the Miminiska Lake area; Ontario Geological Survey, Report 214, 96p.

Wallace, H. 1981b. Geology of the Attwood Lake area; Ontario Geological Survey, Report 203, 49p.

Wang, Z., Wilde, S.A., Wang, K, and Yu, L., 2004. A MORB-arc basalt-adakite association in the 2.5 Ga Wutai greenstone belt: late Archean magmatism and crustal growth in the North China Craton. Precambrian Research, v. 131, pp. 323-343.

Watkinson, D.H., and Melling, D.R., 1992. Hydrothermal origin of platinum-group mineralization in low-temperature copper sulphide-rich assemblages, Salt Chuck Intrusion, Alaska. Economic Geology and the Bulletin of the Society of Economic Geologists, v. 87, pp. 175-184.

Wilson, M., 1989. Igneous petrogenesis: a global tectonic approach. Harper Colins Academic, London.

Winchester, J.A. and Floyd P.A., 1977. Geochemical discrimination of different magma series and their differentiation products using immobile elements. Chemical Geology, v. 20, pp. 325-343.

Wyman, D.A., 1997. Prospectivity of Volcanic Belts for VMS Deposits: A New Exploration Strategy. Project 93E06: Final Report.

Wyman, D.A., 1999. A 2.7 Ga depleted tholeiite suite: evidence of plume-arc interaction in the Abitibi Greenstone Belt, Canada. Precambrian Research, v. 97, pp. 27-42.

Xie, Q, Kerrich, R. and Fan, J., 1991. HFSE/REE fractionations recorded in three komatiite-basalt sequences, Archean Abitibi greenstone belt: Implications for multiple plume sources and depths. Geochemica et Cosmochimica Acta, v. 57, pp.4111-4118.

Young, M. and Helmstaedt, H., 2001. Tectonic evolution of the northern Pickle Lake greenstone belt, northwestern Superior Province, Ontario. Geological Survey of Canada, Current Research 2001-C20, 13 p.

Young, M., 2003. New structural, geochronological, and geochemical constraints on the tectonic assembly of the Archean Pickle Lake greenstone belt, Uchi subprovince, western Superior Province. Unpublished M.Sc thesis, Queen's University, Kingston Ontario.

APPENDIX A

Sample Locations

Sample Locations From Mapping

Sample #	Easting	Northing	Strike/Dip	Rock	XRF/ICP-MS	TIMS
302	469581	5749361		gneiss		
309	470558	5750196	082/70N	ma		
310	470866	5750064		pllw ma		
311	470792	5749541	025-050/~70N	I.F.		
312	472210	5750473	092/-	ma		
313	472254	5750532	075/62N	gab		
	472324	5750655		ma		
315	472813	5750916		ma		
	472863	5750944		ma		
316	472901	5750932	074/-N	sed/ma		
317	473095	5751248		pllw ma		
318	473060	5751276		ma		
319	472979	5751269		ma		
	472854	5751227	068/-N	ma		
320	472654	5751290		pllw ma		
323	471588	5750455		ma		
	471598	5750413	064/-	ma/sed		
	471596	5750399	104/-	I.F.		
324	471541	5750416		px		
325	471160	5751106		ma	yes	
326	470984	5750966	102/-N	ma		
	470967	5750935		ma		
327	470888	5750625		pllw ma		
332	469101	5749346		sed		
333	469205	5749354	074/-N	sed		
	479977	5753650		ma		
347	479976	5753655	110/80-90N	ma		
	480062	5753718		ma		
	480135	5753918	078/N?	ma		
348	480129	5753958		ma/px		
	480128	5754012	080/-	pllw ma		
	480130	5754044		ma		
	480183	5754164	092/-N?	ma		
	480200	5754200		ma		
349	480202	5754204		ma	yes	
352	480444	5754197		pllw ma		
353	480742	5753783		ma/px	yes	yes
354	480581	5753705		ma		
355	480487	5753634		ma		
	480253	5753596		px		
356	480253	5753543		ma		
	480121	5753675		px		
357	479691	5753476		px		
358	479132	5753064		pllw ma		
359	478063	5753360		ma		
360	478032	5753542		pllw ma		
361	477887	5754445	120/60 N?	ma		
362	477905	5754579		ma	yes	
363	477609	5754511	090/80S	ma		
364	477589	5754527		ma/px		

Sample #	Easting	Northing	Strike/Dip	Rock	XRF/ICP-MS	TIMS
	477540	5754585		ma		
365	477506	5754598		fel/ma		
	477450	5754600	110/80N	ma		
	477395	5754597		px		
366	477275	5754429		px		
367	477045	5753632	098/68S	px		
368	477057	5753167	115/-(N?)	px		
	477291	5753130	110/90	ma		
369	477356	5752841	047/80E	ma		
370	478762	5752712	086/-	pllw ma		
	476050	5751670	094/90(S)	ma		
371	476132	5751670	094/90S	pllw ma		
	476030	5751692		ma		
372	475968	5751706		px	yes	
373	475943	5751682		pllw ma	yes	
	475880	5751715	104/-	pllw ma		
374	475425	5751521	040/-	px		
	475400	5751520		ma		
374.5	475316	5751264	085/-	sed/ma		
	475218	5750999	088-098/80-	sed		
376	474620	5751050	086/-	ma	yes	
377	478491	5752438	084/80-90S	ma		
110	471716	5750326		ma		
111	471773	5750319		p ma		
112	471807	5750334		ma/sed		
113	471869	5750346		ma/px		
114	471956	5750293		ma		
115	471946	5750366		ma		
116	471990	5750337		ma		
117	472153	5750286		px		
118	472104	5750095		px		
119	472221	5749900		ma		
120	471627	5750124		ma		
121	471550	5750413		px		
122	471585	5750424		diorite		
123	471896	5750418		granite/px/ma		
124	471599	5750430		sed		
125	471607	5750458		ma px		
126	471615	5750472		ma		
127	471635	5750471		ma		
128	471631	5750424		sed		
129	471602	5750392	265/-	ma		
130	471764	5750241		p ma		
131	471791	5750136		ma		
132	471768	5750060		p ma		
133	471730	5750035		p ma		
134	471653	5750002		ma/px		
137	470615	5749955		p ma		
139	470359	5749926		ma	yes	
140	471823	5750349		ma	yes	
141	471863	5750344		ma/px		

Sample #	Easting	Northing	Strike/Dip	Rock	XRF/ICP-MS	TIMS
142	471863	5750246		ma	yes	yes
143	471915	5750169		ma		
144	471909	5750208		ma		
145	471946	5750241		px	yes	
146	471955	5750292		ma		
147	472080	5750317		ma		
148	472070	5750391		ma		
149	472181	5750650		sed		
151	472249	5750489		ma	yes	
152	472220	5750368		ma		
153	472169	5750181		granite/sed		
154	472149	5750192		ma		
155	472155	5750290		px	yes	yes

Easting and Northing are UTM Zone 16 NAD 27 coordinates.
ma - mafic volcanic
pma - pillowed volcanic
sed - metasedimentary rock
px - pyroxenite/gabbroic

Drill hole locations for core abandoned in map area.

Hole	Easting	Northing
NL-01	476850	5754500
NL-02	476250	5753000
NL-03	475600	5751700
NL-04	477250	5750700
NL-05	477250	5750700
NL-06	477300	5750550
NL-07	473500	5751150
NL-08	471600	5751050
NL-09	471350	5750250
NL-10	470900	5748700
NL-11	472400	5750000
NL-12	471500	5752150
NL-13	471900	5752300
NL-14	472800	5752700
NL-15	473400	5752900
NL-16	474200	5750600
NL-17	474200	5750600
NL-18	474050	5750550
NL-19	474050	5750550
NL-20	474100	5750500
NL-21	473950	5750500
NL-22	475750	5749550

Locator Ltd. diamond drill hole locations listed in UTM Zone 16, NAD 27. Locations approximated from Ministry of Northern Development and Mines assessment files, accuracy +/-100 m.

Hole	No. Holes	Easting	Northing
A	3	47100-472200	576300
AA	1	481500	5749800
CC	1	479900	5753600
D	1	474500	5748800
DD	2	481100-481500	5753700-5753800
F	1	478500	5749900
G	2	471000-4710100	5751000-5751100
H	8	482100-482900	5751900-5752800
I	2	486900-487100	5752900-5753000
K	2	487100-487200	5756200
T	2	475100-575200	5748800-5748900
V	2	472000	5747900-5748100

Wasabi Resources Ltd. diamond drill hole locations listed in UTM Zone 16, NASD 27. Locations approximated from Ministry of Northern Evelopment and Mines assessment files, accuracy +/-200 m. Range of Eastings and Northings are given for multiple drill holes with same designation.

Location of samples selected for geochemistry from abandoned drill core.

Sample	Hole	Depth (m)	Company	XRF/ICP-MS	TIMS
CC1	CC1	96.0	Wasabi Resources Ltd.	yes	yes
F1	F1	21.0	Wasabi Resources Ltd.	yes	
G1	G1	93.0	Wasabi Resources Ltd.	yes	
Hba	H5	34.0	Wasabi Resources Ltd.	yes	
NL-04	NL-04	100.0	Locator Exploration Ltd.	yes	
NL-13c	NL-13	35.0	Locator Exploration Ltd.	yes	
NL-15	NL-15	15.0	Locator Exploration Ltd.	yes	
NL-20	NL-20	75.5	Locator Exploration Ltd.	yes	yes
NL-21	NL-21	75.0	Locator Exploration Ltd.	yes	
NL-22	NL-22	125.0	Locator Exploration Ltd.	yes	
HBb	H5	44.5	Wasabi Resources Ltd.	yes	
NL-13a	NL-13	66.0	Locator Exploration Ltd.	yes	yes
T03	T	58.0	East West Resource Corporation	yes	
O	O	13.3	East West Resource Corporation	yes	
P	P	48.3	East West Resource Corporation	yes	yes
Q	Q	69.2	East West Resource Corporation	yes	

	Drill Hole	Name	From m	To m
A01	A	A01	38.87	39.87
B01	B	B01	57.06	58.06
D03	D	D03	91.00	92.00
E01	E	E01	48.29	49.29
F04	F	F04	60.63	61.63
F01	F	F01	61.63	62.63
F02	F	F02	65.63	66.63
G01	G	G01	41.92	42.92
M01	M	M01	210.96	211.78
N01	N	N01	163.56	164.75
O01	O	O01	47.27	48.27
O02	O	O02	56.27	57.27
T01	T	T01	56.63	57.63
U01	U	U01	32.36	33.19
W01	W	W01	168.94	169.94
U12-01A	U12	U12-01	109.00	111.00
U12-02B	U12	U12-02	111.00	113.50
U12-04	U12	U12-04	111.00	113.50

Location of samples used for SEM and microprobe work.
All materials provided by East West Resource Corporation (EWR). All drill holes excepte U12 are fom EWR work in 2002.
From and To refer to meterage used for bulk rock assay.

APPENDIX B

Whole Rock and

Radiogenic Isotope Geochemistry

Sample	O	P	Q	G1	H5a	H5b	NL04b	NL15
Suite	I	I	I	I	I	I	I	I
SiO2	55.5	53.6	52.5	48.6	48.2	46.7	48.5	48.8
TiO2	1.0	1.0	1.1	0.6	1.0	0.9	1.1	1.1
Al2O3	17.4	17.2	18.1	15.0	16.3	16.0	14.8	14.7
Fe2O3	8.1	9.4	8.9	9.8	9.0	7.9	13.5	13.5
MnO	0.3	0.3	0.3	0.2	0.2	0.2	0.2	0.2
MgO	3.1	3.8	4.1	9.5	3.9	7.1	7.8	7.9
CaO	11.0	11.6	12.0	11.6	11.2	10.6	9.6	10.4
Na2O	2.2	2.3	2.1	1.7	2.8	2.1	2.7	2.4
K2O	0.3	0.4	0.3	0.3	0.2	0.2	0.3	0.2
P2O5	0.1	0.1	0.1	0.0	0.1	0.1	0.1	0.1
LOI	0.2	0.5	0.6	1.6	7.5	8.4	1.2	0.3
Sum	99.4	100.2	100.2	98.9	100.4	100.1	99.8	99.8
Ti	6724	6039	7090	3644	6132	5476	6822	6415
P	384	361	502	233	383	263	423	379
Cr	362	356	419	389	315	346	413	359
Co	52.29	59.64	61.72	49.44	64.69	59.26	60.19	58.32
Ni	175.2	175.9	175.6	184.1	132.6	129.1	125.3	128.8
Rb	11.87	10.88	6.18	13.08	1.04	0.96	1.73	1.47
Sr	151.9	174.1	185.1	119.6	117.6	121.7	155.1	112.8
Cs	0.15	0.87	0.35	2.11	0.10	0.15	0.71	0.28
Ba	178.88	105.33	56.43	71.93	20.60	12.44	22.60	13.53
Sc	46.50	35.65	40.55	33.70	35.99	36.66	40.63	37.25
V	342	342	361	241	314	313	293	260
Ta	0.22	0.20	0.23	0.10	0.17	0.15	0.22	0.21
Nb	3.80	3.58	3.89	2.25	2.85	2.63	3.35	3.05
Zr	63.9	59.2	64.1	32.7	48.9	44.3	65.1	60.7
Hf	1.85	1.75	1.93	0.96	1.46	1.48	1.81	1.76
Th	0.33	0.34	0.33	0.39	0.27	0.25	0.33	0.35
U	0.26	0.11	0.08	0.11	0.12	0.13	0.08	0.08
Y	20.48	20.19	21.32	12.09	21.26	18.26	24.84	25.44
La	4.68	4.11	4.40	1.96	3.19	2.64	3.30	2.99
Ce	11.88	10.34	11.45	5.19	8.53	7.45	9.30	8.61
Pr	1.76	1.62	1.70	0.77	1.31	1.15	1.49	1.37
Nd	8.06	7.85	8.59	3.88	6.24	5.51	7.43	7.14
Sm	2.51	2.39	2.42	1.30	2.14	1.83	2.40	2.43
Eu	1.04	0.90	0.97	0.53	0.86	0.69	0.91	0.92
Gd	3.40	3.14	3.35	1.95	3.05	2.57	3.34	3.33
Tb	0.57	0.54	0.59	0.33	0.54	0.42	0.59	0.57
Dy	3.60	3.72	3.96	2.38	3.55	2.90	4.16	3.78
Ho	0.77	0.77	0.82	0.51	0.74	0.65	0.92	0.82
Er	2.19	2.36	2.36	1.53	2.23	1.93	2.72	2.52
Tm	0.30	0.34	0.33	0.22	0.33	0.28	0.39	0.38
Yb	1.98	2.24	2.24	1.51	2.08	1.72	2.70	2.48
Lu	0.30	0.33	0.29	0.22	0.31	0.24	0.38	0.36
Cu	195.6	105.8	33.3	88.6	157.9	126.4	52.9	134.0
Zn	102.2	130.0	82.0	62.5	68.0	84.2	89.6	86.8
Mo	0.40	ud	ud	0.22	0.55	ud	0.14	0.22
Ag	ud	0.07	ud	ud	0.06	ud	ud	0.06
Tl	ud	ud	ud	0.20	ud	ud	ud	ud
Pb	1.37	1.65	3.15	3.09	0.40	0.39	0.90	0.83
Sn	1.76	2.08	1.01	1.20	1.44	1.00	2.64	1.48
Sb	0.16	0.47	0.72	0.86	0.35	0.68	0.13	0.19
As	4240	ud	ud	114.66	4.95	1.43	0.76	0.60

Sample	NL13	325	349	353	362	NL22	140	142
Suite	I	I	I	I	I	II	II	II
SiO2	47.9	51.3	47.2	43.9	46.5	47.7	49.0	48.1
TiO2	0.8	1.0	1.2	1.4	1.3	0.9	0.8	0.8
Al2O3	15.4	15.3	15.4	16.6	15.0	15.1	15.8	16.0
Fe2O3	11.1	11.4	13.7	14.2	13.9	13.2	11.8	12.1
MnO	0.2	0.2	0.2	0.2	0.3	0.2	0.2	0.2
MgO	8.4	6.5	6.6	6.9	7.4	8.0	8.4	9.1
CaO	11.3	10.3	11.5	11.9	9.2	10.6	12.2	10.7
Na2O	1.7	3.0	2.0	1.9	2.7	2.7	1.4	1.9
K2O	0.2	0.2	0.2	0.2	0.5	0.3	0.1	0.1
P2O5	0.1	0.1	0.1	0.1	0.1	0.0	0.1	0.1
LOI	0.8	0.9	1.9	2.6	1.7	0.7	0.4	0.6
Sum	97.8	100.1	99.8	99.7	98.5	99.4	100.1	99.6
Ti	5189	6657	7889	8426	7632	5651	5051	5277
P	329	453	483	567	511	140	225	297
Cr	465	353	331	345	306	351	399	426
Co	61.68	48.79	59.46	68.20	61.19	68.28	69.67	63.72
Ni	160.1	115.2	122.2	166.3	121.0	163.2	178.3	184.2
Rb	4.46	3.15	0.54	0.71	10.23	4.87	1.22	29.48
Sr	139.0	154.8	175.8	197.9	156.7	191.5	96.4	147.6
Cs	1.10	0.42	ud	ud	0.19	1.15	0.81	13.48
Ba	16.82	31.09	22.73	12.48	51.17	41.19	7.59	5.56
Sc	33.56	34.04	39.27	37.28	59.46	65.94	44.07	40.80
V	236	224	318	333	319	313	331	370
Ta	0.19	0.37	0.22	0.29	0.28	0.16	0.13	0.12
Nb	3.28	6.05	3.40	4.58	4.40	2.47	1.78	1.86
Zr	53.8	92.6	66.0	80.9	80.1	45.1	40.5	39.7
Hf	1.56	2.33	2.09	2.31	2.19	1.28	1.25	1.19
Th	0.35	0.72	0.34	0.46	0.45	0.29	0.14	0.12
U	0.10	0.20	0.08	0.13	0.08	0.07	ud	ud
Y	21.02	36.85	27.04	28.30	28.29	20.36	17.75	17.56
La	3.45	5.60	3.73	5.23	4.73	2.05	1.94	1.84
Ce	9.26	14.95	10.41	14.19	13.01	6.14	5.37	5.44
Pr	1.41	2.31	1.64	2.14	2.01	1.01	0.85	0.88
Nd	6.66	11.52	8.30	10.48	9.49	5.07	4.52	4.32
Sm	2.18	3.68	2.84	3.13	2.88	1.76	1.68	1.67
Eu	0.77	1.20	1.00	1.17	1.09	0.65	0.68	0.58
Gd	2.77	5.19	3.87	4.46	3.82	2.69	2.50	2.34
Tb	0.50	0.91	0.65	0.71	0.70	0.47	0.45	0.40
Dy	3.41	6.27	4.51	4.74	4.71	3.22	2.88	2.79
Ho	0.74	1.32	0.97	1.01	1.05	0.70	0.65	0.62
Er	2.23	4.14	2.95	3.00	3.03	2.09	2.00	1.93
Tm	0.33	0.61	0.45	0.44	0.47	0.32	0.29	0.29
Yb	2.14	3.92	2.91	2.96	3.03	2.14	2.01	2.02
Lu	0.31	0.59	0.41	0.40	0.44	0.30	0.30	0.28
Cu	65.5	66.6	147.9	143.5	137.1	58.2	140.5	284.3
Zn	69.2	87.3	85.2	96.6	92.1	92.4	56.0	87.9
Mo	ud	0.19	ud	0.25	0.29	ud	0.28	ud
Ag	ud	ud	0.09	ud	0.05	0.05	ud	0.07
Tl	0.08	0.05	ud	ud	ud	0.05	ud	0.29
Pb	0.66	0.93	0.90	1.09	0.79	1.64	0.39	0.55
Sn	0.99	1.62	1.93	2.04	1.32	2.50	1.35	1.39
Sb	ud	ud	0.38	0.58	0.07	0.11	0.12	0.08
As	0.33	0.85	14.60	1.12	1.06	1.09	ud	ud

Sample	145	151	155	372	373	376	NL13C	NL20
Suite	II	II	II	II	II	II	IIIa	IIIa
SiO2	49.1	49.0	49.1	47.1	48.2	47.5	53.7	66.8
TiO2	0.7	0.7	0.7	0.5	0.7	0.7	0.4	0.5
Al2O3	15.2	15.6	15.2	15.9	15.0	15.8	13.1	16.1
Fe2O3	12.0	12.0	12.5	10.6	12.0	12.2	1.7	3.3
MnO	0.2	0.2	0.2	0.2	0.2	0.2	0.2	0.2
MgO	7.6	8.0	8.4	9.8	8.5	7.2	0.6	1.1
CaO	11.0	11.3	11.0	11.5	11.1	12.5	14.0	3.4
Na2O	2.5	1.7	2.4	1.3	2.4	1.5	3.9	4.3
K2O	0.1	0.1	0.3	0.3	0.1	0.2	1.3	2.1
P2O5	0.0	0.1	0.1	0.0	0.1	0.1	0.1	0.1
LOI	0.5	0.6	0.5	1.8	0.5	1.1	10.5	1.5
Sum	99.0	99.2	100.4	99.0	98.7	99.0	99.6	99.5
Ti	4650	4602	4452	3342	4454	4441	2303	2829
P	271	255	289	178	226	190	525	412
Cr	400	384	387	371	417	440	56	104
Co	62.06	59.45	61.27	67.45	64.08	68.17	10.36	14.15
Ni	175.8	170.3	166.1	290.4	178.8	187.1	15.8	23.4
Rb	2.36	1.07	12.57	3.11	1.12	1.16	36.02	62.83
Sr	95.9	113.0	74.8	145.5	118.5	130.4	346.1	295.7
Cs	0.32	0.21	2.72	0.53	0.24	ud	1.01	2.77
Ba	23.70	10.25	31.35	19.47	9.66	20.76	319.49	451.34
Sc	47.45	43.32	35.20	50.82	40.20	41.89	12.69	15.65
V	346	357	345	234	293	309	37	62
Ta	0.10	0.10	0.12	0.07	0.10	0.10	0.34	0.42
Nb	1.63	1.66	1.76	1.30	1.60	1.50	3.79	3.81
Zr	39.5	38.4	34.9	26.9	35.7	36.3	101.9	91.7
Hf	1.10	1.15	1.05	0.83	1.11	1.15	2.85	2.65
Th	0.13	0.13	0.13	0.11	0.14	0.14	4.22	4.79
U	ud	0.07	ud	0.02	0.04	0.03	1.58	1.86
Y	17.06	16.97	15.17	14.68	15.58	15.97	6.96	6.99
La	1.49	1.30	1.39	1.34	1.48	1.57	13.92	12.09
Ce	4.54	4.27	4.31	3.84	4.44	4.76	27.06	23.77
Pr	0.72	0.73	0.68	0.62	0.75	0.80	3.13	2.67
Nd	4.40	4.01	3.84	3.14	3.64	4.36	11.09	9.50
Sm	1.58	1.60	1.36	1.15	1.49	1.51	1.89	1.68
Eu	0.60	0.60	0.42	0.48	0.59	0.65	0.62	0.53
Gd	2.30	2.17	1.95	1.72	2.34	2.32	1.82	1.48
Tb	0.41	0.39	0.35	0.31	0.39	0.43	0.22	0.20
Dy	2.83	2.75	2.56	2.24	2.85	2.90	1.30	1.20
Ho	0.59	0.58	0.56	0.50	0.63	0.62	0.24	0.24
Er	1.80	1.81	1.73	1.48	1.90	1.95	0.68	0.71
Tm	0.27	0.26	0.24	0.22	0.28	0.29	0.10	0.10
Yb	1.82	1.96	1.70	1.51	1.87	1.87	0.66	0.69
Lu	0.27	0.28	0.24	0.21	0.27	0.27	0.07	0.09
Cu	125.4	136.0	171.9	123.1	119.8	191.7	43.9	19.8
Zn	86.9	75.5	83.6	63.7	81.3	71.6	21.1	28.7
Mo	0.33	ud	ud	0.11	ud	ud	0.62	1.09
Ag	ud	ud	ud	0.08	ud	0.04	ud	ud
Tl	ud	ud	ud	ud	ud	ud	0.15	0.80
Pb	0.39	0.27	0.52	1.15	0.30	0.26	8.20	6.76
Sn	1.29	1.70	1.12	2.19	0.98	2.03	1.16	1.12
Sb	0.10	0.27	0.11	0.16	0.21	ud	0.65	0.28
As	ud	ud	-1495.74	22.83	0.66	0.29	0.89	20.52

Sample	CC	Fl	NL21	T03	139	160
Suite	IIIb	IIIb	IIIb			
SiO2	52.1	57.0	49.7	45.1	49.6	45.3
TiO2	0.5	0.7	0.9	0.2	1.0	4.3
Al2O3	15.9	15.3	15.7	6.1	15.8	12.5
Fe2O3	10.9	8.2	13.0	13.7	11.5	18.9
MnO	0.2	0.1	0.6	0.3	0.2	0.3
MgO	6.5	5.3	8.0	21.7	9.1	4.7
CaO	9.6	6.2	8.2	7.0	9.3	8.4
Na2O	2.8	4.9	1.3	0.1	2.5	3.1
K2O	0.2	0.2	0.9	0.0	0.1	0.2
P2O5	0.1	0.1	0.1	0.0	0.1	0.2
LOI	1.0	0.7	1.6	4.7	0.4	<0.1
Sum	99.7	98.8	100.0	98.9	99.6	97.9
Ti	3029	4710	5342	1097	6426	30289
P	322	718	384	209	344	1109
Cr	157	228	456	982	322	116
Co	57.20	37.90	52.51	155.17	47.17	58.91
Ni	138.1	89.5	156.3	2173.6	118.8	ud
Rb	1.66	4.13	36.11	0.08	13.21	2.08
Sr	194.8	343.2	190.8	38.1	163.1	125.5
Cs	0.08	1.03	3.29	0.12	3.69	ud
Ba	61.77	72.10	85.66	1.17	10.68	21.76
Sc	37.80	26.24	37.75	22.16	46.83	47.69
V	169	140	262	57	354	239
Ta	0.17	0.41	0.19	0.07	0.16	0.63
Nb	2.54	6.09	2.82	0.86	2.82	10.73
Zr	65.6	125.6	60.9	22.1	53.9	131.7
Hf	1.90	3.46	1.58	0.65	1.58	3.87
Th	1.52	3.47	0.76	0.49	0.22	0.73
U	0.41	0.90	0.22	0.10	0.08	0.21
Y	15.99	17.49	21.48	4.38	20.21	44.56
La	7.67	13.96	4.04	5.42	1.39	5.82
Ce	16.83	32.07	9.18	10.38	4.95	15.09
Pr	2.11	3.96	1.31	1.20	0.93	2.55
Nd	8.14	14.48	6.27	4.80	5.48	13.25
Sm	1.70	2.90	2.29	0.91	1.92	4.59
Eu	0.62	0.88	0.64	0.17	0.71	1.66
Gd	2.20	3.25	2.90	0.80	2.86	6.63
Tb	0.35	0.51	0.52	0.12	0.53	1.19
Dy	2.48	3.11	3.50	0.77	3.37	8.00
Ho	0.60	0.67	0.77	0.17	0.73	1.75
Er	2.02	2.03	2.15	0.49	2.29	5.23
Tm	0.31	0.31	0.33	0.08	0.33	0.76
Yb	2.43	2.06	1.97	0.57	2.23	4.65
Lu	0.36	0.31	0.27	0.09	0.30	0.66
Cu	107.7	68.0	46.5	1314.0	72.9	6.9
Zn	75.1	56.7	129.2	104.8	89.9	71.8
Mo	0.31	0.87	0.25	0.20	ud	0.66
Ag	ud	ud	ud	0.58	ud	ud
Tl	0.03	ud	0.46	0.25	0.14	ud
Pb	2.27	3.44	7.09	1.19	0.98	0.81
Sn	1.40	9.08	5.23	1.04	1.58	2.06
Sb	0.20	0.06	0.39	0.09	0.17	ud
As	0.35	ud	0.49	ud	15392.88	ud

Sample	A1	A2	B1	C1	D1	D2	E1	G1
Suite	EWR-I	EWR-II	EWR-I	EWR-II	EWR-II	EWR-II	EWR-I	EWR-III
SiO2	51.2	50.8	58.7	53.3	44.0	47.1	56.0	45.4
TiO2	1.1	1.1	0.6	1.1	0.8	0.9	0.4	0.2
Al2O3	17.2	17.7	14.5	17.4	12.8	14.4	10.5	8.3
Fe2O3	9.8	10.1	7.7	7.9	16.6	15.5	9.4	16.9
MnO	0.2	0.3	0.1	0.3	0.6	0.5	0.2	1.1
MgO	4.9	4.2	6.7	4.0	6.1	6.1	11.8	18.2
CaO	8.8	11.1	6.3	12.4	14.2	10.9	5.9	5.7
Na2O	3.3	3.1	3.5	2.4	0.9	2.3	1.7	0.5
K2O	1.4	0.4	0.9	0.2	0.5	0.6	2.0	0.1
P2O5	0.3	0.1	0.1	0.1	0.1	0.1	0.1	0.0
LOI	1.1	0.9	0.7	0.7	1.4	0.6	1.5	3.5
Sum	99.4	99.9	99.9	99.8	98.2	99.0	99.5	99.9
Ti								
P								
Cr	330	410	380	400	290	310	740	630
Co	47.5	59	30.5	59.5	102.5	73.5	45	57
Ni	115	150	155	205	170	155	395	1195
Rb	32.2	10.8	36.6	4.4	27.2	9.4	71.6	0.6
Sr	441	136	218	160	86.9	83.3	92.9	3.8
Cs	1	2.4	5.3	0.4	2.4	1	19.1	0.5
Ba	614	62.5	234	28.5	63	78	275	6
Sc								
V	255	295	110	290	240	240	80	80
Ta	<0.5	<0.5	<0.5	<0.5	<0.5	<0.5	<0.5	<0.5
Nb	5	3	5	3	2	3	5	1
Zr	92.5	63	108	55.5	43	49.5	82	21.5
Hf	2	1	3	1	1	1	2	<1
Th	3	<1	4	<1	<1	<1	3	<1
U	0.5	<0.5	1	<0.5	<0.5	<0.5	0.5	<0.5
Y	21.5	22	13.5	20.5	30.5	24	11.5	5
La	22.5	7.5	17.5	7	9	8	14	3
Ce	47.5	12.5	32.5	12	14.5	12	23.5	4
Pr	6.3	1.9	3.5	1.7	1.9	1.6	2.6	0.6
Nd	27	8.5	13	8.5	9	7.5	10.5	2
Sm	5.7	2.6	2.5	2.5	2.7	2.4	2.1	0.5
Eu	1.7	0.9	0.7	0.9	1	0.8	0.5	0.2
Gd	5.5	3	2.8	2.9	3.3	2.8	2.3	0.6
Tb	0.8	0.6	0.4	0.6	0.6	0.6	0.3	0.1
Dy	4.1	3.8	2.3	3.5	4.6	3.8	2	0.8
Ho	0.8	0.9	0.5	0.8	1	0.8	0.4	0.1
Er	2.4	2.5	1.5	2.3	3.3	2.7	1.3	0.6
Tm	0.3	0.4	0.2	0.3	0.5	0.4	0.1	<0.1
Yb	2	2.3	1.3	2	3.1	2.5	1.2	0.6
Lu	0.3	0.4	0.2	0.4	0.6	0.5	0.2	<0.1
Cu	40	110	15	135	4870	1810	325	395
Zn	90	105	70	90	200	300	110	230
Mo	6	6	6	6	26	6	6	2
Ag	<1	<1	<1	<1	1	<1	<1	<1
Tl	<0.5	<0.5	<0.5	<0.5	<0.5	<0.5	<0.5	<0.5
Pb	10	5	10	5	<5	10	5	<5
Sn	1	<1	4	3	4	1	2	5
From (m)	4.9	25	68.15	71.39	9.14	65.32	54.23	
To (m)	5	25.08	68.5	71.63	9.29	65.55	54.44	

Sample	F1	G2	G3	G4	NL04-04	NL04-05	NL04-03	NL04-05
Suite	EWR-III	EWR-I	EWR-I					
SiO2	42.7	58.2	53.9	58.6	62.8	46.2	57.5	58.3
TiO2	0.2	0.5	0.4	0.5	0.9	1.0	0.5	0.5
Al2O3	6.9	14.7	15.1	14.4	15.1	15.4	14.0	15.0
Fe2O3	17.6	7.3	7.5	7.6	7.0	15.2	7.6	7.5
MnO	0.4	0.1	0.2	0.2	0.2	0.4	0.1	0.1
MgO	20.1	7.5	7.8	7.3	2.1	5.6	6.2	6.7
CaO	5.1	6.3	10.0	6.4	6.7	12.3	6.2	6.6
Na2O	0.6	3.1	2.8	3.3	2.6	2.1	3.4	2.5
K2O	0.1	1.0	0.3	0.8	1.1	0.4	1.6	1.6
P2O5	0.0	0.1	0.1	0.1	0.2	0.1	0.1	0.1
LOI	5.2	0.8	1.1	0.6	1.1	1.2	1.5	1.0
Sum	99.1	99.7	99.2	100.0	99.9	99.9	98.8	99.8
Ti								
P								
Cr	1230	340	450		35	73	75	144
Co	122.5	28.5	40.5		15	36	14	17
Ni	890	190	275					
Rb	<0.2	33	3					
Sr	19.2	209	296					
Cs	0.4	3.7	2.1					
Ba	8	230	65.5					
Sc								
V	65	110	210					
Ta	<0.5	<0.5	<0.5					
Nb	1	4	3					
Zr	25	85	58.5					
Hf	<1	2	1					
Th	<1	4	1					
U	<0.5	0.5	0.5					
Y	7.5	11.5	11					
La	4	21.5	11		20	0	10	10
Ce	6.5	40.5	20.5					
Pr	1	4.7	2.3					
Nd	4	16	8					
Sm	1	2.9	1.9					
Eu	0.3	0.6	0.6					
Gd	1.1	2.5	1.8					
Tb	0.1	0.3	0.3					
Dy	1.3	2	1.8					
Ho	0.3	0.4	0.4					
Er	0.8	1.2	1.1					
Tm	0.1	0.1	0.1					
Yb	0.7	1	1					
Lu	0.1	0.1	0.1					
Cu	660	30	70					
Zn	155	60	75					
Mo	2	2	2					
Ag	<1	<1	<1		0	0.7	0	0
Tl	<0.5	<0.5	<0.5					
Pb	5	<5	15					
Sn	5	2	5					
From (m)	58.5	51.21	57.38	51.21	149.14	186.24	181.97	220.83
To (m)	58.63	51.66	57.83	51.66	149.23	186.33	182.03	220.98

Sample	NL04-05	NL04-06	NL04-02	NL04-01	NL04-07	NL04-01	NL04-01
Suite							
SiO2	59.0	50.4	49.8	44.4	53.4	47.5	54.6
TiO2	0.6	0.7	0.4	0.6	0.5	0.3	0.5
Al2O3	14.2	16.4	17.0	11.5	10.1	10.4	8.7
Fe2O3	8.2	10.1	10.8	17.1	11.6	18.7	10.7
MnO	0.1	0.2	0.3	0.4	0.4	1.0	0.2
MgO	6.2	7.0	8.0	8.5	12.9	13.0	14.6
CaO	6.8	7.7	9.6	14.9	6.5	4.4	5.2
Na2O	2.6	2.7	2.2	0.3	2.1	0.6	0.6
K2O	1.0	1.2	0.3	0.2	0.4	1.2	0.5
P2O5	0.1	0.1	0.0	0.1	0.1	0.0	0.1
LOI	0.8	1.9	1.0	1.9	1.9	2.6	3.3
Sum	99.7	99.6	99.5	99.7	100.0	99.7	99.0
Ti							
P							
Cr	126	137	32	18	194	64	330
Co	15	38	25	48	32	48	57
Ni							
Rb							
Sr							
Cs							
Ba							
Sc							
V							
Ta							
Nb							
Zr							
Hf							
Th							
U							
Y							
La	20	10	10	0	10	0	10
Ce							
Pr							
Nd							
Sm							
Eu							
Gd							
Tb							
Dy							
Ho							
Er							
Tm							
Yb							
Lu							
Cu							
Zn							
Mo							
Ag	0.04	0.7	0.2	0.3	0	0.6	0
Tl							
Pb							
Sn							
From (m)	196.45	208.58	240.19	212.75	94.79	208.78	215.07
To (m)	196.60	208.67	240.79	212.83	95.02	208.99	215.19

Sample
Suite
SiO2
TiO2
Al2O3
Fe2O3
MnO
MgO
CaO
Na2O
K2O
P2O5
LOI
Sum
Ti
P
Cr
Co
Ni
Rb
Sr
Cs
Ba
Sc
V
Ta
Nb
Zr
Hf
Th
U
Y
La
Ce
Pr
Nd
Sm
Eu
Gd
Tb
Dy
Ho
Er
Tm
Yb
Lu
Cu
Zn
Mo
Ag
Tl
Pb
Sn
From (m)
To (m)

Data is reproduced, with permission, from East West Resource Corporation internal reports and from the Ministry of Northern Development and Mines assessment files.

Sample Name	NL13A	P2	353	142	155	CC1	NL20	160
AGE	2900	2900	2900	2900	2900	2900	2900	2900
Nd (ppm)	7.45	6.72	10.62	4.96	3.22	7.73	9.53	12.05
$^{143}Nd/^{144}Nd$ (meas)				0.513140	0.513278			
2-sigma				0.000009	0.000017			
Total Sm	2.13	2.06	3.26	1.83	1.23	1.88	1.67	4.34
$^{147}Sm/^{144}Nd$	0.1732	0.1853	0.1856	0.2226	0.2298	0.1471	0.1057	0.2176
$^{143}Nd/^{144}Nd$ init	0.509019	0.508949	0.508939	0.508877	0.508877	0.508749	0.508989	0.508920
Eps Nd (CHUR)T	2.89	1.51	1.32	0.10	0.10	-2.49	2.31	0.95
Tdm (0.214, 0.513115)	2896	3259	3313	436	1563	3501	2939	-1249

Note: 2-sigma precision in $^{143}Nd/^{144}Nd$ = +/- 0.000018 based on repoducibility of standard and duplicates.
So Nd isotope ratios are only good to five decimal places, not the six reported here. Epsilon values are
+/- 0.5 units at 1115 Ma, +/- 0.8 units at 2900 Ma.
See Cousens, 2000, Journal of Geology 108, p. 181, for Sm-Nd analytical details.

Sample	Rb	Sr	87Sr/86Srpres	2-SIGMA	87Rb/86Sr	EpsSr pres	87Sr/86Sr init
353	0.71	160.79	0.701391	0.000011	0.012769	-44.13	0.700854
NL13A	6	101	0.704718	0.000006	0.171837	3.09	0.697494
P	6	143	0.708606	0.000012	0.121413	58.28	0.703502
155	10	59	0.718412	0.000011	0.490925	197.47	0.697774
142	22	115	0.732141	0.000011	0.554849	392.35	0.708815
CC1	4	162	0.702450	0.000014	0.071406	-29.10	0.699448
NL20	69	287	0.729873	0.000006	0.697141	360.16	0.700565
160	2	106	0.703255	0.000009	0.054569	-17.67	0.700961

An assummed age of 200 Ma was used for al calculations. Age is based on correlations with areas of known age.

APPENDIX C

SEM Analyses

Wt %								
Mg								
Al								
Si		0.23						
S	34.80	34.78	35.54	35.13	35.33	35.33	33.95	34.83
Fe	29.87	29.87	30.43	30.33	31.43	31.43	30.14	29.38
Co								
Ni	0.33							1.84
Cu	33.07	32.89	33.25	32.89	34.72	34.72	37.00	34.44
Pt								
Pd								
Sb								
Te								
Bi								
As								
Ag								
Pb								
Mo								
Zn								
Cr								
Total	98.07	97.77	99.22	98.35	101.48	101.48	101.09	100.49
Slide	F02	F02	U01	U01	M01	M01	M01	G01
Mineral	cp	cp	cp	cp	cp	cp	cp	cp

Wt %								
Mg								
Al								
Si								
S	34.78	35.30	34.37	34.17	34.28	34.44	18.01	37.07
Fe	30.48	30.62	29.60	30.52	31.00	30.33	9.56	
Co								
Ni							10.43	
Cu	33.61	33.76	33.92	34.59	33.92	34.36		
Pt								
Pd								
Sb								
Te								
Bi								
As								
Ag								
Pb							62.54	
Mo								63.12
Zn								
Cr								
Total	98.87	99.68	97.89	99.28	99.20	99.13	100.54	100.19
Slide	G01	G01	A01	A01	E01	E01	T01	U12-01a
Mineral	cp	cp	cp	cp	cp	cp	gal	moly

cp-chalcopyrite
gal-galena
moly-molybdenite
pn-pentlandite
po-pyrrhotite
vio-violarite

Wt %								
Mg								
Al								
Si								
S	0.55	33.05	33.08	33.22	33.27	33.14	33.00	33.17
Fe	3.59	28.68	28.16	28.06	28.45	27.59	28.94	29.09
Co		1.55	1.48	1.32	1.32	1.45	1.53	1.19
Ni	0.75	35.39	36.89	36.54	36.83	36.25	35.86	36.98
Cu								
Pt								
Pd	27.41							
Sb								
Te	56.17							
Bi	12.97							
As								
Ag								
Pb								
Mo								
Zn								
Cr								
Total	101.44	98.67	99.61	99.14	99.87	98.43	99.33	100.43
Slide	A01	F02	F02	F02	F02	F02	F02	U12-01a
Mineral	mel	pn	pn	pn	pn	pn	pn	pn

Wt %								
Mg								
Al								
Si								
S	33.47	33.31	32.62	32.97	32.97	32.85	33.11	32.73
Fe	28.56	25.58	27.95	28.14	28.16	28.31	28.42	28.82
Co	0.78		1.45	1.46	1.33	1.21	1.03	1.20
Ni	37.37	41.58	36.98	36.05	36.34	36.62	37.89	37.90
Cu								
Pt								
Pd								
Sb								
Te								
Bi								
As								
Ag								
Pb								
Mo								
Zn								
Cr								
Total	100.18	100.47	99.00	98.62	98.80	98.99	100.45	100.65
Slide	U01	M01	F02	F02	F02	F02	F02	F02
Mineral	pn	pn	pn	pn	pn	pn	pn	pn

cp-chalcopyrite
gal-galena
moly-molybdenite
pn-pentlandite
po-pyrrhotite
vio-violarite

Wt %								
Mg								
Al								
Si								
S	32.70	34.57	33.33	33.07	32.61	32.94	32.75	32.55
Fe	29.03	31.62	27.44	28.79	28.61	28.82	28.65	28.62
Co	1.42	1.13	1.25	1.53	1.29	1.23	1.49	1.61
Ni	36.69	31.05	36.28	36.66	35.68	37.72	36.12	36.19
Cu								
Pt								
Pd								
Sb								
Te								
Bi								
As								
Ag								
Pb								
Mo								
Zn								
Cr								
Total	99.84	98.37	98.30	100.05	98.19	100.71	99.01	98.97
Slide	F02	F02	F02	F02	F02	F02	F02	F02
Mineral	pn	pn	pn	pn	pn	pn	pn	pn

Wt %								
Mg								
Al								
Si								
S	33.43	33.58	33.71	32.68	33.45	36.94	32.46	34.20
Fe	28.47	29.27	28.71	27.15	26.89	26.22	27.73	26.82
Co	1.73	1.45	1.78	1.06	0.61	0.84	0.93	0.72
Ni	36.37	36.50	36.75	37.12	35.99	36.40	37.17	37.17
Cu								
Pt								
Pd								
Sb								
Te								
Bi								
As								
Ag								
Pb								
Mo								
Zn								
Cr								
Total	100.00	100.80	100.95	98.01	96.94	100.40	98.29	98.91
Slide	B01	B01	B01	A01	A01	A01	A01	A01
Mineral	pn	pn	pn	pn	pn	pn	pn	pn

cp-chalcopyrite
gal-galena
moly-molybdenite
pn-pentlandite
po-pyrrhotite
vio-violarite

Wt %								
Mg								
Al								
Si								
S	33.72	34.97	33.14	33.35	31.01	32.55	32.86	32.97
Fe	28.39	26.57	27.97	28.26	29.87	28.39	28.45	29.49
Co	0.92	1.24	1.58	1.63	1.29	1.37	1.70	1.50
Ni	37.50	37.07	37.23	37.28	37.11	36.26	37.68	37.09
Cu								
Pt								
Pd								
Sb								
Te								
Bi								
As								
Ag								
Pb								
Mo								
Zn								
Cr								
Total	100.53	99.85	99.92	100.52	99.28	98.57	100.69	101.05
Slide	A01	A01	A01	A01	E01	E01	E01	E01
Mineral	pn	pn	pn	pn	pn	pn	pn	pn

Wt %								
Mg								
Al								
Si								
S	38.94	39.28	39.23	39.33	39.60	39.58	39.53	40.26
Fe	59.33	57.90	59.39	58.75	59.05	59.55	57.82	59.84
Co								
Ni	0.38	0.52	0.48	0.66	0.70		0.55	
Cu								
Pt								
Pd								
Sb								
Te								
Bi								
As								
Ag								
Pb								
Mo								
Zn								
Cr								
Total	98.65	97.70	99.10	98.74	99.35	99.13	97.90	100.10
Slide	F04	F02	F02	F02	F02	F02	F02	U12-02b
Mineral	po	po	po	po	po	po	po	po

cp-chalcopyrite
gal-galena
moly-molybdenite
pn-pentlandite
po-pyrrhotite
vio-violarite

Wt %								
Mg								
Al								
Si								
S	39.16	39.47	39.82	40.14	39.42	40.12	39.49	39.54
Fe	59.38	59.06	59.01	58.28	59.21	58.74	59.30	59.07
Co								
Ni	0.37	0.56	0.56		0.66	0.47	0.97	0.39
Cu								
Pt								
Pd								
Sb								
Te								
Bi								
As								
Ag								
Pb								
Mo								
Zn								
Cr								
Total	98.91	99.09	99.39	98.42	99.29	99.33	99.76	99.00
Slide	U12-01a	U01	U01	U01	U01	U01	M01	G01
Mineral	po	po	po	po	po	po	po	po

Wt %								
Mg								
Al								
Si								
S	39.78	39.80	39.92	39.74	40.11	39.06	38.99	39.27
Fe	58.65	60.00	60.26	59.56	60.04	58.55	59.75	59.35
Co								
Ni	0.80	0.79	1.10	0.77	0.77	0.76	0.54	0.72
Cu								
Pt								
Pd								
Sb								
Te								
Bi								
As								
Ag								
Pb								
Mo								
Zn								
Cr								
Total	99.23	100.59	101.28	100.07	100.92	98.37	99.28	99.34
Slide	G01	G01	G01	G01	G01	F02	F02	F02
Mineral	po	po	po	po	po	po	po	po

cp-chalcopyrite
gal-galena
moly-molybdenite
pn-pentlandite
po-pyrrhotite
vio-violarite

Wt %								
Mg								
Al								
Si								
S	39.42	39.31	39.43	39.33	39.13	39.45	39.08	39.43
Fe	60.58	59.13	59.63	59.16	58.73	60.04	59.64	59.07
Co								
Ni	0.66	0.51	0.57	0.58	0.35	0.67	0.46	0.71
Cu								
Pt								
Pd								
Sb								
Te								
Bi								
As								
Ag								
Pb								
Mo								
Zn								
Cr								
Total	100.66	98.95	99.63	99.07	98.21	100.16	99.18	99.21
Slide	F02	F02	F02	F02	F02	F02	F02	F02
Mineral	po	po	po	po	po	po	po	po

Wt %								
Mg								
Al								
Si								
S	38.61	39.44	39.39	39.65	40.21	38.69	38.84	38.93
Fe	59.85	59.21	60.22	59.84	60.42	58.15	58.50	59.55
Co								
Ni	0.67	0.71	0.58	0.57	0.47	1.01	1.14	0.83
Cu								
Pt								
Pd								
Sb								
Te								
Bi								
As								
Ag								
Pb								
Mo								
Zn								
Cr								
Total	99.13	99.36	100.19	100.06	101.10	97.85	98.48	99.31
Slide	F02	B01	B01	B01	B01	A01	A01	A01
Mineral	po	po	po	po	po	po	po	po

cp-chalcopyrite
gal-galena
moly-molybdenite
pn-pentlandite
po-pyrrhotite
vio-violarite

Wt %								
Mg								
Al								
Si								
S	39.43	39.44	39.77	39.21	39.12	39.25	39.48	39.54
Fe	58.15	59.44	58.19	59.68	59.11	59.92	59.66	59.86
Co							0.00	
Ni	1.03	0.86	1.20	0.71	0.90	0.74	0.93	0.76
Cu								
Pt								
Pd								
Sb								
Te								
Bi								
As								
Ag								
Pb								
Mo								
Zn								
Cr								
Total	98.61	99.74	99.16	99.60	99.13	99.91	100.07	100.16
Slide	A01	A01	A01	A01	A01	A01	A01	A01
Mineral	po	po	po	po	po	po	po	po

Wt %								
Mg								
Al								
Si								
S	40.18	39.04	39.01	39.09	39.06	42.62	43.89	41.22
Fe	60.47	60.07	60.28	60.26	58.55	26.72	26.08	36.39
Co						0.40	2.94	
Ni	0.69			0.79	0.76	29.82	28.18	22.10
Cu								
Pt								
Pd								
Sb								
Te								
Bi								
As								
Ag								
Pb								
Mo								
Zn								
Cr								
Total	101.34	99.11	99.29	100.14	98.37	99.56	101.09	99.71
Slide	A01	E01	E01	E01	F02	G01	G01	A01
Mineral	po	po	po	po	po	vio	vio	vio

cp-chalcopyrite
gal-galena
moly-molybdenite
pn-pentlandite
po-pyrrhotite
vio-violarite

Wt %								
Mg								
Al								
Si								
S	41.87	41.51	53.16	52.91	53.25	52.95	53.87	53.27
Fe	22.36	42.78	46.15	43.66	44.31	44.26	44.40	43.85
Co	0.84	1.67		1.49	0.95	0.61	1.17	1.83
Ni	34.79	13.69	0.16					
Cu								
Pt								
Pd								
Sb								
Te								
Bi								
As								
Ag								
Pb								
Mo								
Zn								
Cr	0.20							
Total	100.06	99.65	99.47	98.06	98.51	97.82	99.44	98.95
Slide	A01	A01	T01	F02	F02	F02	F02	U01
Mineral	vio	vio	py	py	py	py	py	py

Wt %								
Mg								
Al								
Si								
S	53.71	52.59	52.36	54.14	54.09	53.71	53.55	52.58
Fe	44.43	43.62	44.58	45.45	46.17	45.60	46.09	44.81
Co	1.14		1.31	2.23			0.65	
Ni		3.11				1.38		
Cu			2.46					
Pt		1.61			2.20	2.18		1.71
Pd								
Sb								
Te								
Bi								
As								
Ag								
Pb								
Mo								
Zn								
Cr								
Total	99.28	100.93	100.71	101.82	102.46	102.87	100.29	99.10
Slide	U01	G01	G01	G01	G01	G01	F02	F02
Mineral	py	py	py	py	py	py	py	py

cp-chalcopyrite
gal-galena
moly-molybdenite
pn-pentlandite
po-pyrrhotite
vio-violarite

Wt %				
Mg				
Al				
Si			0.16	
S	53.47	52.92	52.75	52.82
Fe	46.42	45.77	40.89	45.81
Co		0.73		
Ni			4.88	1.25
Cu				
Pt				
Pd				
Sb				
Te				
Bi				
As				
Ag				
Pb				
Mo				
Zn				
Cr				
Total	99.89	99.42	98.68	99.88
Slide	F02	F02	A01	A01
Mineral	py	py	py	py

Wt %				
Mg				
Al				
Si				
S	52.89	53.20	53.27	
Fe	44.67	46.44	41.79	
Co	1.90		4.03	
Ni				
Cu				
Pt				
Pd				
Sb				
Te				
Bi				
As				
Ag				
Pb				
Mo				
Zn				
Cr				
Total	99.46	99.64	99.09	
Slide	E01	E01	T01	
Mineral	py	py	py	

cp-chalcopyrite
gal-galena
moly-molybdenite
pn-pentlandite
po-pyrrhotite
vio-violarite

py-pyrite

py-pyrite

py-pyrite

py-pyrite

py-pyrite

py-pyrite

py-pyrite

py-pyrite

py-pyrite

Wt%							
Mg			0.64		0.88		
Al			0.32		0.82		
Si			2.07		1.35		0.65
S	5.98	4.77		1.22		2.48	1.28
Fe	7.22	5.61	1.63	3.59	3.45	5.54	2.89
Co							
Ni	0.52			1.68			
Cu			1.30				1.09
Pt							
Pd	22.45	21.59	22.22	22.73	23.83	23.68	22.52
Sb		2.23	4.37	1.12	9.56	11.56	6.69
Te	46.00	29.71	30.96	48.51	32.40	29.78	32.53
Bi	16.58	35.39	37.44	21.45	28.79	27.73	33.58
Rh							
Au							
Ag							
Pb							
Se							
As							
Total	98.75	99.30	100.95	100.30	101.08	100.77	101.23
Slide	O02	B01	T01	U12-02B	B01	E01	F04
Mineral	mich	mich	mich	mich	mich	mich	mich

Wt%							
Mg							
Al							
Si							0.63
S	3.27	1.75	1.71	1.05	1.14	0.48	
Fe	4.73	3.70	4.00	3.54	1.95	2.28	2.29
Co							
Ni						1.83	
Cu					1.45		1.03
Pt							
Pd	24.00	22.72	23.38	23.22	23.60	22.88	23.07
Sb	5.13	4.48	6.12	6.35	6.95	4.54	5.00
Te	30.26	30.97	30.64	32.90	33.62	32.33	33.15
Bi	34.66	36.04	34.15	33.99	33.12	36.69	34.96
Rh							
Au							
Ag							
Pb							
Se							
As							
Total	102.05	99.66	100.00	101.05	101.83	101.03	100.13
Slide	U12-01a	U12-02B	U12-01a	G01	G01	U12-02B	F02
Mineral	mich	mich	mich	mich	mich	mich	mich

mich-michenerite/testibiopalladite
kot-kotulskite
meren-merenskyite
hess-hessite
sperry-sperrylite
acanthite

Wt%							
Mg							
Al							
Si		1.07					0.86
S	0.98		0.71	1.60		0.58	
Fe	2.54	1.66	2.49	3.01	2.14	2.39	1.80
Co							
Ni					2.10		
Cu							
Pt							
Pd	23.37	24.13	23.29	24.35	23.29	23.07	23.17
Sb	6.86	7.39	5.94	4.20	5.47	6.34	6.20
Te	31.74	37.86	31.81	30.73	31.57	31.11	35.29
Bi	34.47	28.94	36.04	38.02	35.42	36.20	29.14
Rh							
Au							
Ag							
Pb							
Se							
As							
Total	99.96	101.05	100.28	101.91	99.99	99.69	96.46
Slide	F04	F04	U12-01a	U12-02B	B01	U12-02B	G01
Mineral	mich	mich	mich	mich	mich	mich	mich

Wt%							
Mg							
Al	0.33						
Si	0.51						
S	0.51	0.34	1.91		0.53		
Fe	2.05	2.30		1.51	1.43	3.52	1.97
Co							
Ni							0.85
Cu				1.28			
Pt		1.02		0.72			
Pd	23.57	22.79	23.73	23.20	23.40	23.20	23.13
Sb	4.64	2.10	4.51	5.52	6.19		5.49
Te	31.10	31.98	34.11	32.03	31.59	32.95	31.01
Bi	36.32	40.45	36.11	36.95	35.36	41.00	36.89
Rh							
Au							
Ag							
Pb							
Se							
As					1.20		
Total	99.03	100.98	100.37	101.21	99.70	100.67	99.34
Slide	U12-01a	G01	O02	T01	U12-01a	U12-01a	U12-02B
Mineral	mich	mich	mich	mich	mich	mich	mich

mich-michenerite/testibiopalladite
kot-kotulskite
meren-merenskyite
hess-hessite
sperry-sperrylite
acanthite

Wt%							
Mg							
Al							
Si				0.59			
S		0.35					0.37
Fe	3.63	2.82	2.99	2.49	3.01	2.65	1.94
Co							
Ni							
Cu							
Pt							
Pd	24.21	23.60	24.19	24.08	24.39	24.36	23.70
Sb	8.64	5.77	5.58	5.44	9.50	6.60	3.17
Te	31.72	31.93	36.80	32.96	34.49	33.65	34.55
Bi	32.13	34.60	31.32	34.41	28.60	35.38	36.88
Rh							
Au							
Ag							
Pb							
Se							
As							
Total	100.33	99.07	100.88	99.97	99.99	102.64	100.61
Slide	U12-02B	U12-01a	E01	U12-02B	B01	G01	G01
Mineral	mich	mich	mich	mich	mich	mich	mich

Wt%							
Mg							
Al							
Si							
S		0.49					
Fe	1.07	1.61	2.04	0.87	0.82	1.40	1.16
Co							
Ni							
Cu					1.18		
Pt	1.97			1.95			
Pd	24.13	23.87	23.49	23.44	23.45	23.32	23.00
Sb	14.54	6.82	5.80	9.31	6.75	4.88	5.39
Te	33.13	34.55	34.00	32.92	33.43	33.21	32.45
Bi	25.08	31.69	34.18	31.91	33.17	37.60	37.35
Rh							
Au							
Ag							
Pb							
Se							
As							
Total	99.92	99.03	99.51	100.40	98.80	100.41	99.35
Slide	U01	G01	U12-01a	U01	G01	T01	T01
Mineral	mich	mich	mich	mich	mich	mich	mich

mich-michenerite/testibiopalladite
kot-kotulskite
meren-merenskyite
hess-hessite
sperry-sperrylite
acanthite

Wt%							
Mg							
Al							
Si							
S							
Fe	1.06	2.64	1.19	0.87	2.02	1.26	2.20
Co							
Ni						1.53	
Cu			1.56	0.89			
Pt	1.37						
Pd	23.34	23.61	24.49	23.84	24.09	23.78	24.10
Sb	9.20	2.72	6.94	6.34	7.36	3.94	4.02
Te	31.92	32.68	33.09	34.94	35.57	30.59	34.49
Bi	31.92	38.43	34.49	32.76	29.23	39.24	36.06
Rh							
Au							
Ag							
Pb							
Se							
As							
Total	98.81	100.08	101.76	99.64	98.27	100.34	100.87
Slide	U01	B01	G01	G01	G01	U12-01a	G01
Mineral	mich	mich	mich	mich	mich	mich	mich

Wt%							
Mg							
Al							
Si							
S							
Fe	1.41		0.91	1.17	2.05	0.82	2.20
Co							
Ni							
Cu							
Pt							
Pd	25.62	23.32	22.60	23.85	24.47	23.31	24.36
Sb	19.10	5.76	2.09	4.38	7.75	3.39	4.81
Te	34.57	36.27	32.81	34.79	31.90	34.04	34.08
Bi	19.46	34.52	39.56	36.40	34.67	37.76	34.65
Rh							
Au							
Ag							
Pb							
Se							
As							
Total	100.16	99.87	97.97	100.59	100.84	99.32	100.10
Slide	U01	F02	G01	O02	B01	U12-01a	U12-02B
Mineral	mich	mich	mich	mich	mich	mich	mich

mich-michenerite/testibiopalladite
kot-kotulskite
meren-merenskyite
hess-hessite
sperry-sperrylite
acanthite

Wt%							
Mg							
Al							
Si							
S							
Fe	1.09	1.04	1.81	2.18	1.65	1.38	
Co							
Ni							
Cu							
Pt							
Pd	24.34	23.31	25.02	24.68	24.16	24.29	23.79
Sb	7.59	4.37	8.19	5.93	5.57	5.98	5.37
Te	33.94	33.76	35.73	32.71	32.31	32.62	35.03
Bi	33.85	35.25	29.85	34.64	36.04	36.23	36.15
Rh							
Au							
Ag							
Pb							
Se							
As							
Total	100.81	97.73	100.60	100.14	99.73	100.50	100.34
Slide	W01	O02	B01	U12-01a	U12-01a	U12-01a	F02
Mineral	mich	mich	mich	mich	mich	mich	mich

Wt%							
Mg							
Al							
Si							
S							
Fe	1.22	1.69	1.31	0.87	1.42	0.68	1.29
Co							
Ni							
Cu							
Pt							
Pd	24.13	24.47	25.09	23.64	24.66	24.69	25.05
Sb	5.63	5.29	8.64	4.49	6.07	6.94	11.51
Te	33.89	32.99	35.02	33.54	33.59	36.04	31.73
Bi	34.44	36.02	30.91	35.21	34.60	31.62	30.02
Rh							
Au							
Ag							
Pb							
Se							
As							
Total	99.31	100.46	100.97	97.75	100.34	99.97	99.60
Slide	U12-01a	U12-02B	B01	T01	U12-01a	G01	U01
Mineral	mich	mich	mich	mich	mich	mich	mich

mich-michenerite/testibiopalladite
kot-kotulskite
meren-merenskyite
hess-hessite
sperry-sperrylite
acanthite

Wt%							
Mg							
Al							
Si							
S							
Fe	0.70	1.89		1.24	1.80		
Co							
Ni							
Cu							
Pt							
Pd	24.84	24.83	25.06	25.39	24.42	26.01	25.32
Sb	11.51	4.96	12.31	6.59		15.01	8.85
Te	35.27	31.52	33.36	35.02	34.26	34.04	35.49
Bi	24.92	37.80	29.05	32.83	38.99	26.66	31.67
Rh							
Au							
Ag							
Pb							
Se							
As							
Total	97.24	101.00	99.78	101.07	99.47	101.72	101.33
Slide	W01	U12-02B	W01	F04	U12-01a	F04	B01
Mineral	mich	mich	mich	mich	mich	mich	mich

Wt%							
Mg							
Al							
Si							
S				0.28			
Fe			2.65	2.32	1.68	1.44	1.30
Co							
Ni				3.21			
Cu							
Pt							
Pd	25.34	25.25	25.44	32.21	28.55	34.27	36.98
Sb	9.03	10.17		27.00	12.66	17.37	10.04
Te	34.29	33.80	30.91	32.26	39.59	29.13	33.48
Bi	33.22	31.43	41.95	3.57	17.44	16.39	15.85
Rh							
Au							
Ag							
Pb							
Se							
As							
Total	101.88	100.65	100.95	100.85	99.92	98.60	97.65
Slide	F04	U12-01a	E01	T01	F02	U12-02B	O02
Mineral	mich	mich	mich	mich	mich	kot	kot

mich-michenerite/testibiopalladite
kot-kotulskite
meren-merenskyite
hess-hessite
sperry-sperrylite
acanthite

Wt%							
Mg							
Al							
Si							0.50
S					0.28		
Fe	0.49				2.11	1.71	0.62
Co							
Ni							
Cu							
Pt							
Pd	39.14	37.17	41.49	26.23	25.99	25.72	24.83
Sb	14.04	9.67	15.59				1.56
Te	32.99	36.36	36.18	59.05	52.07	53.86	50.19
Bi	12.95	15.06	9.29	15.43	19.40	18.56	20.50
Rh							
Au							
Ag							
Pb							
Se							
As							
Total	99.61	98.26	102.55	100.71	99.85	99.85	98.20
Slide	F02	N01	N01	N01	U12-01a	N01	B01
Mineral	kot	kot	kot	meren	meren	meren	meren

Wt%							
Mg							
Al							
Si						0.31	
S							
Fe	1.19	1.66	1.14	1.50	0.78	2.28	2.31
Co							
Ni					0.69	0.67	1.72
Cu					0.66		
Pt			0.93				
Pd	25.75	24.84	24.64	24.65	24.91	24.90	24.02
Sb	1.39				1.07	0.92	
Te	60.31	50.86	53.80	53.67	56.27	49.61	53.29
Bi	10.87	23.70	18.23	20.18	15.16	22.03	19.65
Rh							
Au							
Ag							
Pb							
Se							
As							
Total	99.51	101.06	98.74	100.00	99.54	100.72	100.99
Slide	G01	N01	G01	B01	W01	U12-02B	B01
Mineral	meren	meren	meren	meren	meren	meren	meren

mich-michenerite/testibiopalladite
kot-kotulskite
meren-merenskyite
hess-hessite
sperry-sperrylite
acanthite

Wt%							
Mg							
Al							
Si							
S	0.51	0.24			0.90	0.36	
Fe	2.21	0.57		1.16	2.62	3.16	2.10
Co							
Ni	0.58	1.19			3.19	2.62	1.84
Cu							
Pt		0.84	2.74	1.26			
Pd	23.96	23.76	21.91	23.50	21.86	20.71	21.11
Sb	0.59			1.51			
Te	50.79	53.81	55.49	65.53	61.10	53.68	54.00
Bi	20.03	17.74	19.26	5.22	10.69	19.12	15.74
Rh							
Au							
Ag							
Pb							6.11
Se							
As							
Total	98.67	98.15	99.40	98.18	100.36	99.65	100.90
Slide	U12-02B	G01	F02	G01	O02	O02	B01
Mineral	meren	meren	meren	meren	meren	meren	meren

Wt%							
Mg							
Al							
Si							
S							1.55
Fe	3.42	2.09	2.72	1.48	0.89	0.89	2.84
Co							
Ni	2.14	2.64	1.92	2.75	14.53	14.53	12.47
Cu							
Pt	1.29			5.52			
Pd	21.86	21.55	22.10	18.73	5.14	5.14	7.09
Sb		1.15					
Te	54.73	54.29	55.38	55.49	78.22	78.22	75.08
Bi	17.12	18.56	19.55	17.53			2.31
Rh							
Au							
Ag							
Pb							
Se							
As							
Total	100.56	100.28	101.67	101.50	98.78	98.78	101.34
Slide	F02	O02	F02	F02	G01	G01	N01
Mineral	meren	meren	meren	meren	meren	meren	meren

mich-michenerite/testibiopalladite
kot-kotulskite
meren-merenskyite
hess-hessite
sperry-sperrylite
acanthite

Wt%							
Mg							
Al							
Si							0.23
S		24.49	21.32	2.30	1.32	2.33	0.66
Fe	1.32	19.72	21.41	4.09	2.84	3.07	1.23
Co							
Ni	7.45						1.60
Cu		5.08			0.47		
Pt							
Pd	15.28						
Sb							
Te	71.18	20.50	21.81	40.41	38.03	36.26	39.99
Bi	4.76						
Rh							
Au							
Ag		32.54	34.60	54.01	55.20	58.25	56.33
Pb							
Se							
As							
Total	99.99	102.33	99.14	100.81	97.86	99.91	100.04
Slide	B01	W01	F02	E01	W01	U12-01a	U12-01a
Mineral	meren	hess	hess	hess	hess	hess	hess

Wt%							
Mg							
Al							
Si							
S	1.91	0.62	1.29	0.52		0.18	0.83
Fe	3.75	2.40	2.11	3.42	2.53	1.22	1.39
Co							
Ni	1.21		1.75				1.29
Cu							
Pt							
Pd							
Sb							
Te	33.65	40.37	35.31	38.37	40.69	41.66	36.45
Bi							
Rh							
Au							
Ag	59.35	54.93	59.10	58.79	56.84	57.58	60.89
Pb							
Se							
As							
Total	99.87	98.32	99.56	101.10	100.06	100.64	100.85
Slide	U12-01a	G01	U12-01a	F04	U12-01a	W01	W01
Mineral	hess	hess	hess	hess	hess	hess	hess

mich-michenerite/testibiopalladite
kot-kotulskite
meren-merenskyite
hess-hessite
sperry-sperrylite
acanthite

Wt%							
Mg							
Al							
Si			0.49				
S	0.83	0.27	0.34				0.44
Fe	1.39	0.99	1.22	1.06	1.78	2.45	2.20
Co							
Ni	1.29						
Cu		1.45					
Pt							
Pd							
Sb							
Te	36.45	37.64	37.84	40.94	39.27	38.10	36.33
Bi							
Rh							
Au							
Ag	60.89	58.64	59.34	58.64	59.13	60.58	60.53
Pb							
Se							
As							
Total	100.85	98.99	99.23	100.64	100.18	101.13	99.50
Slide	W01	F04	U12-01a	U12-01a	U12-01a	F02	W01
Mineral	hess	hess	hess	hess	hess	hess	hess

Wt%							
Mg							
Al							
Si							
S		0.57		0.61			
Fe	2.64	2.13	1.72	0.64	1.13		
Co							
Ni							
Cu			1.40	0.79	1.17		
Pt							
Pd							
Sb							
Te	37.18	36.80	36.24	36.97	36.98	38.25	37.62
Bi							
Rh							
Au							
Ag	60.93	61.97	61.17	61.95	62.33	62.55	62.53
Pb							
Se							
As							
Total	100.75	101.47	100.53	100.96	101.61	100.80	100.15
Slide	U12-01a	W01	T01	W01	T01	F02	N01
Mineral	hess	hess	hess	hess	hess	hess	hess

mich-michenerite/testibiopalladite
kot-kotulskite
meren-merenskyite
hess-hessite
sperry-sperrylite
acanthite

Wt%					
Mg					
Al					
Si	0.32				2.70
S	11.12				0.59
Fe	0.59		2.06		2.80
Co					
Ni					
Cu					
Pt		41.73	50.30	55.17	53.74
Pd					
Sb					
Te					
Bi					
Rh					
Au					
Ag	81.66				
Pb					
Se					
As		54.40	52.22	49.21	37.47
Total	93.69	96.13	104.58	104.38	97.30
Slide	G01	W01	G01	O02	U12-01a
Mineral	acanthite	sperry	sperry	sperry	sperry

Wt%				
Mg				
Al				
Si				
S				
Fe	1.62		2.24	
Co				
Ni				
Cu				
Pt	53.88	54.04	55.72	
Pd				
Sb				
Te				15.32
Bi				
Rh				
Au				72.03
Ag				9.86
Pb				
Se				
As	47.30	41.60	39.26	
Total	102.80	95.64	97.22	97.21
Slide	G01	W01	U12-01a	G01
Mineral	sperry	sperry	sperry	unknown

mich-michenerite/testibiopalladite
kot-kotulskite
meren-merenskyite
hess-hessite
sperry-sperrylite
acanthite

APPENDIX D

Microprobe Analyses

Sample	Detection limit (ppm)	d-03	d-03	t-01	d-03	g-01	m-01	w-01
Fe	0.0200	29.52	29.51	30.82	29.91	29.06	30.71	29.27
Co	0.0200	0.03	0.04	0.04	0.04	0.00	0.00	0.03
Ni	0.0200	0.00	0.00	0.00	0.00	0.00	0.03	0.00
Cu	0.0200	34.10	34.41	34.20	34.13	33.11	34.10	33.45
Zn	0.0200	0.03	0	0	0	0	0	0
Ru	0.0250	0	0	0	0	0	0	0
Rh	0.0250	0	0	0	0	0	0	0
Pd	0.2500	0	0	0	0	0	0	0
Ag	0.1200	0	0	0	0.13	0.22	0	0
Cd	0.0250	0	0	0	0	0	0	0
Re	0.3000	0.09	0.08	0	0.06	0.05	0	0.04
Os	0.6000	0	0	0	0	0	0.10	0.09
Ir	0.6000	0	0.18	0.10	0	0	0	0
Pt	0.5000	0	0	0	0	0	0	0
Au	0.6000	0	0.08	0	0	0	0	0
Pb	0.2000	0.20	0.13	0.10	0.09	0.08	0.07	0.05
S	0.2000	35.53	34.83	34.16	35.27	35.51	32.36	34.30
Total		99.58	99.30	99.52	99.72	98.17	97.40	97.30
Mineral		cp	cp	cp	cp	cp	cp	cp

Sample	Detection limit (ppm)	t-01	w-01	w-01	d-03	d-03	g-01	m-01
Fe	0.0200	31.11	19.02	29.58	29.79	29.74	29.43	3.10
Co	0.0200	0.05	0.00	0.00	0.02	0.03	0.06	0.03
Ni	0.0200	0.00	0.02	0.00	0.00	0.00	0.41	0.03
Cu	0.0200	33.42	18.11	33.60	34.57	34.53	33.62	1.56
Zn	0.0200	0	0	0	0	0	0	0
Ru	0.0250	0	0	0	0	0	0	0
Rh	0.0250	0	0	0	0	0	0	0
Pd	0.2500	0	0	0	0	0	0	0
Ag	0.1200	0	0	0	0.27	0	0	0.18
Cd	0.0250	0	0	0	0	0	0	0.11
Re	0.3000	0	0	0	0.09	0.04	0	1.24
Os	0.6000	0	0	0.07	0	0	0	0
Ir	0.6000	0	0.11	0	0	0	0	0
Pt	0.5000	0	0	0	0	0	0	0
Au	0.6000	0	0	0	0	0	0	0
Pb	0.2000	0.03	0	0	0	0	0	80.66
S	0.2000	33.32	21.02	36.49	36.46	35.04	34.49	11.86
Total		97.99	58.32	99.81	101.21	99.46	98.04	98.77
Mineral		cp	cp	cp	cp	cp	cp	ga

cp-chalcopyrite
ga-galena
pn-pentlandite
py-pyrite
po-pyrrhotite

Sample	w-01	g-01	d-03	u12-04	o-01	w-01	o-01	u12-04
Fe	28.13	21.32	25.51	28.56	29.88	28.87	30.01	28.62
Co	1.32	1.73	1.56	1.69	1.69	1.45	1.82	1.61
Ni	36.41	30.64	27.77	35.30	36.16	36.06	36.06	35.65
Cu	0.00	0.00	0.09	0.00	0.00	0.00	0.00	0.00
Zn	0	0	0	0	0	0	0	0
Ru	0	0	0	0	0	0	0	0
Rh	0	0	0	0	0	0	0	0
Pd	0	0	0	0	0	0	0	0
Ag	0	0	0.30	0	0	0.14	0	0
Cd	0.05	0	0.04	0	0	0	0	0.04
Re	0.07	0.04	0	0.04	0	0.04	0	0.08
Os	0	0	0	0	0.15	0	0	0.14
Ir	0	0.06	0.06	0	0	0.12	0	0
Pt	0.0747	0	0	0	0	0	0	0
Au	0	0.13	0	0	0	0	0	0
Pb	0.32	0.25	0.21	0.18	0.10	0.10	0.08	0.08
S	33.47	39.52	40.97	33.09	32.48	32.97	32.96	31.84
Total	99.90	93.68	96.57	98.93	100.49	99.82	100.95	98.09
Mineral	pn	pn	pn	pn	pn	pn	pn	pn

Sample	u12-04	g-01	f-01	u12-04	g-01	d-03	t-01	o-01
Fe	28.73	24.81	29.39	28.87	25.08	26.40	29.82	29.45
Co	1.62	1.49	1.79	1.71	1.54	1.27	1.16	1.70
Ni	35.77	29.63	36.25	35.03	28.78	27.36	36.09	35.67
Cu	0.00	0.07	0.00	0.04	0.03	0.09	0.00	0.00
Zn	0	0	0	0	0	0	0	0
Ru	0	0	0	0	0	0	0	0
Rh	0	0	0	0.05	0	0	0	0
Pd	0	0	0	0.03	0	0	0	0
Ag	0	0	0	0.36	0.17	0	0	0
Cd	0	0	0	0	0	0	0	0.02
Re	0.05	0	0	0	0	0	0	0
Os	0	0	0	0	0	0	0	0
Ir	0	0.09	0	0	0	0	0	0
Pt	0	0	0	0	0	0.0861	0	0
Au	0	0	0	0.09	0	0	0	0
Pb	0.08	0.05	0.05	0.05	0.05	0.05	0.04	0.02
S	32.47	39.34	32.02	31.49	39.97	39.83	32.05	32.42
Total	98.78	95.48	99.58	97.73	95.64	95.11	99.30	99.48
Mineral	pn	pn	pn	pn	pn	pn	pn	pn

cp-chalcopyrite
ga-galena
pn-pentlandite
py-pyrite
po-pyrrhotite

Sample	m-01	m-01	g-01	w-01	g-01	g-01	d-03	u12-04
Fe	26.62	26.09	23.50	27.70	21.51	25.14	26.34	29.51
Co	0.02	0.00	1.68	1.31	2.09	1.46	1.12	1.68
Ni	40.71	41.19	29.80	36.51	32.05	27.66	27.02	35.69
Cu	0.00	0.00	0.37	0.00	0.00	0.00	0.00	0.00
Zn	0	0	0	0	0	0	0	0
Ru	0	0	0	0	0	0	0	0
Rh	0	0	0	0	0	0.05	0	0
Pd	0	0	0	0	0	0	0	0
Ag	0	0	0.38	0	0	0	0	0
Cd	0.03	0	0	0	0	0	0.03	0
Re	0	0	0.07	0.09	0	0	0	0.09
Os	0	0	0	0	0	0	0	0
Ir	0	0	0	0	0	0	0.12	0
Pt	0	0	0	0	0	0	0	0
Au	0	0	0	0.11	0.10	0.07	0	0
Pb	0	0	0	0	0	0	0	0
S	31.50	30.76	39.37	33.24	39.81	37.90	41.13	33.32
Total	98.93	98.08	95.17	99.13	95.62	92.28	95.81	100.36
Mineral	pn	pn	pn	pn	pn	pn	pn	pn

Sample	w-01	w-01	g-01	m-01	o-01	u12-04	t-01	d-03
Fe	28.93	29.45	23.18	27.15	29.50	29.76	30.03	26.89
Co	1.40	1.38	1.10	0.02	1.73	1.51	1.47	1.41
Ni	36.04	34.64	29.62	40.50	36.45	33.90	36.01	26.48
Cu	0.00	0.00	0.00	0.00	0.00	0.00	0.00	0.29
Zn	0	0	0	0	0	0	0	0
Ru	0	0	0	0	0	0	0	0
Rh	0	0.03	0	0	0	0	0	0.03
Pd	0	0	0	0	0	0	0	0
Ag	0	0.12	0	0.15	0	0	0	0
Cd	0	0	0.07	0.04	0	0	0	0
Re	0.07	0.07	0	0	0	0	0	0
Os	0	0	0	0	0	0	0	0
Ir	0	0	0	0	0	0	0	0
Pt	0	0	0	0	0	0	0	0
Au	0	0	0	0	0	0	0	0
Pb	0	0	0	0	0	0	0	0
S	34.00	33.38	38.22	31.36	32.71	34.17	32.06	38.20
Total	100.69	99.09	92.29	99.26	100.49	99.46	99.57	93.32
Mineral	pn	pn	pn	pn	pn	pn	pn	pn

cp-chalcopyrite
ga-galena
pn-pentlandite
py-pyrite
po-pyrrhotite

Sample	w-01	t-01	d-03	g-01	u12-04	m-01	w01	o-01
Fe	28.19	29.58	24.90	46.08	45.72	47.93	45.56	46.56
Co	1.36	1.28	1.16	1.42	2.44	1.05	1.74	1.81
Ni	36.74	36.54	27.91	0.04	0.04	0.00	0.00	0.00
Cu	0.00	0.00	0.85	0.00	0.00	0.00	0.00	0.00
Zn	0	0	0	0	0.02	0	0.04	0
Ru	0	0	0	0	0.06	0	0	0
Rh	0	0	0	0	0	0	0	0
Pd	0	0	0	0	0	0	0.04	0
Ag	0	0	0	0	0.15	0	0	0
Cd	0	0	0	0	0	0	0	0
Re	0	0	0	0.04	0.11	0	0.10	0
Os	0	0	0	0	0	0	0.07	0
Ir	0	0	0	0	0	0	0	0
Pt	0.1436	0	0.0594	0	0	0	0	0
Au	0	0	0	0	0	0	0	0
Pb	0	0	0	0.96	0.25	0.20	0.19	0.15
S	34.47	31.68	37.72	53.06	55.39	49.99	51.58	49.88
Total	101.02	99.18	92.65	101.75	104.23	99.30	99.34	98.49
Mineral	pn	pn	pn	py	py	py	py	py

Sample	m-01	d-03	u12-04	d-03	d-03	d-03	u12-04	o-01
Fe	48.28	46.25	45.69	45.55	47.05	46.46	44.96	47.32
Co	0.09	0.05	2.15	0.05	0.06	0.05	3.00	0.95
Ni	0.00	0.79	0.00	0.84	0.11	0.76	0.00	0.00
Cu	0.00	0.00	0.00	0.00	0.00	0.00	0.03	0.00
Zn	0.02	0	0.02	0	0	0	0	0
Ru	0	0.06	0	0	0.11	0	0	0
Rh	0	0	0	0	0	0	0	0
Pd	0	0	0	0	0	0.03	0	0
Ag	0.12	0.26	0.23	0	0	0	0	0
Cd	0	0	0	0	0.04	0.02	0	0
Re	0	0.10	0.10	0.05	0.09	0.05	0.15	0
Os	0	0	0	0	0	0	0	0
Ir	0	0	0	0	0	0	0	0
Pt	0	0.0845	0.0609	0.0649	0.0699	0	0	0
Au	0	0	0	0	0	0	0	0
Pb	0.13	0.10	0.09	0.09	0.09	0.08	0.07	0.06
S	50.63	51.00	52.13	53.32	52.71	53.11	53.75	52.43
Total	99.33	98.73	100.51	100.07	100.36	100.59	102.07	100.90
Mineral	py	py	py	py	py	py	py	py

cp-chalcopyrite
ga-galena
pn-pentlandite
py-pyrite
po-pyrrhotite

Sample	u12-04	f-01	u12-04	w01	o-01	f-01	u12-04	w01
Fe	45.91	47.14	46.05	46.75	46.67	46.65	45.40	46.00
Co	1.74	1.02	2.17	1.41	1.84	1.23	2.31	1.01
Ni	0.00	0.00	0.09	0.00	0.00	0.00	0.00	0.02
Cu	0.00	0.00	0.00	0.00	0.00	0.00	0.00	0.03
Zn	0	0	0	0.03	0	0	0	0
Ru	0	0	0	0	0	0	0	0
Rh	0.03	0	0	0	0	0	0	0
Pd	0	0	0	0.04	0	0	0	0
Ag	0	0	0	0	0	0	0	0
Cd	0	0	0	0	0	0	0	0
Re	0.14	0	0.12	0.12	0	0	0.12	0.11
Os	0	0	0	0.08	0.09	0.07	0	0
Ir	0.06	0	0.06	0	0	0	0	0
Pt	0	0	0	0	0	0	0.0562	0
Au	0	0	0.07	0.07	0	0	0	0
Pb	0.05	0.05	0	0	0	0	0	0
S	54.51	51.18	53.29	54.32	51.34	50.62	52.25	54.21
Total	102.49	99.48	101.87	102.87	99.98	98.61	100.25	101.46
Mineral	py	py	py	py	py	py	py	py

Sample	w01	g-01	g-01	w01	m-01	g-01	m-01	g-01
Fe	45.82	45.90	43.00	46.10	47.40	42.36	60.29	58.20
Co	1.55	1.86	0.07	1.10	1.44	0.07	0.09	0.12
Ni	0.00	0.05	4.11	0.00	0.00	4.60	0.46	0.70
Cu	0.00	0.03	0.00	0.00	0.00	0.00	0.00	0.00
Zn	0	0	0	0.02	0	0	0	0
Ru	0	0	0	0	0	0	0	0
Rh	0	0	0	0	0	0.08	0	0
Pd	0	0	0	0.03	0	0	0	0
Ag	0	0.55	0	0	0	0	0	0
Cd	0	0	0	0	0	0.05	0	0
Re	0.10	0.07	0.06	0	0	0.11	0	0.08
Os	0	0	0	0	0	0	0	0
Ir	0	0	0	0	0	0	0	0
Pt	0	0	0	0	0	0.1085	0	0
Au	0	0	0	0	0	0	0	0
Pb	0	0	0	0	0	0.31	0.20	0.15
S	52.25	51.31	53.67	55.12	49.37	51.65	36.48	41.19
Total	99.84	99.87	100.91	102.43	98.27	99.48	97.58	100.48
Mineral	py	py	py	py	py	po	po	po

cp-chalcopyrite
ga-galena
pn-pentlandite
py-pyrite
po-pyrrhotite

Sample	u12-04	g-01	d-03	t-01	w-01	t-01	w-01	g-01
Fe	58.61	58.42	58.90	59.21	58.68	60.07	58.94	45.85
Co	0.04	0.06	0.04	0.08	0.07	0.06	0.08	0.05
Ni	0.57	0.49	0.53	0.43	0.42	0.52	0.47	1.54
Cu	0.00	0.00	0.00	0.00	0.03	0.07	0.00	0.00
Zn	0	0	0	0	0	0	0	0
Ru	0	0	0	0	0	0	0	0
Rh	0	0	0	0	0	0	0.03	0
Pd	0	0	0	0	0	0	0	0
Ag	0	0.37	0	0	0	0	0	0.35
Cd	0	0	0.05	0	0	0	0	0
Re	0.04	0.12	0.07	0	0.07	0	0.08	0.10
Os	0	0	0	0	0	0	0	0.10
Ir	0	0	0	0	0	0	0	0
Pt	0	0.0973	0.0612	0	0	0	0.087	0.0699
Au	0.11	0.10	0	0	0.12	0	0	0
Pb	0.13	0.12	0.12	0.09	0.08	0.07	0.07	0.06
S	40.05	40.14	41.82	37.69	39.76	38.36	40.69	53.77
Total	99.70	99.98	101.76	97.58	99.31	99.19	100.47	101.93
Mineral	po	po	po	po	po	po	po	po

Sample	o-01	f-01	t-01	d-03	m-01	g-01	o-01	w-01
Fe	60.02	60.28	60.38	56.48	60.98	59.18	60.20	53.52
Co	0.04	0.09	0.06	0.08	0.04	0.08	0.06	0.05
Ni	0.48	0.44	0.55	0.90	0.46	0.44	0.46	0.73
Cu	0.00	0.00	0.00	0.08	0.03	0.00	0.00	0.02
Zn	0.02	0	0	0	0	0	0.04	0
Ru	0	0	0	0	0	0	0	0
Rh	0	0	0	0	0	0	0	0
Pd	0	0	0	0	0	0.02	0	0.04
Ag	0	0	0	0	0	0	0	0
Cd	0	0	0.02	0	0	0	0	0
Re	0	0	0	0.09	0	0.10	0	0
Os	0	0	0	0	0	0	0	0
Ir	0	0	0	0	0	0	0	0
Pt	0	0	0	0	0	0	0	0
Au	0	0	0	0.12	0	0	0	0.16
Pb	0.05	0.05	0.04	0.04	0.03	0.02	0.02	0.0046
S	38.41	38.65	38.10	42.26	37.13	41.29	38.84	36.18
Total	99.03	99.58	99.17	100.09	98.67	101.23	99.65	90.74
Mineral	po	po	po	po	po	po	po	po

cp-chalcopyrite
ga-galena
pn-pentlandite
py-pyrite
po-pyrrhotite

Sample	u12-04	w-01	w-01	u12-04	g-01	g-01	u12-04	u12-04
Fe	58.81	58.37	56.19	58.74	57.93	58.55	58.18	58.47
Co	0.06	0.05	0.07	0.05	0.05	0.04	0.08	0.08
Ni	0.57	0.44	0.44	0.53	0.73	0.59	0.53	0.53
Cu	0.00	0.00	0.00	0.00	0.00	0.00	0.00	0.00
Zn	0.02	0	0	0	0.03	0	0	0
Ru	0	0	0	0	0	0	0.05	0
Rh	0	0	0	0	0	0	0	0
Pd	0	0	0	0	0.03	0	0	0
Ag	0.16	0	0	0	0.37	0	0	0
Cd	0	0	0	0	0	0	0	0
Re	0	0.10	0	0	0.14	0.08	0.05	0.04
Os	0	0	0.31	0.08	0	0	0	0
Ir	0	0.08	0	0	0	0	0	0
Pt	0	0	0	0	0	0.051	0	0
Au	0.10	0	0	0	0	0	0	0
Pb	0	0	0	0	0	0	0	0
S	41.23	41.37	38.49	40.98	42.03	41.13	38.96	40.48
Total	101.02	100.49	95.62	100.45	101.32	100.45	97.87	99.63
Mineral	po	po	po	po	po	po	po	po

Sample	g-01	o-01	u12-04	t-01	t-01	d-03	d-03
Fe	58.05	60.13	58.79	60.49	60.34	6.21	6.13
Co	0.08	0.06	0.06	0.08	0.02	0.06	0.03
Ni	0.63	0.53	0.59	0.55	0.57	0.00	0.00
Cu	0.00	0.00	0.00	0.03	0.00	0.35	0.24
Zn	0	0	0.02	0	0	60.32	59.82
Ru	0	0	0	0	0	0	0
Rh	0	0	0	0	0	0	0
Pd	0	0	0	0	0	0	0.05
Ag	0	0	0.15	0	0	0	0
Cd	0	0.05	0	0	0	0.64	0.67
Re	0.04	0	0	0	0	0.05	0
Os	0	0	0	0	0	0	0.11
Ir	0	0	0	0	0	0	0
Pt	0.0874	0	0	0	0	0	0.066
Au	0	0	0	0	0	0	0.06
Pb	0	0	0	0	0	0.11	0
S	39.12	38.04	39.50	38.19	37.50	34.97	33.21
Total	98.08	98.96	99.18	99.47	98.53	102.77	100.41
Mineral	po	po	po	po	po	sph	sph

cp-chalcopyrite
ga-galena
pn-pentlandite
py-pyrite
po-pyrrhotite

Sample	g-01	g-01
Fe	24.24	0.00
Co	0.02	0.00
Ni	0.12	0.00
Cu	30.86	0.00
Zn	0	0
Ru	0	0
Rh	0	0
Pd	0	0
Ag	0	0
Cd	0	0
Re	0	0.11
Os	0	0
Ir	0.10	0
Pt	0	0
Au	0.15	0
Pb	0.20	0
S	0.00	102.29
Total	55.72	102.44
Mineral	unknown	unknown

Sample	d-03
Fe	22.35
Co	0.00
Ni	0.03
Cu	26.14
Zn	15.05
Ru	0
Rh	0
Pd	0
Ag	0
Cd	0.22
Re	0.11
Os	0
Ir	0
Pt	0
Au	0
Pb	0.09
S	34.58
Total	98.61
Mineral	unknown

cp-chalcopyrite
ga-galena
pn-pentlandite
py-pyrite
po-pyrrhotite